IN VITRO CHARACTERIZATION OF WILD-TYPE AND RIFAMYCIN-RESISTANT *MYCOBACTERIUM TUBERCULOSIS* RNA POLYMERASES

by

Sumandeep Kaur Atwal

A dissertation submitted in partial fulfillment
of the requirements for the degree of
Doctor of Philosophy
(Chemical Biology)
in The University of Michigan
2012

Doctoral Committee:

Professor George A. Garcia, Chair
Professor Carol A. Fierke
Assistant Professor Patrick J. O'Brien
Assistant Professor Oleg V. Tsodikov
Research Professor Hollis D. Showalter

To my husband

Ranjit Atwal,

and both of my families

the Atwal's and the Gill's

ACKNOWLEDGEMENTS

It would not have been possible to write this doctoral thesis without the help and support of several individuals who in one way or another contributed in the preparation and completion of this dissertation.

First and foremost, I am grateful to God for blessing me with so much in my life. I would like to thank my husband and best friend, Ranjit Atwal, for his encouraging words, personal support, and great patience at all times. I am indebted to my parents who have given me the opportunity of an education from great institutions. I would also like to thank my brothers and my in-laws for their unconditional love and support.

I offer my sincerest gratitude to my advisor, Professor George Garcia, whose encouragement, guidance and support has made me a better scientist. I would also like to thank my committee members, Professor Carol Fierke, Professor Patrick O'Brien, Professor Oleg Tsodikov, and Professor Hollis Showalter, for providing me with excellent advice and support throughout the years.

This thesis would not have been possible without our collaborators. I would like to thank Professor Hollis Showalter and his lab for synthesizing the rifamycin analogues especially Ms. Yafei Jin, Hao Xu, and Dr. AJ Turbiak. I am grateful to Dr. Paul Kirchoff for providing us with the modeling data. I would also like to thank Dr. Scott Franzblau for conducting the anti-TB studies. I appreciate the financial support from Program of

Chemical Biology, College of Pharmacy, and Rackham Graduate School of the University of Michigan for funding this project.

I cherish the friendships that I have made at the University of Michigan especially the ones within the GAG lab. It was an honor to work with Dr. Julie Hurt, Dr. Yi-Chen Chen, and Anthony Emanuele. I am going to miss our No Thai lunches!

I owe my gratitude to everyone mentioned here along with others I did not mention who have made this dissertation possible and because of whom my graduate experience has been one that I will cherish forever.

TABLE OF CONTENTS

LIST OF FIGURES

Figure

LIST OF TABLES

Table

ABSTRACT

IN VITRO CHARACTERIZATION OF WILD-TYPE AND RIFAMYCIN-RESISTANT *MYCOBACTERIUM TUBERCULOSIS* RNA POLYMERASES

by

Sumandeep Kaur Atwal

Chair: George A. Garcia

Rifampin (a semi-synthetic rifamycin derivative) is one of the first-line anti-tuberculosis drugs. Rifampin inhibits transcription by binding to the β-subunit of the RNA polymerase (RNAP). The majority of the clinically-relevant *Mycobacterium tuberculosis* (MTB) rifamycin-resistant (RifR) mutations result from amino acid substitutions of one of the following three residues: βAsp435, βHis445, and βSer450 in a highly conserved 27 amino acid region of the RNAP β-subunit.

The core subunits of wild-type and RifR mutants (Asp435Val, His445Tyr, Ser450Leu) of MTB RNAP were overexpressed in and purified from *E. coli*. The rifamycins were all found to bind tightly (IC_{50}) to the wild-type MTB and *E. coli* RNAPs, whereas dramatic ($\sim 10^2$-10^5 fold) losses of affinity for rifamycins were observed for the RifR mutants from both bacteria. Additional studies with efflux pump-deficient *E. coli* (EC2880) confirm that the differential sensitivity of MTB and *E. coli* to rifamycin antibiotic activity is due to rifamycin efflux from *E. coli*, rather than any differences in

the target RNAPs. The activities of C-8 modified rifamycins are consistent with X-ray crystal structures that show Ser450 acting as a hydrogen bond donor to the C-8 hydroxyl of rifamycins and that rifamycin resistance in the Ser450 mutants is likely due to loss of this hydrogen bond and loss of affinity. A series of novel benzoxazinorifamycin analogues displayed superior affinity toward wild-type and RifR mutants of the MTB RNAP than rifampin and rifalazil (RifR mutants, but not WT), but the IC_{50} values were still in the 10^{-6} M (μM) range with the RifR MTB RNAPs.

Rifampin exhibits significant drug-drug interactions via potent induction of cytochrome P450 3A4 (CYP3A4). Selected commercially available rifamycins and our synthetic analogues were screened in the human pregnane X receptor (hPXR) activation assay to determine their extents of hPXR activation as an indicator of potential for CYP3A4 induction. One of our analogues exhibited very low (similar to rifalazil) activation of hPXR, while the others did show significant activation and some cytotoxicity.

The results of these studies have provided encouraging evidence that rifamycins with improved activity against RifR MTB RNAP and lower drug-drug interaction liabilities can be developed.

CHAPTER I

Introduction

Even after successful prevention and control efforts, infectious diseases remain the second leading cause of death in developing countries and the third leading cause of death in developed countries (*1, 2*). These diseases include tuberculosis, HIV/AIDS, diarrheal diseases, and acute lower respiratory infections (*1*). After the "era of antibiotics" (1930-1970s), infectious diseases seemed to be controlled and the attention was shifted to the threat of chronic diseases. In the 1980s, pharmaceutical companies considered the number of antibiotics to be sufficient, and the development of new drugs was redirected away from antibiotics (*2, 3*). Unfortunately due to antimicrobial resistance, infectious diseases have reemerged as important human health threats. This has become an issue of great global concern because antimicrobial resistance reduces the effectiveness of current antibiotics leading to a greater risk of death and the possibility of returning to the pre-antibiotic era. Many factors may enhance antibiotic resistance including the incorrect use of antimicrobials (*i.e.*, not completing the full course; poor quality antibiotics are used at sub-therapeutic dosing) (*4*). Three major mechanisms of resistance are: inability of an antibiotic to permeate through cell wall or increased efflux, modification of the target that reduces the affinity for antibiotics, and inactivation of antibiotics by molecular modification (*3*). Since infectious diseases have been neglected for the past few decades, the development of new antibiotics has been a slow process. It is crucial to understand

the mechanisms of resistance and interactions of antibiotics with the resistance targets to allow for more potent and effective antibiotics to be designed and synthesized.

Mycobacterium tuberculosis and Tuberculosis

Tuberculosis (TB), an infectious disease caused by *Mycobacterium tuberculosis* (MTB), is a worldwide health threat being one of the most widespread and persistent bacterial infections (*5, 6*). In 2009, approximately 9.4 million new cases of TB were reported, along with 1.7 million deaths caused by TB. Furthermore, the emergence of antibiotic resistant MTB strains has increased to half a million cases (*5, 7*). TB is the leading cause of death in persons with HIV infection due to the fact that the one infection accelerates the progression of the other (*5, 8, 9*).

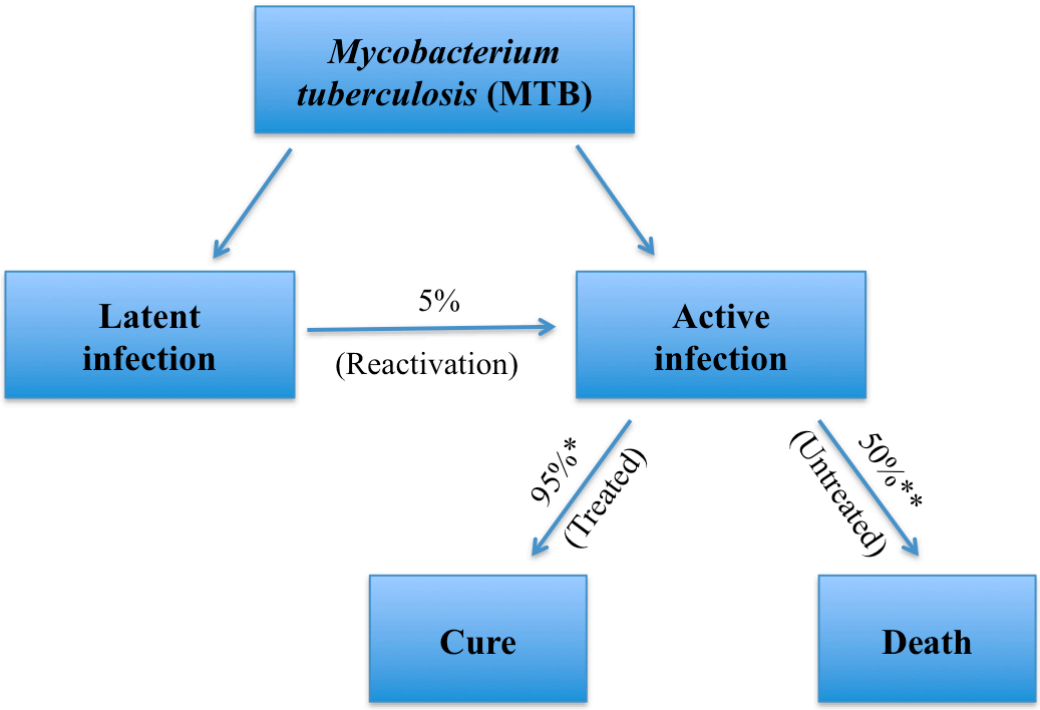

Figure I-1: Stages of *Mycobacterium tuberculosis* (MTB) Infection. TB exists as either latent or active infection. There is a 5-10% chance of the latent form developing into the active infection. Patients with the drug-susceptible TB recover 95% of the time (denoted by two asterisks) with a 5% chance of relapse. If TB is untreated this results in high mortality (50%; denoted by two asterisks).

The TB infection exists in two forms (Figure I-1), active TB and latent TB, with one-third of the world's population being infected with the latent/dormant form where there is ~5% (~10% for HIV/AIDs patients) chance of it converting to the active form (*9, 10*). Latent TB is not infectious and exists in a nonreplicative metabolic state in hypoxic environments thus making it difficult for antibiotics to be effective against it. On the other hand, active TB is infectious and can be transmitted from the infected host to a healthy individual via air by coughing, sneezing, and talking (*5, 9*).

Anti-TB Drugs and Resistant TB

The hydrophobic and waxy cell wall that is rich in mycolic acids, provides a formidable barrier to the penetration of drugs through the MTB cell envelop, thus limiting the number of effective anti-TB drugs. The current anti-TB treatment includes the following first-line drugs: rifampin, isoniazid, pyrazinamide, ethambutol, and streptomycin (Table I-1) (*8, 11-14*). Due to the high rate of spontaneous mutations (10^{-8} to 10^{-9} per bacterium per cell division), the anti-TB drugs are given in combination and the extensive treatment usually lasts six to nine months (*12-16*). The recommended regimen for a drug-susceptible strain is the combination of isoniazid, rifampin, pyrazinamide, and ethambutol (optional) for the first two months. During the next four to seven months (continuation phase), only rifampin and isoniazid (the two most potent anti-TB drugs) are administered (*12, 17, 18*). Approximately 95% of patients infected with a drug-susceptible strain can be cured in six months with only these four first line anti-TB drugs with only a 5% chance of relapse (*10*).

Unfortunately, alternative regimens have to be implemented for multidrug-resistant TB (MDR-TB) strains that are resistant to both rifampin and isoniazid (*7, 19*).

This therapy (usually lasting 18-24 months) consists of second line antibiotics (Table I-1) that are usually more expensive, more difficult to administer, less effective, and have more toxic side effects than first line drugs, which limit their usefulness (*11-14, 18*). Some of the side effects include nephrotoxicity, hepatotoxicity and dysglycaemia (*20*). The cure rate of MDR-TB with suboptimal therapy is only 50-70%, with 30% exhibiting treatment failure (*10, 19*). Furthermore, strains that are MDR and resistant to any fluoroquinolone and at least one of the injectable drugs (kanamycin, capreomycin, or amikacin) are classified as extensively drug-resistant TB (XDR-TB) with very high mortality rates (*7, 19*). Treatment failure is usually observed due to nonadherence to drug regimen, drug resistance, or malabsorption of drugs (*18*). To improve patient compliance, the directly observed therapy short course (DOTS) has been introduced where the patients are observed to ingest each dose in order to complete therapy and decrease the chance of acquired resistance (*5*).

Table I-1: Anti-Tuberculosis Drugs, MICs, Mechanism of Action

Drugs	**MIC (μM)**	**Mechanism of Action**
(First line)		
Rifampin	0.06 – 0.12	Inhibition of RNA synthesis
Isoniazid	0.15 – 1.5	Inhibition of cell wall mycolic acid synthesis
Pyrazinamide	130 – 410	Disrupts membrane potential via accumulation of pyrazinoic acid
Streptomycin	3.4 – 13.8	Inhibition of protein synthesis
Ethambutol	4.9 – 25	Inhibition of cell wall arabinogalactan synthesis
(Second line)		
Amikacin/kanamycin	3.7 – 7.5	Inhibition of protein synthesis
Fluoroquinolones	1.1 – 5.7	Inhibition of DNA gyrase/DNA synthesis
Ethionamide	15 – 60	Inhibition of mycolic acid synthesis
Capreomycin/viomycin	2.9 – 5.9	Inhibition of protein synthesis
p-aminosalicylic acid	3.3 – 50	Inhibition of folate biosynthesis pathway and mycobactin synthesis (unclear)

Recently, a new resistant strain has been identified as totally drug-resistant (TDR) TB; therefore, the issue of resistance and the necessity for new antibiotics is becoming of even greater concern (*21*). The existing anti-TB drugs are inadequate to address the issue of resistance; furthermore, anti-TB drugs with a new mechanism of action have not been introduced since rifampin in the 1960s (*10, 19*). The classes of anti-TB drugs currently in clinical trials (Phase 1 and 2; Figure I-2) include the following: diarylquinolines, nitroimidazoles, diamines, β-lactams, oxazolidinones, fluoroquinolones, and rifamycins, with only a 10% chance of any of these agents advancing to Phase 3 (*10, 13, 14, 21*). Unfortunately, mutations that confer resistance have already been identified for some of these drugs (*13*).

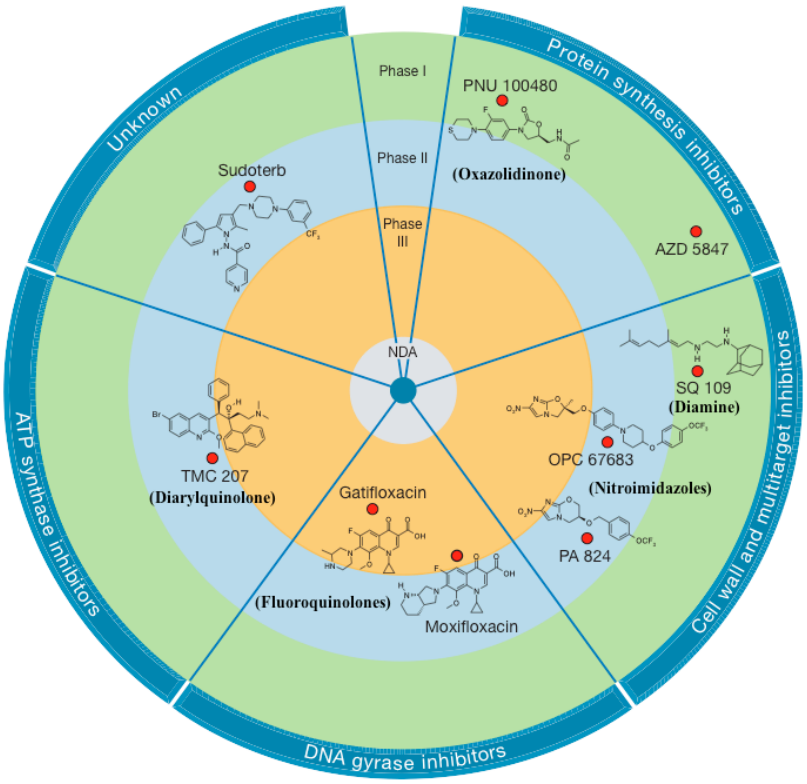

Figure I-2: The nine current anti-TB drugs in the clinical pipeline. The different classes the antibiotics belong to are listed in parentheses. (Reproduced and modified with permission from Koul 2011 (*10*))

Targeting the RNAP

An alternative to determining new classes of antibiotics/novel targets that are more potent is to chemically modify existing anti-TB drugs since their targets are already known. Rifampin (one of the most effective anti-TB drugs) inhibits RNA synthesis by binding to the bacterial DNA-dependent RNA polymerase (RNAP), a nucleotidyl transferase enzyme (*22-25*). RNAP is a vital enzyme responsible for transcription, an essential cellular process responsible for translating DNA into RNA in all organisms (*3, 26*). The core RNAP is composed of four different subunits ($\alpha_2\beta\beta'\omega$); whereas, the holoenzyme is formed upon the binding of the sigma factor (σ) to the core enzyme (Table I-2) (*24, 25*). The inhibition of bacterial RNAP leads to cell death thus making RNAP an attractive target. Additionally, bacterial RNAP is highly conserved among other prokaryotes but not eukaryotes hence allowing for therapeutic selectivity (*16, 27*). Furthermore, a bacterial RNAP inhibitor has the potential of being a broad-spectrum antibacterial drug because of the high level of conservation (*27*). The best characterized bacterial RNAP is the *E. coli* enzyme and to a lesser extent that of *Bacillus subtilis* (*22*). Other selective and non-selective RNAP inhibitors include the following: streptolydigin, myxopyronin, sorangicin, CBR703, guanosine tetraphosphate, tagetitoxin, lipiarmycin, daunomycin, marcellomycin, and microcin J25; however, rifampin was the first rifamycin to be approved for clinical use (*23-25, 27*).

Table I-2: Composition of the DNA-dependent RNAP holoenzyme

Subunit	Gene	MW of MTB subunits (kDa)	Function
α	*rpoA*	37.7	Assembly of the enzyme and the recognition of regulatory factors
β	*rpoB*	129.9	Chain initiation and elongation
β'	*rpoC*	146.7	Binds to the DNA template and contains most of the active site
ω	*rpoZ*	11.8	Aids β' binding and restores denatured RNAP
σ^A	*rpoD*	57.8	Recognizes and initiates transcription from promoters of house-keeping genes (SigA, note there are 13 sigma factors in MTB)

History and Development of Rifampin and Rifamycins

Rifampin is a semi-synthetic rifamycin derivative. Rifamycins belong to the greater ansamycin class of polyketide natural products (*16, 25, 28-31*). The generic ansamycin structure is composed of a flat aromatic ring system (naphthalene or benzene) and a 17-atom aliphatic ansa bridge connecting two non-adjacent atoms of the ring system (*29*). A mixture of rifamycins (Rifamycins A – E) was first isolated from *Amycolatopsis mediterranei* (previously classified as *Streptomyces mediterranei* and *Nocardia mediterranea*) where rifamycin B was the only stable product isolated in pure crystalline form (5-10% of the mixture) (*16, 28, 29*). The pathway from the weakly active rifamycin B to the more active rifamycin SV is illustrated in Figure I-3. In brief, rifamycin B is spontaneously oxidized to rifamycin O that is then hydrolyzed to rifamycin S with the loss of glycolic acid, and under mild reduction conditions, the more active rifamycin SV is formed (*28, 31*). Rifamycin SV is also a biosynthetic precursor of rifamycin B in the polyketide synthesis pathway (*16, 25*).

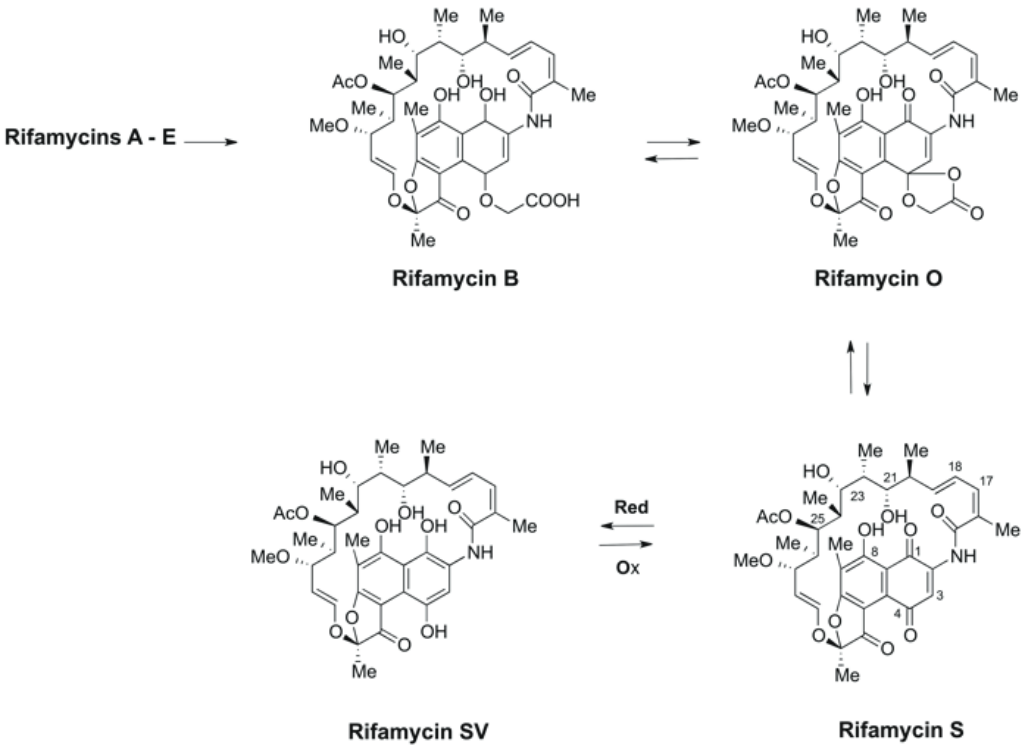

Figure I-3: Biological Transformation of rifamycin B into rifamycin SV

Although rifamycin SV was active, an improved rifamycin derivative was required with better oral absorption, prolonged antibacterial levels in blood, and greater antimicrobial activity (*28*). Several rifamycin derivatives have been synthesized, and the following relationships between structures of rifamycins and their antibacterial activities have been determined (some of the positions mentioned below are numbered on the rifamycin S structure in Figure I-3) (*32*):

- Both naphthohydroquinone and naphthoquinone rifamycin derivatives were equally active
- Acetylation of the hydroxyl group at position C8 resulted in an inactive rifamycin
- Opening of the ansa bridge resulted in loss of all activity
- Hydrogenation of the double bonds of the ansa bridge decreased activity
- Epoxidation of the C16-C17 and C18-C19 double bonds reduced activity

- Acetylation of –OH groups C21 and C23 led to inactive derivatives
- Hydrolysis of the acetoxyl group at C25 involved no loss of activity
- Substituents added to C3 and/or C4 position increased activity

Certain modifications of critical groups resulted in a decrease or loss of activity, and the minimal requirements for an active rifamycin were the hydroxyl groups at C21 and C23 of the ansa ring, the polar groups at C1 and C8 of the naphthol ring, and the specific ansa configuration (*29, 30, 32*). Modifications at C3 and C3/C4 of the aromatic ring are well tolerated and such derivatized rifamycins are active (*29, 32*). Rifampin (a C3 derivative) was found to be the most active with the following favorable qualities: broad-spectrum antibiotic, unique mechanism of action, good oral absorption, active against latent TB, and reduced TB therapy from 18 to 9 months (*28, 30, 33*).

Rifampin was first reported to inhibit the initiation of *E. coli* RNA synthesis by Hartmann and colleagues (*34, 35*). Rifampin binds tightly to the RNAP to form a stable noncovalent 1:1 complex with a binding constant in the range of 10^{-8} M (*36*). The binding of rifampin had no effect on promoter binding or the formation of the first phosphodiester bond but decreased the binding affinity of NTPs (by a factor of two) under *in vitro* conditions (*36-38*). Rifampin was able to bind to both the core RNAP and the holoenzyme (with a slightly higher affinity for the holoenzyme); therefore, the sigma factor is not required for binding (*39*). The rate of inhibition decreased in the presence of DNA template since the enzyme was protected to a certain degree. No inhibition was observed when rifampin was added after the addition of nucleotides since transcription was already in the elongation phase and the rifamycin binding site was inaccessible (*40, 41*).

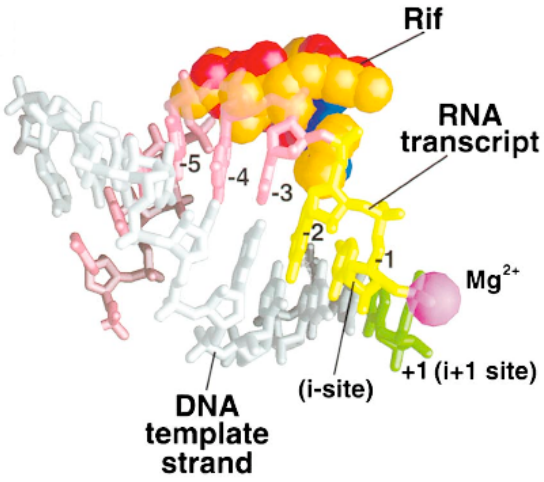

Figure I-4: A cartoon of the "steric occlusion" model. In this overlay of two structures, rifampin (carbon atoms, orange; oxygen, red; nitrogen, blue) is bound to the β subunit of the RNAP (RNAP and nucleic acids are omitted for clarity). The active site is indicated by the Mg^{2+} ion (the magenta sphere) and the 9bp RNA/DNA hybrid (+1 to -8) is only numbered from +1 to -5. The first nucleotide (green) binds at the +1 position as the chain grows, it is able to translocate to positions -1 and -2 (seen in yellow). However, the triphosphate of the first nucleotide clashes with the rifampin (illustrated in pink; -3 to -8) upon the addition of another nucleotide thus inhibiting RNA synthesis and releasing dinucleotides. (Reproduced with permission from Campbell 2001 (*41*))

McClure and Cech proposed the "steric occlusion" model as the principal mechanism of action. The 5' phosphates of the 5' NTP clash with the bound rifampin thus inhibiting the formation of the second phosphodiester bond. The RNAP is unable to translocate and dinucleotides are released. If transcription is initiated by NDP or NMP, the third phosphodiester bond is inhibited. The 3.3 Å crystal structure of *Thermus aquaticus* core RNAP in complex with rifampin supports the steric occlusion theory (Figure I-4) (*41*).

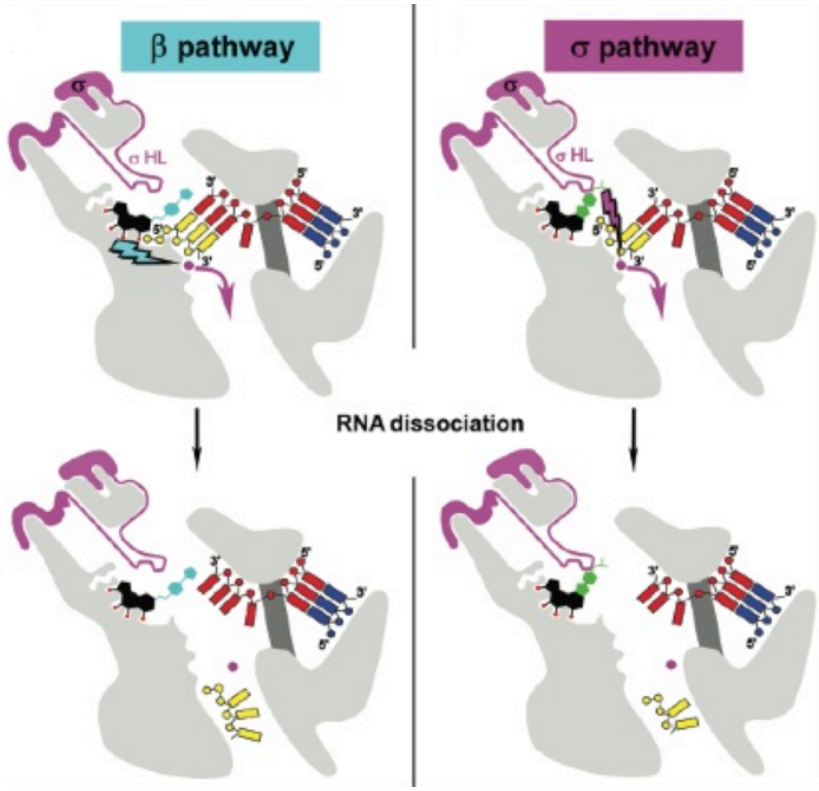

Figure I-5: The two pathways involved in the inhibition of RNAP via "allosteric mechanism". The β pathway (on the left) is activated when the ansa bridge and the β subunits interact. The allosteric signal (blue lightning bolt) from this pathway inhibits the formation of the second phosphodiester bond. The signal from the σ pathway (the purple lightning bolt; on the right) is activated when the C3/C4 rifamycin tail interacts with the hairpin loop of the σ factor (σHL) and inhibits the formation of the first phosphodiester bond. Both pathways release the catalytic Mg^{2+} ion (magenta sphere; bent arrow) thus releasing unstably bound RNAs (yellow) from the initiation complex. (The other components of the complex are as follows: core RNAP, gray; DNA template strand, red; DNA nontemplate strand, blue; RNA, yellow; σ and hairpin loop; magenta.) (Reproduced with permission from Artsimovitch 2006 (*46*))

However, the steric occlusion theory alone is not sufficient to explain the difference in activity with different rifamycin derivatives that only vary at the C3 and C3/C4 positions (*42-45*). It was observed that the rifamycin analogues with C3 tail modifications inhibited the formation of the second phosphodiester bond; whereas, the analogues with C3/C4 tail modifications inhibited the formation of the first

phosphodiester bond. Artsimovitch and colleagues proposed the "allosteric inhibition mechanism" with two pathways (the β pathway and the σ pathway) to explain these differences (Figure I-5) (*44*). The β pathway is activated by the interactions of the ansa bridge with the β residues and inhibits the formation of the second or third phosphodiester bond. Whereas, the σ pathway inhibits the formation of the first phosphodiester bond where the C3/C4 tail interacts with the hairpin loop of the σ factor (σHL) and this induces an allosteric signal (over 19 Å) and decreases the affinity for the catalytic Mg^{2+} ion thus slowing down transcription (*44, 46*). These two pathways were supported by the crystal structures of *Thermus thermophilus* RNAP in complex with rifapentine (C3 rifamycin; β pathway) and rifabutin (C3/C4 rifamycin; σ pathway).

Feklistov *et al*. reinvestigated the "allosteric mechanism" and found no evidence to support the hypothesis. The predominant effect of rifamycins was the inhibition of the formation of the second or third phosphodiester bond, consistent with the original steric occlusion model theory (*37, 47*). The results of Feklistov *et al.* are compelling and the steric occlusion model seems to be the most logical working hypothesis. This model suggests that if one were to incorporate new binding interactions between the rifamycin and the RNAP, one could achieve higher affinity and efficacy.

Rifamycin-resistance

The rifamycin-resistant (RifR) mutations arise spontaneously at a frequency of 10^{-8} where approximately 95% of these mutations are within 4 regions of the β subunit (N-terminal cluster and clusters I, II, III; Figure I-6) (*16, 41, 48*). Rifamycin resistance is mainly due to single amino acid substitutions and a few deletions or insertions of residues that alter the rifamycin binding site thus reducing the affinity for rifamycins (*43, 49, 50*).

All but one of the 15 different residues that have been identified from MTB RifR clinical isolates mapped to the 27 amino acid region of cluster I (also known as the Rifamycin Resistance Determining Region (RRDR)), a highly conserved region among prokaryotic RNAPs (*42, 49*).

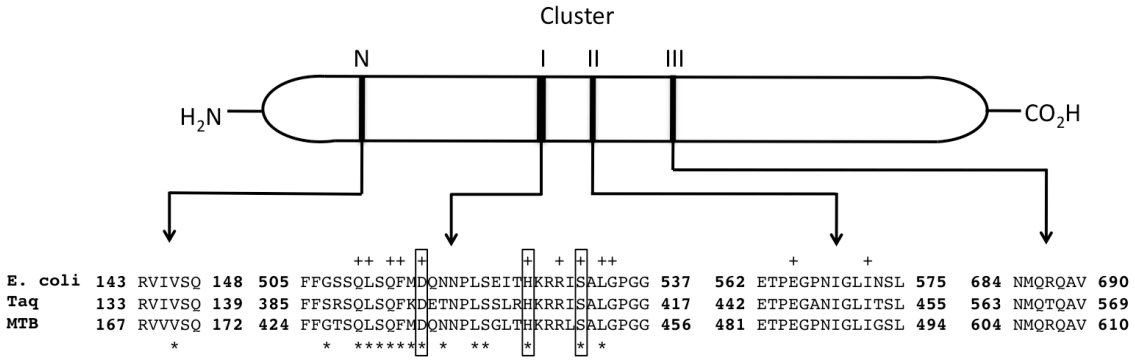

Figure I-6: Selected Sequences from Rifamycin-resistance Determining Regions of the RNAP β Subunits from *E. coli, Thermus aquaticus* (Taq), and *Mycobacterium tuberculosis* (MTB) (Cluster N and Clusters I, II, and III). The 12 amino acids of the β subunit that interact directly with rifampin are indicated with + above the *E. coli* sequence. The 15 RifR mutation positions that have been identified in MTB RifR clinical isolates are indicated with * below the MTB amino acid sequence. The three most frequently mutated residues are seen within the boxes. (Data from Campbell 2001)

From the co-crystal structure of Taq RNAP and rifampin, it was determined that the rifamycin binding site is located ~12.1 Å away from the active site (*38, 41*). Rifampin binds to the β subunit and directly interacts with twelve β subunit residues (via hydrogen bonding or van der Waals interactions) as can be seen in Figure I-7 (*41, 51*). The four critical groups at C1, C8, C21, and C23 of the rifamycins (discussed earlier) are involved in hydrogen bond interactions to ensure protein binding. Most of these twelve residues are found within the RRDR, and mutations of 11 out of the 12 residues result in RifR strain (Figure I-6) (*16, 41*).

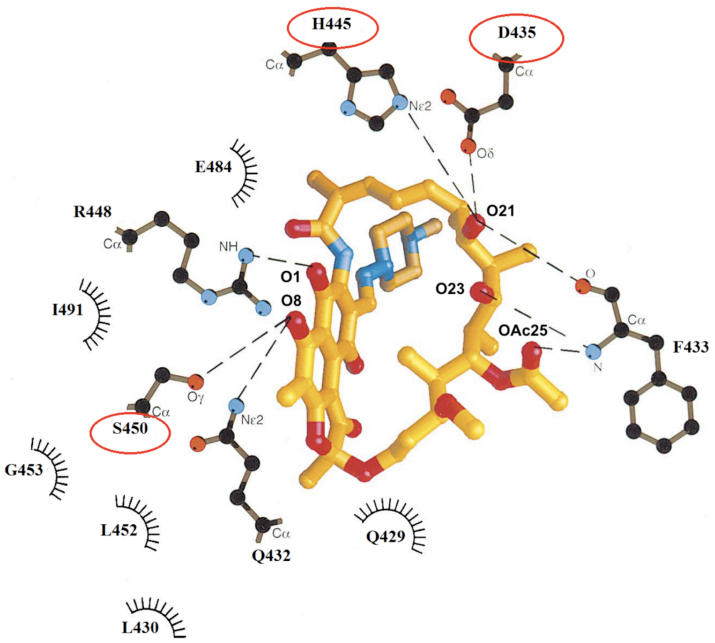

Figure I-7: Interaction of Rifampin with the Amino Acids of *Thermus aquaticus* RNA polymerase (RNAP) in the Antibiotic-Enzyme Complex. The amino acid numbering is for MTB *rpoB*. The amino acids interact with rifampin via van der Waals and hydrogen-bonding interactions. The oxygens of rifampin that form hydrogen bonds are numbered as in Figure I-3. The three most prevalent RifR mutation sites (re: Figure I-6) are circled. (Reproduced and modified with permission from Campbell 2001 (*41*))

Among these residues, the individual substitutions of three residues (Asp435, His445, and Ser450; MTB numbering; Figures I-6 and I-7) together account for more than 84% of MTB RifR strains found in clinical isolates. The most abundant amino acids substituted in place of these residues are as follows: 435 Val, 445 Tyr, and 450 Leu, respectively (*42, 49*). The three wild-type residues interact with the critical groups of rifampin via hydrogen bonds (Figure I-7): Asp435 and His445 H-bond with the hydroxyl at C21 and Ser450 H-bonds with the hydroxyl at C8. Mutations of these residues lead to the loss of important interactions; therefore, rifampin is unable to bind as tightly to the RifR RNAP, consistent with the results and conclusions of Feklistov *et al*. (*47*). These

resistant mutants are able to survive well with little decrease in fitness, most likely due to the distance between the rifamycin binding site and the RNAP active site (*52*).

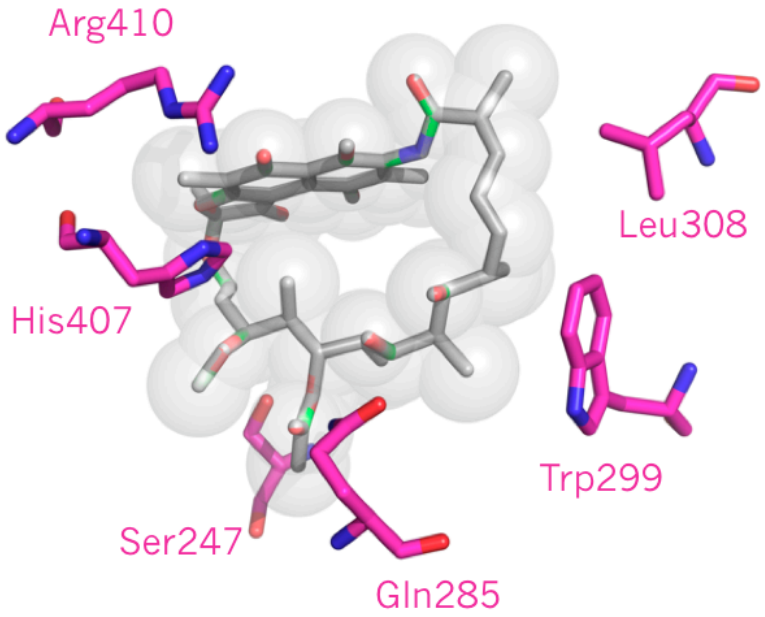

Figure I-8: The hPXR ligand-binding pocket with rifampin bound. The hPXR residues are shown in magenta. (Reproduced with permission from Chrencik 2005 (*53*))

One of the drawbacks of rifampin is that it is a potent agonist of the human pregnane X receptor (hPXR), which is responsible for transcriptional regulation of certain drug metabolizing enzymes and transporters (*54*). Most importantly, the activation of hPXR by rifampin leads to the up-regulation of expression of cytochrome P450 3A4 (CYP3A4), which results in metabolic clearance of drugs, failure of therapy, and reduced efficacy (*53, 54*). The relative potency of CYP3A4 induction is rifampin > rifapentine > rifabutin > rifalazil (a benzoxazinorifamycin derivative) where rifalazil does not induce the expression of CYP3A4 at ~10^5 x its IC_{50} for WT RNAP (*55*). Additionally, not all PXRs from different species are activated by rifampin (*e.g.,* mouse and rat PXRs). Recently, the x-ray crystal structures of activators bound to the ligand-binding domain of

hPXR have been determined including one with RMP bound (Figure I-8). From these structures, it was concluded that the hPXR ligand-binding pocket is large, flexible, and capable of adapting itself to bind a large variety of ligands (*53*). Also, rifampin is one of the largest hPXR activators and fills the binding pocket quite well, most likely the reason for its very potent activation of hPXR.

Due to the existence of resistant mutants and other unfavorable properties of rifampin (*i.e.,* heptatoxicity, flu-like syndrome, induction of cytochrome p450, and inhibition of hepatic transporters), a more effective rifamycin that will shorten treatment time, target resistant strains, be active against the latent form of TB, and eliminate drug-drug interactions is highly desirable (*10, 55*). In the past 40 – 50 years several rifamycin derivatives have been synthesized with the focus on C3 or C3/C4 modified rifamycin derivatives to produce a more effective antibiotic (*29*). However, there have been only three other rifamycins approved in the United States along with rifampin: rifapentine, rifabutin, and rifaximin (Figure I-9). While these rifamycins have improved antibacterial activity, they still exhibit cross-resistance with RifR mutants (*42, 55*). Recently, a new class of rifamycin derivatives, the benzoxazinorifamycins, have been shown to demonstrate more potent activity against mycobacteria and are effective against certain RifR strains, especially rifalazil (*56, 57*). But due to serious side effects during clinical trials, the development of rifalazil has been halted (*55*).

Although many rifamycin derivatives have been synthesized, it has been observed that the pharmacokinetic properties of rifamycins can be improved, the drug-drug interactions can be reduced/eliminated, levels of toxicities can be changed, and potency

against resistant strains can be improved. Most importantly the availability of the crystal structure allows for a structure-based approach to develop improved rifamycins (*55*).

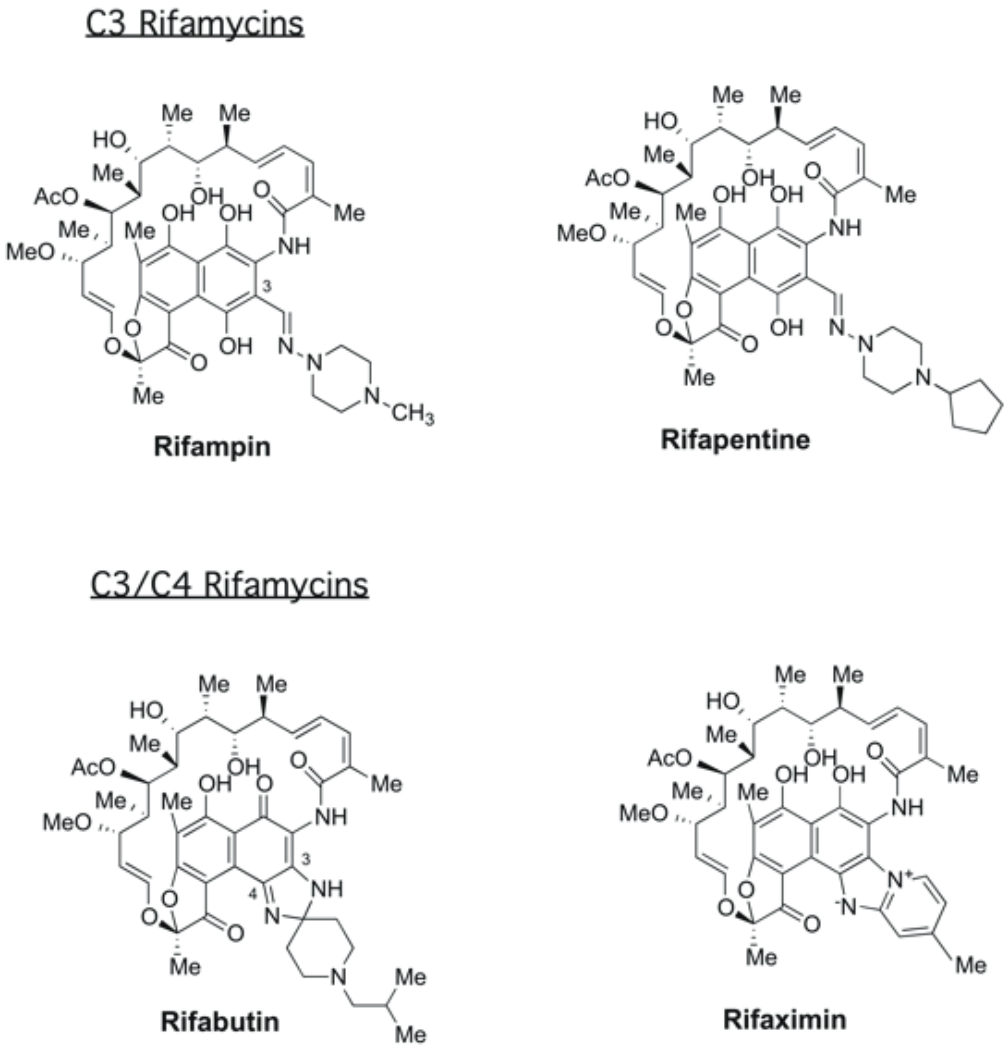

Figure I-9: Rifamycins approved in the United States. The C3 rifamycin derivatives are shown on top and the C3/C4 derivatives are on the bottom.

Research Objectives

There is an urgent need for anti-TB drugs that are effective against antibiotic resistant strains. The current treatment consists of anti-TB drugs that are 50 years old and that are ineffective against antibiotic resistant TB strains (MDR and XDR). Due to the difficulties of discovering new drugs against novel targets, in many cases focus has

returned to modifying existing antibiotics interacting with known, effective targets. In order to modify antibiotics to control the resistant strains, a better understanding of resistance needs to be achieved at the molecular level. The resistance mechanisms of known drugs (*i.e.,* rifampin and other rifamycins) need to be thoroughly understood, thus leading to improved drug design and better understanding of the RifR mutants to guide further research.

The overall focus of this dissertation is to understand the molecular interactions between rifampin and rifamycin analogues and the wild-type and RifR mutant MTB RNAPs. Although studies have been conducted previously using the *E. coli* RNAP, it is important to characterize the MTB RNAP with rifampin and other rifamycins. Even though there is a high level of conservation of the *rpoB* gene and the rifamycin binding site among prokaryotes, the sensitivity toward rifampin has been observed to be different for different bacterial strains (*41, 58*). Harshey *et al*. were able to purify MTB RNAP from MTB $H_{37}R_v$ strain and reported that MTB RNAP was 1000 times more sensitive to rifampin than *E. coli* RNAP (*58*). Furthermore, the three most prevalent RifR mutations (D435V, H445Y, and S450L) have been clinically isolated and studied in resistant MTB strains, but no *in vitro* studies of purified RifR MTB RNAPs with rifamycins have been reported.

This dissertation is focused on the detailed *in vitro* characterization of wild-type and RifR mutants of the MTB RNAP to elucidate the molecular interactions that are responsible for resistance. The ultimate goal is to provide information that can help drive the development of novel rifamycins that overcome the issue of resistance. The primary questions addressed in each chapter of this dissertation are listed below.

- Chapter II: How does the sensitivity of the MTB RNAPs (WT and selected RifR mutants) to rifamycins compare to that of *E. coli* RNAPs and how does this correlate with the differential sensitivities of MTB and *E. coli* to rifamycins?
- Chapter III: Do any of our novel C8 rifamcyin analogues (probing the interaction between S450 and the C8 OH) result in a more potent/effective rifamycin against the RifR MTB RNAP (S450L)?
- Chapter IV: Do any of our novel, structure-based designed benzoxazinorifamycin analogues result in a more potent/effective rifamycin against the wild-type and RifR MTB RNAPs?
- Chapter V: Can a dansyl-conjugated rifamycin be used as a fluorescent probe for a direct binding assay?
- Appendix: Can a MTB promoter based plasmid assay be developed for use in a high throughput screening assay to search for inhibitors representing novel chemotypes?

References

1. A. S. Fauci, Infectious diseases: Considerations for the 21st century. *Clinical Infectious Diseases* **32**, 675 (Mar, 2001).

2. M. L. Cohen, Changing patterns of infectious disease. *Nature* **406**, 762 (Aug, 2000).

3. H. Yoneyama, R. Katsumata, Antibiotic resistance in bacteria and its future for novel antibiotic development. *Bioscience Biotechnology and Biochemistry* **70**, 1060 (May, 2006).

4. World-Health-Organization, Antimicrobial resistance. http://www.who.int/mediacentre/factsheets/fs194/en/, (2012).

5. World-Health-Organization, "WHO Report 2010: Global Tuberculosis Control" *Report* (2010).

6. D. M. Morens, G. K. Folkers, A. S. Fauci, The challenge of emerging and re-emerging infectious diseases. *Nature* **430**, 242 (Jul, 2004).

7. WHO, Multidrug and Extensively Drug-Resistant TB (M/XDR-TB): 2010 Global Report on Surveillance and Response. http://whqlibdoc.who.int/publications/2010/9789241599191_eng.pdf, (2010).

8. J. M. Musser, Antimicrobial agent resistance in mycobacteria: molecular genetic insights. *Clin. Microbiol. Rev.* **8**, 496 (October 1, 1995, 1995).

9. G. Lamichhane, Novel targets in M. tuberculosis: search for new drugs. *Trends Mol. Med* **17**, 25 (Jan, 2011).

10. A. Koul, E. Arnoult, N. Lounis, J. Guillemont, K. Andries, The challenge of new drug discovery for tuberculosis. *Nature* **469**, 483 (Jan, 2011).

11. Y. L. Janin, Antituberculosis drugs: Ten years of research. *Bioorg. Med. Chem.* **15**, 2479 (Apr, 2007).

12. Y. Zhang, W. W. Yew, Mechanisms of drug resistance in Mycobacterium tuberculosis. *Int. J. Tuberc. Lung Dis.* **13**, 1320 (Nov, 2009).

13. P. E. A. Da Silva, J. C. Palomino, Molecular basis and mechanisms of drug resistance in Mycobacterium tuberculosis: classical and new drugs. *J. Antimicrob. Chemother.* **66**, 1417 (Jul, 2011).

14. Y. Zhang, K. Post-Martens, S. Denkin, New drug candidates and therapeutic targets for tuberculosis therapy. *Drug Discovery Today* **11**, 21 (Jan, 2006).

15. S. H. Gillespie, Tuberculosis: evolution in millennia and minutes. *BIOCHEMICAL SOCIETY TRANSACTIONS* **35**, 1317 (Nov, 2007).

16. H. G. Floss, T.-W. Yu, Rifamycin-mode of action, resistance, and biosynthesis. *Chem. Rev.* **105**, 621 (2005).

17. S. H. Gillespie, Evolution of drug resistance in Mycobacterium tuberculosis: Clinical and molecular perspective. *Antimicrob. Agents Chemother.* **46**, 267 (Feb, 2002).

18. American Thoracic Society/Centers for Disease Control and Prevention/Infectious Diseases Society of America: Treatment of tuberculosis. *American Journal of Respiratory and Critical Care Medicine* **167**, 603 (Feb, 2003).

19. N. R. Gandhi *et al.*, Multidrug-resistant and extensively drug-resistant tuberculosis: a threat to global control of tuberculosis. *Lancet* **375**, 1830 (May, 2010).

20. Z. K. Ma, C. Lienhardt, H. McIlleron, A. J. Nunn, X. X. Wang, Global tuberculosis drug development pipeline: the need and the reality. *Lancet* **375**, 2100 (Jun, 2010).

21. C. E. Barry, J. S. Blanchard, The chemical biology of new drugs in the development for tuberculosis. *Current Opinion in Chemical Biology* **14**, 456 (Aug, 2010).

22. S. A. Darst, Bacterial RNA polymerase. *Current Opinion In Structural Biology* **11**, 155 (Apr, 2001).

23. S. D. Zorov, J. V. Yuzenkova, K. V. Severinov, Low-molecular-weight inhibitors of bacterial DNA-dependent RNA polymerase. *Molecular Biology* **40**, 875 (Nov-Dec, 2006).

24. I. Chopra, Bacterial RNA polymerase: a promising target for the discovery of new antimicrobial agents. *Curr. Opin. Invest. Drugs* **8**, 600 (2007).

25. R. Mariani, S. I. Maffoli, Bacterial RNA polymerase inhibitors: an organized overview of their structure, derivatives, biological activity and current clinical development. *Current Med. Chem*. **16**, 430 (2009).

26. P. Villain-Guillot, M. Gualtieri, L. Bastide, J.-P. Leonetti, In vitro activities of different inhibitors of bacterial transcription against Staphylococcus epidermidis biofilm. *Antimicrob Agents Chemother* **51**, 3117 (Sep, 2007).

27. M. Ho, B. Hudson, K. Das, E. Arnold, R. Ebright, Structures of RNA polymerase–antibiotic complexes. *Current Opinion in Structural Biology* **19**, 715 (2009).

28. P. Sensi, History of the development of rifampin. *Rev. Infectious Dis.* **5**, S402 (1983).

29. W. Wehrli, Ansamycin –chemistry, biosynthesis and biological activity. *Topics in Current Chemistry* **72**, 21 (1977).

30. S. Riva, Silvestr.Lg, RIFAMYCINS - GENERAL VIEW. *Annu. Rev. Microbiol.* **26**, 199 (1972).

31. W. Wehrli, M. Staehelin, Actions of the rifamycins. *Bacteriological Reviews* **35**, 290 (1971).

32. W. Wehrli, M. Staehelin, The rifamycins-relation of chemical structure and action on RNA polymerase. *Biochim. Biophys. Acta* **182**, 24 (1969).

33. D. A. Mitchison, The search for new sterilizing anti-tuberculosis drugs. *Frontiers in Bioscience* **9**, 1059 (2004).

34. G. Hartmann, K. O. Honikel, F. Knusel, J. Nuesch, The specific inhibition of the DNA-directed RNA synthesis by rifamycin. *Biochim. Biophys. Acta* **145**, 843 (1967).

35. A. Sippel, G. Hartmann, MODE OF ACTION OF RIFAMYCIN ON RNA POLYMERASE REACTION. *Biochimica Et Biophysica Acta* **157**, 218 (1968).

36. W. Wehrli, F. Knusel, K. Schmid, M. Staehelin, Interaction of rifamycin with bacterial RNA polymerase. *Proc. Nat. Acad. Sci. USA* **61**, 667 (1968).

37. W. R. McClure, C. L. Cech, On the mechanism of rifampicin inhibition of RNA synthesis. *J. Biol. Chem.* **253**, 8949 (1978).

38. D. C. Hinkle, Chamberl.Mj, W. F. Mangel, STUDIES OF BINDING OF ESCHERICHIA-COLI RNA-POLYMERASE TO DNA .4. EFFECT OF RIFAMPICIN ON BINDING AND ON RNA CHAIN INITIATION. *JOURNAL OF MOLECULAR BIOLOGY* **70**, 209 (1972).

39. W. Bahr, W. Stender, K. Scheit, T. Jovin, in *RNA Polymerase,* R. Losick, M. Chamberlin, Eds. (Cold Spring Harbor Laboratory Press, Cold Spring Harbor, 1976), pp. 369-396.

40. G. Hartmann, W. Behr, K.-A. Beissner, K. Honikel, A. Sippel, Antibiotics as inhibitors of nucleic acid and protein synthesis. *Angew. Chem. internat. Edit.* **7**, 693 (1968).

41. E. A. Campbell *et al.*, Structural mechanism for rifampicin inhibition of bacterial RNA polymerase. *Cell* **104**, 901 (2001).

42. D. L. Williams *et al.*, Contribution of rpoB mutations to development of rifamycin cross-resistance in Mycobacterium tuberculosis. *Antimicrob. Agents Chemother.* **42**, 1853 (1998).

43. D. J. J. a. C. A. Gross, Mapping and Sequencing of Mutations in the *Escherichia coli rpoB* Gene that Lead to Rifampicin Resistance. *Journal of Molecular Biology* **202**, 45 (1988).

44. I. Artsimovitch *et al.*, Allosteric modulation of the RNA polymerase catalytic reaction is an essential component of transcription control by rifamycins. *Cell* **122**, 351 (Aug 12, 2005).

45. W. Schulz, W. Zillig, RIFAMPICIN INHIBITION OF RNA-SYNTHESIS BY DESTABILIZATION OF DNA-RNA POLYMERASE-OLIGONUCLEOTIDE-COMPLEXES. *Nucleic Acids Res.* **9**, 6889 (1981).

46. I. Artsimovitch, D. G. Vassylyev, Is it easy to stop RNA polymerase? *Cell Cycle* **5**, 399 (Feb, 2006).

47. A. Feklistov *et al.*, Rifamycins do not function by allosteric modulation of binding of Mg2+ to the RNA polymerase active center. *Proceedings of the National Academy of Sciences of the United States of America* **105**, 14820 (Sep 30, 2008).

48. S. T. Cole, A. Telenti, DRUG-RESISTANCE IN MYCOBACTERIUM-TUBERCULOSIS. *Eur. Resp. J.* **8**, S701 (Sep, 1995).

49. P. I. A. Telenti, F. Marchesi, D. Lowrie, S.T. Cole, J. Colston, L. Matter, K. Schopfer, and T. Bodmer., Detection of rifampicin-resistance mutation in *Mycobacterium tuberculosis*. *Lancet* **341**, 647 (1993).

50. W. Wehrli, Rifampin: mechanisms of action and resistance. *Reviews of Infectious Diseases* **5**, S407 (1983).

51. E. Wyss, W. Wehrli, USE OF DEXTRAN-COATED CHARCOAL FOR KINETIC MEASUREMENTS - INTERACTION BETWEEN RIFAMPICIN AND DNA-DEPENDENT RNA-POLYMERASE OF ESCHERICHIA-COLI. *Analytical Biochemistry* **70**, 547 (1976).

52. O. J. Billington, T. D. McHugh, S. H. Gillespie, Physiological cost of rifampin resistance induced in vitro in Mycobacterium tuberculosis. *Antimicrobial Agents and Chemotherapy* **43**, 1866 (Aug, 1999).

53. J. E. Chrencik *et al.*, Structural disorder in the complex of human pregnane X receptor and the macrolide antibiotic rifampicin. *Molecular Endocrinology* **19**, 1125 (May, 2005).

54. M. W. Sinz, Pregnane X receptor: prediction and attenuation of human CYP3A4 enzyme induction and drug-drug interactions. *In Annual Reports in Medicinal Chemistry* **43**, 405 (2008).

55. P. A. Aristoff, G. A. Garcia, P. D. Kirchhoff, H. D. H. Showalter, Rifamycins - Obstacles and opportunities. *Tuberculosis* **90**, 94 (Mar, 2010).

56. H. Saito *et al.*, In vitro antimycobacterial activities of newly synthesized benzoxazinorifamycins. *Antimicrob. Agents Chemother.* **35**, 542 (1991).

57. A. M. Dhople, A. A. Dhople, M. A. Ibanez, Comparative in vitro activities of rifamycin analogues against rifampin-sensitive and rifampin-resistant Mycobacterium tuberculosis. *Internat. J. Antimicrob. Agents* **8**, 209 (1997).

58. R. M. Harshey, T. Ramakrishnan, Purification and properties of DNA-dependent RNA polymerase from Mycobacterium tuberculosis H37Rv. *Biochimica et Biophysica Acta (BBA) - Nucleic Acids and Protein Synthesis* **432**, 49 (1976).

CHAPTER II

In vitro Investigation of Wild-type and Rifamycin-resistant Mutants of the *Mycobacterium tuberculosis* RNA polymerase

Rifampin (RMP) is a first line anti-tuberculosis drug that inhibits the prokaryotic RNA polymerase (RNAP) by binding to the β subunit. Previously, the interaction of RMP with various prokaryotic RNAPs has been investigated but *in vitro* data for wild-type (WT) and rifamycin-resistant (RifR) MTB RNAPs is lacking *(1-6).* The various bacterial RNAPs have been reported to possess different levels of sensitivity towards RMP (*1, 3, 4, 7*). Even though the rifamycin-binding site is conserved among prokaryotes, differences in key residues that directly interact with RMP lead to differential inhibition (*1*). RMP is a broad spectrum antibiotic with more potent activity against Gram-positive bacteria (particularly mycobacteria) than Gram-negative bacteria (*6, 8*). Additional factors include permeability issues where the reduced penetration of RMP through the outer membrane of Gram-negative bacteria has been invoked to explain the lower sensitivity to RMP (*6*).

Even though the RifR mutations in MTB have been clinically isolated and studied in RifR MTB strains, no *in vitro* studies of purified RifR MTB RNAPs with rifamycins have been reported (*9, 10*). Previously, Harshey and colleagues have isolated WT MTB RNAP ($\alpha\beta\beta'\sigma$) from MTB $H_{37}R_V$ cells and reported that RMP is a thousand-fold more potent against MTB RNAP than *E. coli* RNAP and the difference in sensitivity to

RMP could be due to the differences in the beta subunits (*7*). Recently, the MTB RNAP ($\alpha\beta\beta'\sigma$) has been reconstituted as recombinant proteins expressed in *E. coli,* but the activity of the MTB RNAP in the presence of rifamycins was not assessed (*11*). In order to understand rifamycin resistance further, it is important to obtain *in vitro* data for WT and the three most prevalent RifR MTB RNAPs. The individual substitutions of three residues (Asp435, His445, and Ser450; MTB numbering) together account for more than 84% of MTB RifR strains found in clinical isolates. The most abundant amino acids substituted in place of these residues are as follows: 435 Val, 445 Tyr, and 450 Leu, respectively (*9, 10*).

Due to the increase of RifR strains, the focus has been on synthesizing improved rifamycins that are active against RifR mutations. Many of the modifications on rifamycin resulted in decrease or loss of activity, but alterations at C3 and C3/C4 positions of the aromatic ring are well tolerated (*6*). Therefore, the focus over the past 40 or so years has been to synthesize C3 or C3/C4 modified rifamycin derivatives to produce a more effective antibiotic. However, there have only been three other rifamycins approved in the United States along with RMP: rifapentine (RPN), rifabutin (RBN), and rifaximin (RFX), where these rifamycins have improved antibacterial activity but still exhibit cross-resistance with RifR mutants (Figure II-1) (*12-18*).

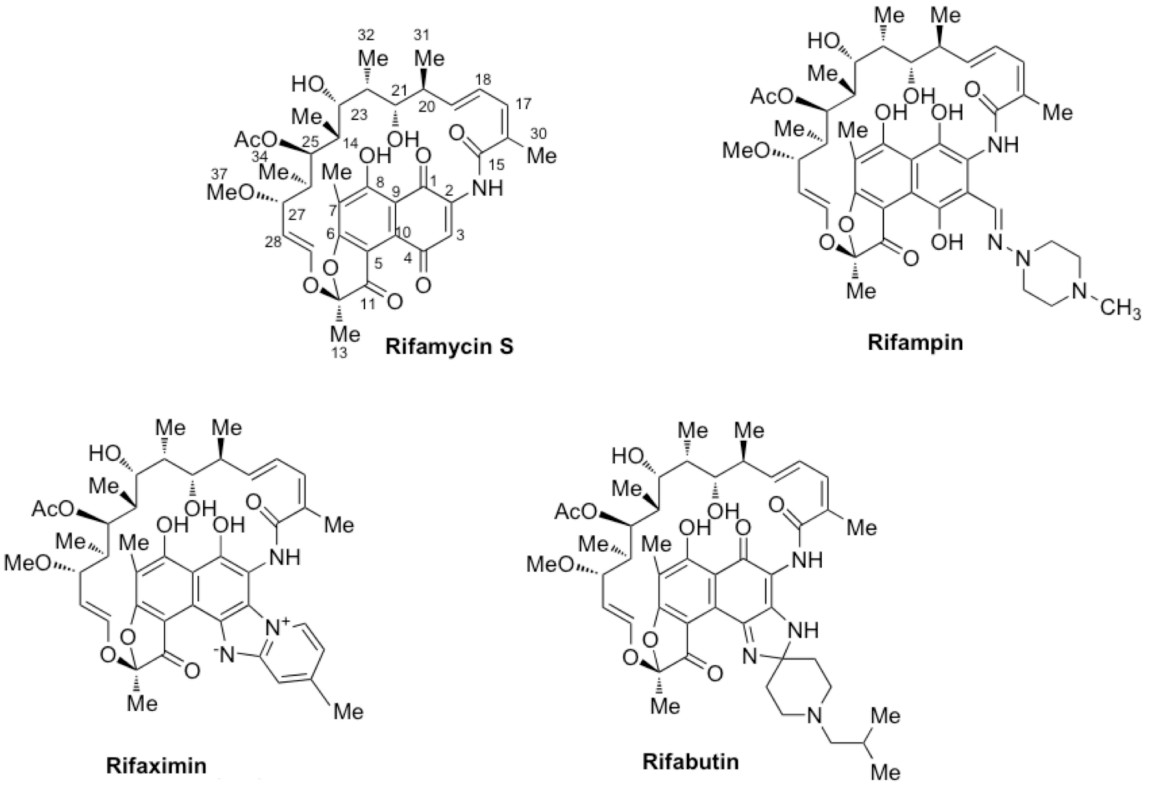

Figure II-1: Structures of Key Rifamycins (typical rifamycin numbering system is shown with Rifamycin S).

To better understand the interaction between the rifamycins and wild-type/RifR mutant MTB RNAPs, we report here the cloning and expression and *in vitro* activity of MTB RNAP. The three most prevalent RifR mutations (Asp435Val, His445Tyr, Ser450Leu) found in the MTB clinical isolates were generated to express the mutant β subunit of the RNAP in the *rpoB* gene via site directed mutagenesis. We also report the results of the *in vitro* screen of three key rifamycins (RMP, RBN, and RFX) along with the MICs of these rifamycins in MTB and *E. coli*. These results will help to inform the development of novel rifamycins with enhanced activity against RNAPs containing single amino acid substitutions.

Materials and Methods

Reagents

Unless otherwise specified, all reagents were purchased from Sigma-Aldrich (St. Louis, MO). Gelase™ Agarose-Gel Digesting Preparation and Kool™ NC-45™ Universal RNA Polymerase template were from Epicentre (Madison, WI). The QIAprep Spin Miniprep and Maxiprep Kit were from Qiagen (Valencia, CA). Carbenicillin (disodium salt), Corning microplates, bactotryptone, and yeast extract were from Fisher Scientific (Hampton, NH). The *E. coli* BL21 (DE3) CodonPlus-RIPL and *Epicurian coli* XL2-Blue Ultracompetent cells were from Agilent Technologies (Santa Clara, CA). All restriction enzymes and Vent® DNA polymerase were from New England Biolabs (Ipswich, MA). SeaPlaque® Agarose was from Lonza (Rockland, ME). T4 DNA Ligase, Quanti-iT™ RiboGreen RNA Reagent, RNaseOUT™ Recombinant Ribonuclease Inhibitor, pEXP-5-NT/TOPO® TA Expression Kit, and all synthetic oligonucleotides were from Invitrogen (Carlsbad, CA). Lysonase™ Bioprocessing Reagent and Ni-NTA His•Bind® resin were from Novagen (San Diego, CA). The nucleotide triphosphates (NTPs) were from Roche Applied Science (Indianapolis, IN). PhastGel Precast Gels and SDS Buffer Strips were from VWR (Arlington Heights, IL). The Bio-Rad Protein Assay kit was from Bio-Rad (Hercules, CA). The avirulent *Mycobacterium tuberculosis* strain ($H_{37}R_a$) was a generous gift from the TB center of Colorado State University. The pVS10 vector, containing the *E. coli rpo* genes encoding the RNAP subunits, was a generous gift from Professor Irina Artsimovitch (Ohio State University). The plasmids containing the individual MTB *rpo* genes (pSR52 (*rpoA*), pJF09 (*rpoB*), pJF10 (*rpoC*)) were a generous gift from Dr. Sébastien Rodrique (MIT). The EC2880 strain (permeable

strain with *tolC*$^-$ and *imp*$^-$ mutations) was a generous gift from Dr. Michael Hubband (Pfizer Scientific).

Cloning MTB rpo Genes into an E. coli Co-overexpression Plasmid

For *in vitro* studies, the wild-type MTB core RNAP was obtained from the co-overexpression plasmid pMTBRP-5 (Figure II-4). The MTB core RNAP subunit encoding genes (*rpoA* (α), *rpoB* (β), *rpoC* (β'), and *rpoZ* (ω)) were amplified from pSR52, pJF09, pJF10, and genomic MTB $H_{37}R_a$ DNA, respectively (Figure II-2).

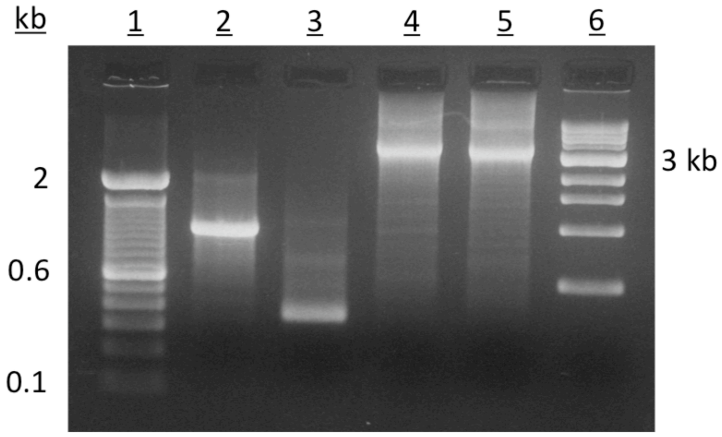

Figure II-2: PCR amplified MTB genes on 1% agarose gel: lane 1, 100 bp DNA ladder; lane 2, MTB *rpoA* (1044 bp); lane 3, MTB *rpoZ* (333 bp); lane 4, MTB *rpoB* (3519 bp); lane 5, MTB *rpoC* (3951 bp); lane 6, 1 kb DNA ladder

The individual genes were then cloned into pEXP5-NT/TOPO vector to generate pEXP5-NT/TOPO(*rpoA*), pEXP5-NT/TOPO(*rpoB*), pEXP5-NT/TOPO(*rpoC*), pEXP5-NT/TOPO(*rpoZ*). Reactions were performed according to the manufacturer's instructions and then chemical transformation of the resulting plasmids into host cells was carried out. Each one of the MTB RNAP genes was PCR amplified with Vent® DNA polymerase using specific primers introducing unique restriction enzyme sites to assist in gene cloning. The oligonucleotides used for PCR amplification are listed in

Table II-A2 in Appendix II-1. The pVS10 plasmid encodes the *E. coli rpoA*-*rpoB*-*rpoC*[His_6]-*rpoZ* ORFs under the control of a single T7 promoter and terminator sequence and was used as the template where the *E. coli rpo* genes were replaced with MTB *rpo* genes following the scheme presented in Figure II-3. The PCR product of the 1.0 kb MTB *rpoA* was digested with *NcoI* and *NdeI* and cloned into pVS10 treated with *NcoI* and *NdeI* replace of *E. coli rpoA*. The *E. coli rpoB* and *rpoC* genes were replaced with a 165 bp linker in order to facilitate the incorporation of the smaller MTB *rpoZ* gene. The resultant plasmid, pMTBRP-1 and the 0.3 kb *rpoZ* gene were treated with *AflII* and *NotI*. The ribosome-binding site (RBS) was introduced to the beginning of the *rpoZ* ORF producing pMTBRP-3. Additional alterations had to be made to the ORFs of *rpoC* and *rpoB* to eliminate internal restriction sites and/or to correct PCR induced mutations by site directed mutagenesis before being amplified with PCR primers. The amplification of *rpoB* gene was divided into two parts where a hexahistidine tag was introduced first and then the unique restriction site to the 3' end of the *rpoB* ORF. After these changes the plasmid containing the 4.0 kb *rpoC* gene and pMTBRP-3 were treated with *AvrII* and *AscI*. The *rpoC* cassette was subcloned into the treated plasmid to form pMTBRP-4. The plasmid containing the 3.5 kb *rpoB* gene and pMTBRP-4 were digested with *AvrII* and *BmtI*. Sequences confirmed that the resultant plasmid, pMTBRP-5, contained the four MTB *rpo* genes in the following order: *rpoA*-*rpoB*[His_6]-*rpoC*-*rpoZ* (Figure II-4).

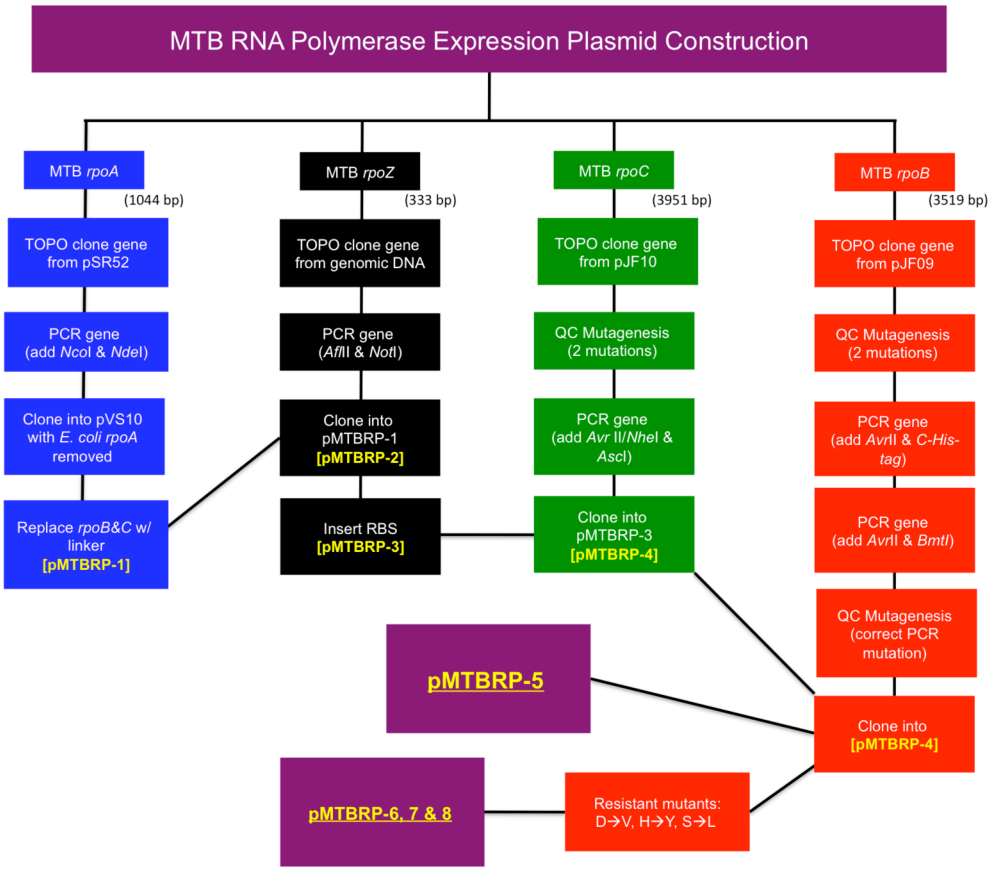

Figure II-3: Construction Scheme for expression vectors for wild-type MTB RNAP (pMTBRP-5) and rifamycin-resistant mutants (pMTBRP-6, 7, 8).

Construction and Preparation of MTB RNAP Mutant Plasmids

The single nucleotide mutations (D435V (GAC-GTC), H445Y (CAC-TAC), and S450L (TCG-TTG)) were independently incorporated into pEXP-5/TOPO (*rpoB*) by PCR site-directed mutagenesis using the primers listed in Table II-A2 in Appendix II-1. The resultant plasmids were transformed into *Epicurian coli* XL2-Blue ultracompetent cells. After verification of mutant *rpoB* by DNA sequencing, the plasmids containing the mutant *rpoB* genes and the wild-type pMTBRP-5 were digested with *AvrII* and *SbfI* and ligated to create the MTB mutant RNAP vectors: pMTBRP-6(D435V), -7(H445Y), and -8(S450L) (Figure II-3 and II-4).

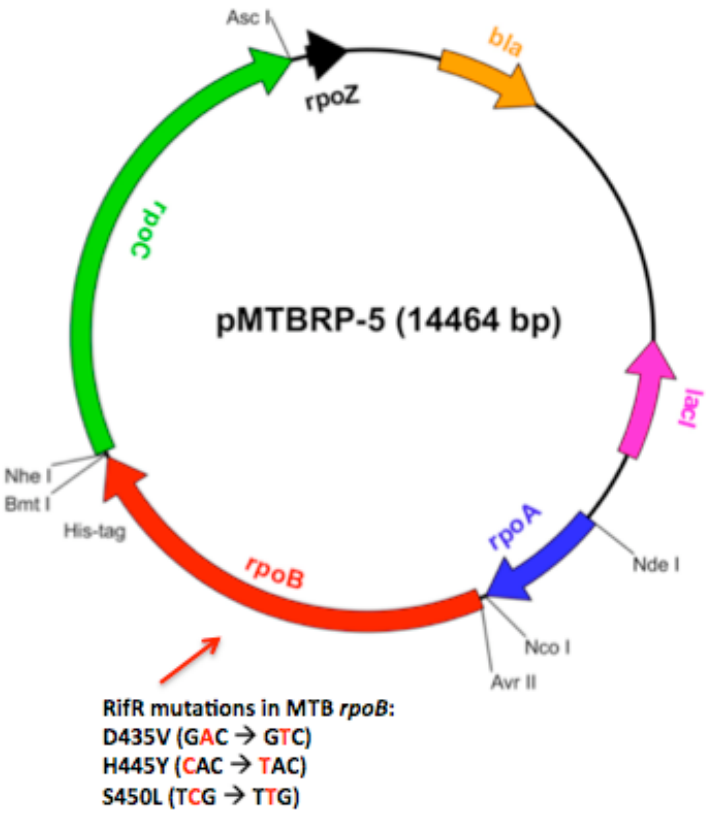

Figure II-4: Co-overexpression Vector pMTBRP-5 Containing the MTB *rpoA*(α)-*rpoB*(β)-*rpoC*(β')-*rpoZ*(ω) Genes Encoding the 4 Subunits of the Wild-type MTB Core RNAP. The hexahistidine tag is fused to the C-terminus of *rpoB* gene for purification. Artsimovitch and colleagues' co-overexpression plasmid, pVS10 (expressing the *E. coli* core RNAP), was used as a template for the construction of pMTBRP-5.

Expression and Purification of MTB Core RNAPs

The co-expression vectors (pMTBRP-5, 6, 7, 8) were transformed into *E. coli* BL21(DE3) CodonPlus-RIPL cells. The cells were grown in 500 mL of 2xTY liquid cultures containing 100 µg/mL carbenicillin and 30 µg/mL chloramphenicol at 37°C with vigorous shaking until cell density reached OD_{600nm}=0.5-0.6. The protein was induced by the addition of isopropyl β-D-thiogalactoside (IPTG) to a final concentration of 1 mM. The cultures were allowed to incubate for an additional 20-24 hours at 19°C. The cells were harvested by centrifugation (6000x*g*, 15 min, 4°C). The cell pellet of each 500 mL

culture was re-suspended in 10 mL of Ni^{2+}-NTA bind buffer (300 mM NaCl, 50 mM NaH_2PO_4, 10 mM imidazole, pH 8.0). The freeze/thaw method was followed to lyse the cells, and it was repeated a total of three times. The sample was supplemented with 10 µL of Lysonase™ Bioprocessing Reagent and 100 µM of phenylmethylsulfonyl fluoride (PMSF), and then the resulting lysate was cleared by centrifugation (21,000x*g*, 30 min, 4°C). All further purification steps were performed at 4°C. The lysate was incubated with 2 mL Ni^{2+}-NTA His•Bind Resin overnight with gentle shaking. Each supernatant-resin mixture was applied to individual columns. The columns were washed twice with 4 mL of Ni^{2+}-NTA wash buffer (300 mM NaCl, 50 mM NaH_2PO_4, 20 mM imidazole, pH 8.0), and the protein was then eluted in 6 mL of Ni^{2+}-NTA elute buffer (300 mM NaCl, 50 mM NaH_2PO_4, 250 mM imidazole, pH 8.0). The MTB RNAPs were concentrated to a final volume of ~500 µL and then sterile-filtered with 0.22-µm syringe before being applied to a HiPrep 16/60 Sephacryl S-200 HR (GE Healthcare) column and the running buffer was RNAP storage buffer (10 mM Tris-HCl (pH 7.9), 0.1 mM EDTA, 0.1 mM DTT, 0.1 M NaCl). The fractions containing the MTB RNAP were pooled together and concentrated to a final volume of ~100-200 µL using Amicon Centrifugal Filter Units (MWCO=100 kDa). The enzyme was mixed with one volume of 100% glycerol and stored in liquid nitrogen. The final concentration of the enzymes was determined via Bradford assay using the Bio-Rad Protein Assay Kit.

Construction, Expression and Purification of Wild-type and Mutant E. coli RNAPs

The corresponding RifR mutations (D516V (GAC-GTC), H526Y (CAC-TAC), and S531L (TCG-TTG); *E. coli* numbering) were introduced to the wild-type *E. coli* *rpoB* gene of pVS10 via site-directed mutagenesis. For the construction of the *E. coli*

mutant RNAP expression vectors, the plasmids containing the mutant *rpoB* genes and the wild-type pVS10 were digested with *XbaI* and *SbfI* and ligated to create pVS10 (D516V), pVS10 (H526Y), and pVS10 (S531L) following the general laboratory protocol. These plasmids were then confirmed by DNA sequencing. The *E. coli* RNAPs were purified in the same fashion as the MTB RNAPs with a few modifications. The *E. coli* expression vectors were transformed into *E. coli* BL21 (DE3) strain. The cells were grown in 500 mL of 2xTY liquid culture containing 100 µg/mL carbenicillin at 37°C until OD_{600nm} reached ~0.6, at which point the protein production was induced with 1 mM IPTG. The cells were grown for an additional 4 hours at 37°C and harvested by centrifugation (6000x*g*, 15 min, 4°C). The cell pellets were resuspended in 10 mL of bind buffer and supplemented with 10 µL Lysonase™ Bioprocessing Reagent and 100 µM PMSF. The cell suspension was incubated at room temperature for 20 min before the cells were disrupted by sonication (seven 13-sec pulses) on ice. The resulting lysate was cleared as described above. The lysate was incubated with 2 mL Ni^{2+}-NTA His•Bind Resin with gentle shaking for 1 h. The mixture was then applied to the column. The protein was purified from the column as described above and then concentrated before being applied to a size exclusion column. The fractions containing the *E. coli* RNAP were pooled together and concentrated to a final volume of ~300-500 µL using Amicon Centrifugal Filter Unit (MWCO=100 kDa). The enzyme was mixed with one volume of 100% glycerol and stored in liquid nitrogen. The concentration of the enzymes was determined as stated before for MTB RNAPs.

Determination of the in vitro Transcriptional Activity of MTB RNAPs

The activity of the WT and RifR mutant MTB and *E. coli* RNAPs was measured via rolling circle transcription assay using the Kool^{TM} NC-45^{TM} Universal RNA Polymerase template in the absence and presence of rifamycins (Figure II-5). The supplier's protocol for end-point detection using RiboGreen (a fluorescent nucleic acid dye) was followed. The assays were performed on a SpectraMax M5 (Molecular Devices) microplate reader using 96-well half-area black plates. The *in vitro* transcription conditions were as follows for a 25 µL reaction: RNAP (10 nM), *E. coli* RNAP 5X reaction buffer (200 mM Tris-HCl (pH 8.0), 250 mM KCl, 50 mM $MgCl_2$, 0.05% Triton X-100), DTT (8 mM), RNase inhibitor (1.12 U/µL), Kool NC-45 template (80 nM), and NTP solution (500 µM of each NTP). The reaction was initially incubated at 37^{o}C for 10 min in the absence of Kool NC-45 template and NTP solution to ensure the binding of RNAP and rifamycin. Then the template was added and the reaction was initiated upon the addition of the NTPs. Aliquots were taken every 30 min for 2 h from each reaction and quenched in TE buffer (10 mM Tris-HCl (pH 7.5), 1 mM EDTA). The amount of RNA synthesized was measured by the addition of 1:200 diluted RiboGreen (an ultrasensitive fluorescent nucleic acid stain). The excitation and emission wavelengths for RiboGreen were 480 nm and 520 nm, respectively.

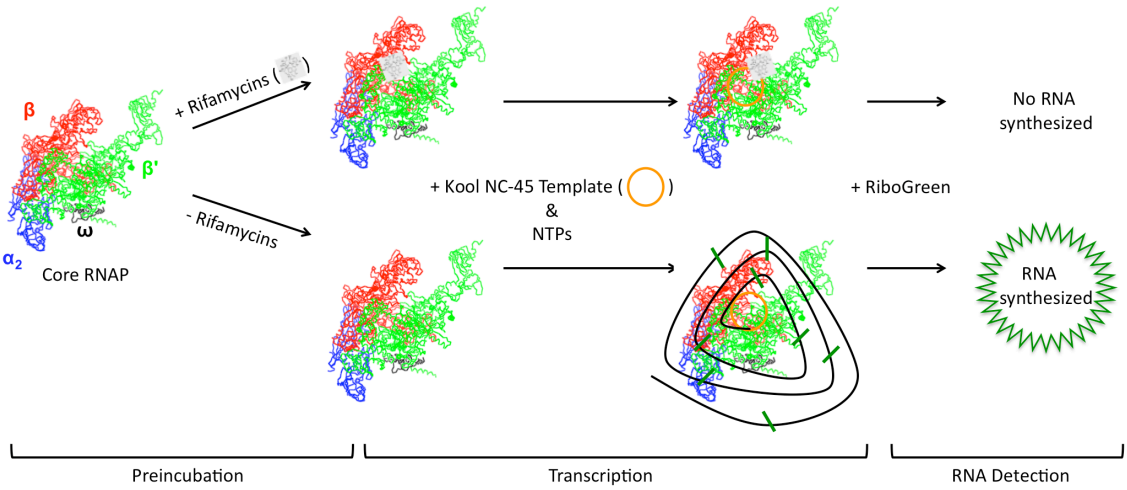

Figure II-5: RNAP Rolling Circle Transcription Assay. RNAP is pre-incubated with varying concentrations of rifamycins. The 45mer DNA nanocircle, Kool NC-45 Template, binds to the free bacterial RNAP. In the absence of rifamycins, the RNAP is able to transcribe multiple copies of the 45 base template (indicated by the green ticks on the growing RNA strand). The concentration of RNA is detected using a fluorescent dye, RiboGreen and an RNA concentration standard curve as described in Materials and Methods.

Inhibitory Effect of Rifamycins on MTB and E. coli RNAPs

Dose response studies with different rifamycins were performed on WT and RifR RNAPs after it had been confirmed that the enzymes were active. Each of the rifamycins (RMP, RBN, RFX-Figure II-1) was tested in duplicate where the concentration ranges were as follows for the different enzymes: for wild-type MTB RNAP (1.56-100 nM rifamycins); for wild-type *E. coli* RNAP (3.12-200 nM rifamycins); for MTB RNAP (D435V) (78-5000 µM RMP and 39-5000 µM RBN/RFX), for MTB RNAP (H445Y) (19.5-2500 µM RMP and 78-5000 µM RBN/RFX), for MTB RNAP (S450L) (19.5-2500 µM RMP and 4-2500 µM RBN/RFX), for *E. coli* RNAP (D516V and S531L) (78-10000 µM RMP, 4-2500 µM RBN, and 39-5000 µM RFX), for *E. coli* RNAP (H526Y) (78-20000 µM RMP and 39-10000 µM RBN/RFX).

An RNA standard curve was made using varying concentrations of tRNA, and the curve was used to convert the fluorescence values to the amount of RNA synthesized. The replicate data points were averaged and both the original data points and the average values were plotted as function of log concentration versus percent activity. The average values were then fit by non-linear regression to a modified four parameter logistic equation (below) as described (http://www.curvefit.com/introduction89.htm) using Kaleidagraph (Synergy Software, Essex, VT):

$$y = M3 + [(100 - M3)/(1 + 10^{[(M0-M1)*M2]})],$$

where M3 is the lower limit of the assay, and 100 is the upper limit of the assay, M0 is the log of the rifamycin concentration, M1 is the log of the IC_{50}, and M2 is the Hill slope. The data were normalized such that the upper limit of the raw data (manually set to either the no inhibitor value or to the average of the first two-three data points) was 100% activity. M1, M2 and M3 were fit by the regression. The logIC_{50}s and their standard errors (of the fit) are reported in Table II-A4 in Appendix II-1.

Determination of Minimal Inhibitory Concentration (MIC) of Rifamycins Against MTB and E. coli Strains

The MIC values of RMP for *Mycobacterium tuberculosis* ($H_{37}R_v$) were determined by Dr. Scott Franzblau (Institute for Tuberculosis Research, University of Illinois, Chicago) using two different assays (Table II-2). The Microplate Alamar Blue Assay (MABA) was conducted as described earlier (*19*). The second assay was Low Oxygen-Recovery Assay (LORA) where MTB was adapted to low oxygen conditions and kept under an anaerobic environment for 10 days to resemble the conditions for the

latent form of MTB (*20*). The RMP concentration ranged from 0.04-4.9 μM for MABA and 0.15-19 μM for LORA.

The MIC of each rifamycins was also determined for *E. coli* by the microdilution method described previously (*21*). In brief, the wild-type *E. coli* strains (DH5α and TG2) and mutant *E. coli* strain (EC2880) were grown on LB plates. A colony was grown in 2xTY media at 37°C for 3-4 h until the culture reached the McFarland 0.5 standard (OD_{625nm} 0.08-0.13) corresponding to approximately 1 x 10^8 cfu/mL. The susceptibilities of these strains to rifamycins (Rifamycin SV, RMP, RBN, RFX) were determined by adding 50 μL aliquots of culture to 50 μL serial two-fold dilutions of rifamycins. Concentrations of the rifamycins were 0.049-100 μM for DH5α and TG2 strains and 0.006-12.5 μM for EC2880 strain. Rifamycins were initially dissolved in DMSO and the two-fold dilutions were made in 2xTY media. Drug-free controls consisted of 50 μL culture and 2xTY media; whereas, the positive control consisted of 50 μL culture and 20 μg/mL carbenicillin. The assays were performed on a SpectraMax M5 (Molecular Devices) microplate reader using sterile 96-well polystyrene plates. The plates were covered and incubated at 37°C for 20 hours. OD_{600nm} absorbance was measured on the SpectraMax M5 microplate reader. MIC_{90} values were defined as the concentration of rifamycin that results in 90% inhibition of growth.

Results

Construction of pMTBRP-5, 6, 7, and 8 vectors

To investigate the activity and inhibition of MTB RNAP, we have constructed a co-overexpression vector to express the MTB RNAP, pMTBRP-5 (Figure II-4). To allow for simple expression, assembly, and purification of MTB RNAP, the co-overexpression

vector pVS10 (expressing the *E. coli* RNAP) was used as the template. The MTB *rpo* genes (encoding the MTB RNAP subunits) were initially modified to introduce unique restriction sites to the ends of each *rpo* gene open reading frame (ORF) and then subcloned into pVS10, replacing the *E. coli rpo* genes. To facilitate cloning further, additional modifications were made to the *rpoB* and *rpoC* ORFs to introduce silent mutations to eliminate internal restriction sites and/or to correct PCR induced mutations (see Materials and Methods). A hexahistidine tag was introduced to the 3' end of the *rpoB* ORF, which allowed for the purification of the assembled MTB RNAP from other proteins. The resultant pMTBRP-5 vector contained a single T7 RNAP promoter before the *rpoA* ORF and a T7 terminator following the *rpoZ* ORF where each *rpo* gene was preceded by a ribosome-binding site. To assess the affect of the three most prevalent amino acid substitutions found in clinical isolates (D435V, H445Y, S450L), point mutations were introduced to the MTB *rpoB* gene. The altered genes were subcloned individually, replacing the wild-type MTB *rpoB* gene in the pMTBRP-5, resulting in the following mutant vectors: pMTBRP-6 (D435V), pMTBRP-7 (H445Y), and pMTBRP-8 (S450L).

Expression of MTB RNAPs

Initially when the pMTBRP-5 plasmid was transformed into an expression cell line only a single distinct band was observed corresponding to the MTB α subunit with a molecular weight of approximately 38 kDa (Figure II-6). (The identity of MTB α subunit was confirmed by Michigan Proteome Consortium via mass spectrometry, Table II-A3 in Appendix II-1.) Along with testing different expression cell lines (BL21(DE3), HMS174(DE3), and JM109(DE3)), the temperature and IPTG concentration was also

varied, but the MTB α subunit was the only over-expressed subunit observed. Since the wild-type and RifR MTB RNAPs are heterologous proteins, the plasmids were then expressed in *E. coli* BL21 (DE3) CodonPlus-RIPL strains. During the expression trials, the lower temperature induction (19^{o}C) was found to be optimal for greater protein expression levels.

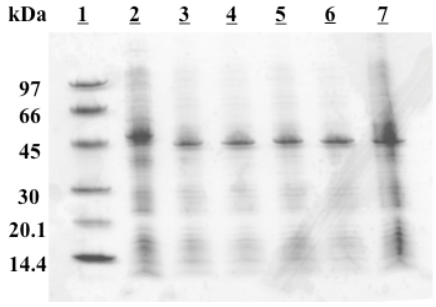

Figure II-6: SDS-PAGE of pMTBRP-5 expressed in HMS174(DE3) cells at 25^{o}C. Lane 1, LMW; lane 2, uninduced sample; lane 3, 0.5 mM IPTG induced sample; lane 4, 1 mM IPTG induced sample; lane 5, 2.5 mM IPTG induced sample; lane 6, 5 mM IPTG induced sample, lane 7, sample via autoinduction

The freeze/thaw method was preferred over sonication for cell lysis because that resulted in a greater yield of protein. Although impurities were present, the specific activity was comparable (Figure II-7B); therefore, these contaminating proteins did not affect the activity of the enzyme. The purities of these MTB enzyme preparations after chromatography were confirmed by SDS-PAGE analysis (Figure II-7C left), and the concentration of each enzyme was determined via Bradford assay. This approach yielded ~0.05 to 0.3 mg MTB RNAP which was sufficient for the assay which only required 0.1 μg of enzyme for each reaction.

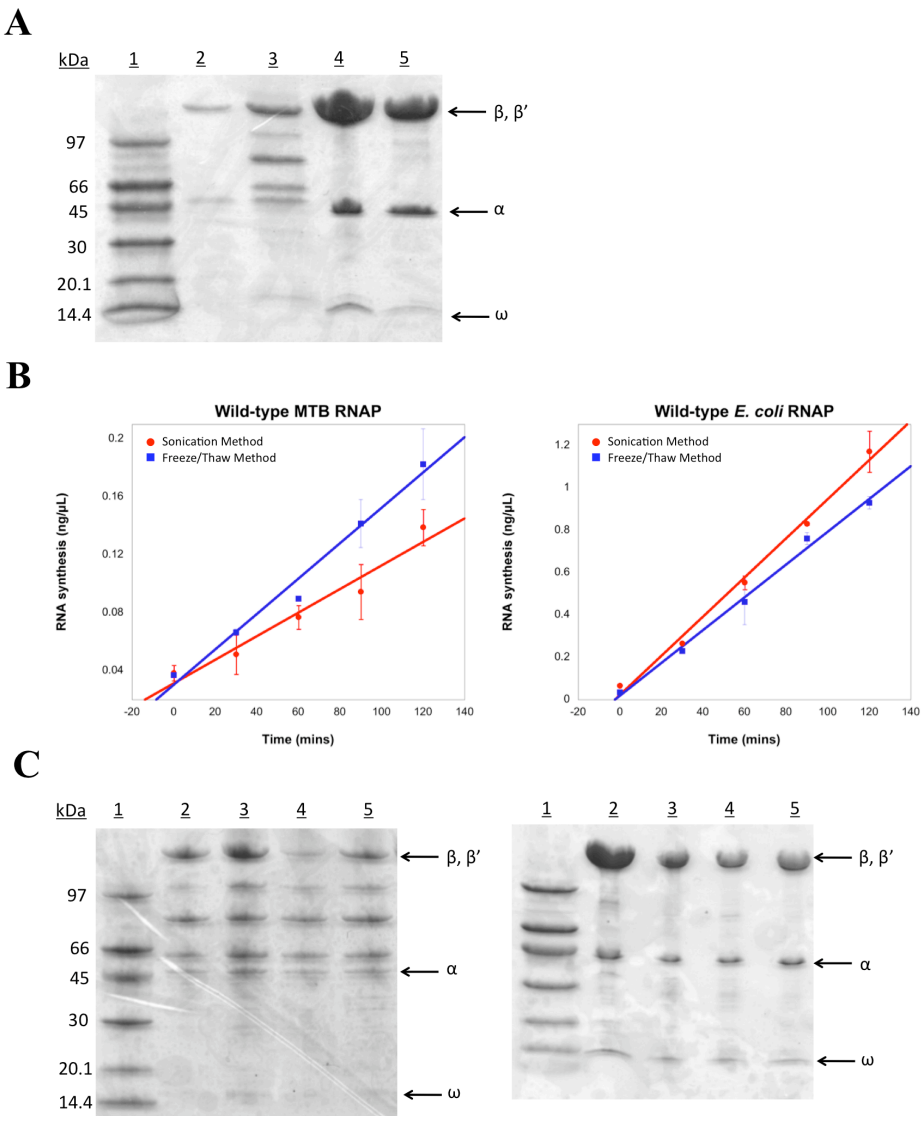

Figure II-7. (A) SDS-PAGE of wild-type MTB and *E. coli* RNAPs prepared via sonication or freeze/thaw method: lane 1, LMW std; lane 2, MTB RNAP (sonication) [0.5 µM]; lane 3, MTB RNAP (freeze/thaw) [3.5 µM]; lane 4, *E. coli* RNAP (sonication) [4.1 µM]; lane 5, *E. coli* RNAP (freeze/thaw) [2.2 µM]. (B) Activity of wild-type MTB and *E. coli* RNAPs prepared using different purification methods (red: sonication method; blue: freeze/thaw method). (C) SDS-PAGE of WT and Mutant RNAPs After Size Exclusion Chromatography. (On the left) lane 1, LMW std; lane 2, MTB RNAP (WT) [2.2 µM]; lane 3, MTB RNAP (D435V) [3.5 µM]; lane 4, MTB RNAP (H445Y) [0.8 µM]; lane 5, MTB RNAP (S450L) [2.0 µM] (On the right) lane 1, LMW std; lane 2, *E. coli* RNAP (WT) [4.1 µM]; lane 3, *E. coli* RNAP (D516V) [1.6 µM]; lane 4, *E. coli* RNAP (H526Y) [4.4 µM]; lane 5, *E. coli* RNAP (S531L) [4.1 µM] (Note the intensity of β and β' band on SDS-PAGE is due to the larger size and the overlapping of these two subunits.)

Additionally, the corresponding RifR mutations were introduced to the *E. coli* *rpoB* gene in pVS10 and the *E. coli* RNAPs were expressed in *E. coli* BL21 (DE3) strains. For *E. coli* RNAPs, lower temperature induction was not necessary because optimal protein yield was obtained after 4 h induction at 37^{o}C. The cells were disrupted via sonication, and the enzyme was purified by metal ion affinity chromatography and gel filtration (Figure II-7C right). The highest yield of *E. coli* RNAP was obtained via the sonication method; whereas, the lowest yield was obtained of MTB RNAP for this same method. The expression levels of MTB core RNAP subunits in the *E. coli* host were lower even with freeze/thaw method compared to levels observed for the *E. coli* core RNAP subunits.

Activity of the RNAPs and Determination of IC_{50} values

The activities of the overexpressed enzymes were assessed using an *in vitro* rolling circle transcription assay (Figure II-5). The core RNAP transcribed a small 45 base single-stranded DNA nanocircle, the Kool^{TM} NC-45^{TM} Universal RNA Polymerase template. To achieve optimal RNAP activity, the pH of the reaction buffer was varied where the optimal pH was determined to be 8.0 (data not shown). The MTB RNAPs from pMTBRP-5, 6, 7, and 8 were active; however, the magnitude of activity of the MTB RNAPs was approximately 10 fold less than the corresponding *E. coli* RNAPs (data not shown). Although the activity was lower, the fluorescent dye (RiboGreen) was sensitive enough to detect the RNA synthesized by the MTB RNAPs.

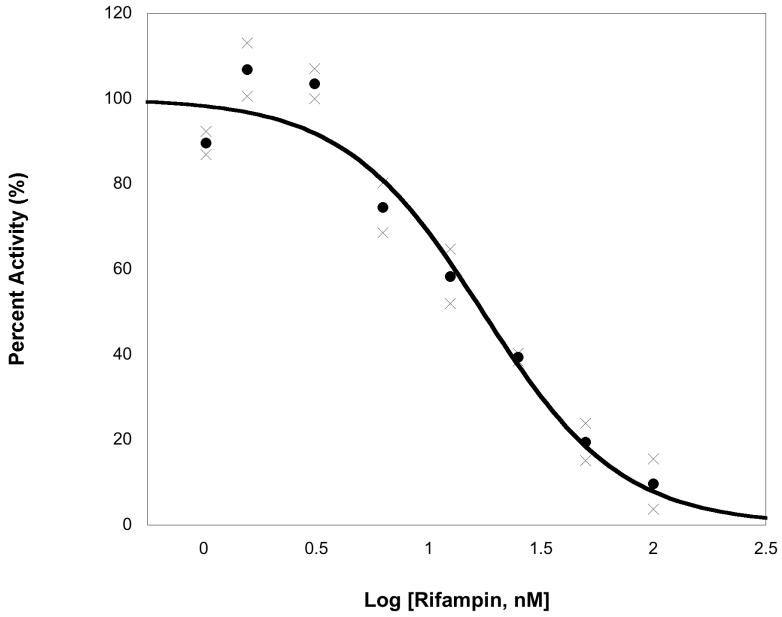

Figure II-8: Example Dose-Response Plot for Rifampin–MTB RNAP (WT) IC_{50} Determination. All of the individual data points (x) and the average data points (•) were plotted. The average data were fit by nonlinear regression to determine the IC_{50} values. The concentrations of rifampin were 1.56-100 nM.

The inhibition of the different MTB RNAPs by rifamycins was investigated via dose-response studies with three of the rifamycins shown in Figure II-1: RMP, RBN, and RFX. Each compound was tested in duplicate in dilutions ranging in concentrations specified in Materials and Methods. The data were plotted (% activity vs log rifamycin concentration) and then fit by nonlinear regression (Figure II-8). This was then repeated with the *E. coli* RNAPs. The logIC_{50} values and their standard errors (of the fit) are reported in Table II-A4 in Appendix II-1. The standard errors of the logIC_{50}s roughly translate into a 20-25% error in the IC_{50} values. The Hill slopes are all very close to one (mean Hill slope = 1.07). Note that for seven of the inhibitor•enzyme combinations, the data plateaued above zero. In these cases the regression was allowed to fit the lower limit. The reason for the lack of complete inhibition in these cases is unclear, but may have to do with the processive nature of the RNAP reaction. That is, a small fraction of enzyme

may enter the elongation phase and, due to the insensitivity of the elongation phase to rifamycin inhibition, it may generate a long enough strand of RNA to give an above-zero lower limit.

The apparent IC_{50} values are listed on Table II-1. As shown in Table II-1, rifamycins inhibit the wild-type MTB and *E. coli* RNAPs in the 10^{-9} M (nM) range. Whereas, the IC_{50} values for the RifR mutants of MTB and *E. coli* were in the 10^{-6} M (μM) range. The most frequently observed MTB RifR mutant in clinical isolates, S450L (*9, 10*), was inhibited at lower concentrations of rifamycins relative to the other MTB mutants. Additionally, the MTB D435V and S450L mutants were the most sensitive to RBN. Overall, the *E. coli* enzymes followed a similar inhibition trend compared to their MTB counterparts.

Table II-1. *In vitro* RNAP IC_{50} Values (μM) for Selected Rifamycins

RNAP	Rifampin	Rifabutin	Rifaximin
MTB (WT)	0.017	0.023	0.007
MTB β(D435V)	465	171	506
MTB β(H445Y)	610	1200	506
MTB β(S450L)	109	20	113
E. coli (WT)	0.012	0.042	0.058
E. coli β(D516V)	233	13	296
E. coli β(H526Y)	1130	1360	1520
E. coli β(S531L)	171	4.9	85

IC_{50} is the concentration of rifamycin resulting in 50% inhibition of transcription. Errors of the logIC_{50} values are reported in Table II-A4 in Appendix II-1 as described in Materials and Methods. The errors of the IC_{50} values are approximately ±25%.
Comparative data for Rifampin: *E. coli* (wt): <12.2 nM[1], 2 nM[2]; *E. coli* (D516V): 12.2 μM[1], 4 μM[2]; *E. coli* (H526Y): > 122 μM[1]; *E. coli* (S531F): 12.2 μM[1].
[1] Jin *et al., J. Mol. Biol* **202**, 45-58, 1988. (only observed S531F mutation in *E. coli* RifR strains rather than S531L)
[2] Feklistov *et al., PNAS* **105 (39)**, 14820-14825, 2008

MICs of Rifamycins

The MICs of rifamycins against the MTB $H_{37}R_V$ strain were determined using two different assays (Microplate Alamar Blue Assay (MABA) and Low Oxygen-Recovery Assay (LORA)) and are reported in Table II-2. Higher MIC values for RMP were observed for LORA compared to MABA, where the former assay resembled the environment in which the latent MTB resides.

Table II-2. MIC Values (μM) for Selected Rifamycins Against MTB Clinical Isolates

MTB Strain	Rifampin	Rifabutin
$H_{37}R_V$[1] MABA	0.24	-
LORA	3.3	-
$H_{37}R_V$[2]	0.3	≤ 0.018
RNAP β(D435V)[2]	38.9	≤ 0.6
RNAP β(H445Y)[2]	> 78	≥ 37.8
RNAP β(S450L)[2]	> 78	37.8

[1] MIC_{90} is the concentration of rifamycin that results in 90% inhibition of growth. (Data from Prof. Scott G. Franzblau (UIC).)
[2] MIC_{99} is the concentration of rifamycin that results in 99% inhibition of growth. (Williams *et al., Antimicrobial Agents and Chemotherapy* **42 (7)**, 1853-1857, 1998.)

The susceptibility of *E. coli* wild-type strains (DH5α and TG2) and mutant strain (EC2880) to rifamycins is summarized in Table II-3. The MIC values of the different rifamycins were analyzed and correlated to what has been previously reported for MTB and *E. coli* (Tables II-2 and II-3). The MICs of rifamycins against wild-type *E. coli* strains were approximately 100-500 fold greater than the MICs observed for EC2880. RMP and RBN had comparable MICs to one another when assayed in the wild-type and mutant *E. coli* strains; whereas, MICs of RFX were 2-4 fold higher compared to RMP and RBN against these strains.

Table II-3. MIC Values (μM) for Selected Rifamycins Against *E. coli*

***E. coli* strains**	**Rifamycin S**	**Rifampin**	**Rifabutin**	**Rifaximin**
WT				
TG2	**> 92**	**6.25**	**6.25**	**25**
DH5α	**> 100**	**25**	**12.5**	**50**
DH5α[1]	573 (Rif SV)	7.60	14.76	NR
Δ*tolC*				
EC2880	**0.78**	**0.05**	**0.10**	**0.20**
D21f/tolC[1]	1.12 (Rif SV)	0.12	0.06	NR

MIC_{90} is the concentration of rifamycin that results in 90% inhibition of growth. Results from this study are in **bold**. NR: not reported.
Comparative data for Rifampin in *E. coli* isolates[2]: *E. coli* (wt): <12.2 μM; *E. coli* (D516V): ≥ 1220 μM; *E. coli* (H526Y): ≥ 1220 μM; *E. coli* (S531F): ≥ 1220 μM.
[1] Feklistov *et al., PNAS* **105 (39)**, 14820-14825, 2008.
[2] Jin *et al., J. Mol. Biol* **202**, 45-58, 1988.

Discussion

The three aforementioned RifR mutants have been identified from clinical isolates and these strains have been studied. However, no *in vitro* studies of purified MTB RifR RNAPs have been reported. Herein, we describe a co-overexpression system for wild-type and RifR MTB RNAPs in *E. coli* and its use to investigate the effect of the mutation on inhibition by rifamycins. Artsimovitch and colleagues developed a co-overexpression plasmid for the *E. coli* core RNAP (pVS10, $\alpha_2\beta\beta'\omega$) (*22*). We adopted the same concept and used pVS10 as the template to construct our co-overexpression plasmid for the MTB core RNAP (pMTBRP-5; Figure II-4). However, we encountered a few obstacles using the co-overexpression method. Due to the enormous size of the plasmid (~14.4 kb), the number of unique sites present was limited. After multiple trials, optimal PCR conditions were obtained to modify the MTB ORFs to incorporate unique sites. Additionally, the large size of the plasmid made the integration of the MTB *rpoZ* gene (~0.3 kb) difficult. Therefore, a 165 bp linker was designed (containing the unique restriction enzyme sites

required to subclone in MTB *rpoB* and *rpoC* genes) and introduced to replace the *E. coli rpoB* and *rpoC* genes. The reduced size of the plasmid facilitated the incorporation of MTB *rpoZ*. After following the multi-step scheme illustrated in Figure II-3, the *E. coli rpo* genes were replaced by MTB *rpo* genes. The resulting plasmid, pMTBRP-5, was verified via DNA sequencing. The plasmid was then transformed into an expression cell line and successfully purified via nickel affinity chromatography and gel filtration. A hexahistidine tag fused to the C-terminus of the β subunit allowed for the separation of the target enzyme from contaminating *E. coli* RNAP. The resulting MTB RNAP was pure enough for a microtiterplate-based *in vitro* transcription assay. In previous studies, the wild-type MTB RNAP has been obtained from crude extracts of MTB $H_{37}R_V$ cells and from *in vitro* reconstitution by renaturation of mixtures of denatured subunits (*7, 11*). Altogether, the co-overexpression method allowed for the purification of the assembled core RNAP in a convenient manner avoiding the denaturing and renaturing steps required to obtain RNAP from crude extracts or via reconstitution from individual subunits. To determine how the RifR mutants influence inhibition by rifamycins, the three most prevalent mutations found in clinical isolates (D435V, H445Y, S450L) were introduced individually to the MTB *rpoB* ORF to yield the following vectors: pMTBRP-6 (D435V), -7 (H445Y), -8 (S450L) (Figure II-3 and II-4). The mutations were also introduced to the corresponding residues in *E. coli rpoB* (D516V, H526Y, S531L) of pVS10. The activity of the wild-type and RifR RNAPs of MTB and *E. coli* was assessed via *in vitro* rolling circle transcription assay (Figure II-5), which confirmed that these enzymes were active. A single-stranded nanocircle is used as the DNA template. Previously, nanocircle templates have proven to be efficient substrates for various bacterial and phage RNAPs

(*23, 24*). The RNAP produced long RNA repeats of the nanocircle in the absence of RNAP inhibitor, and RiboGreen was used to measure the amount of RNA transcribed.

It has been reported that MTB is more sensitive to RMP than *E. coli* and other prokaryotes (*25*). Previously, Zenkin *et al.* reconstituted a chimeric *E. coli* RNAP containing MTB Clusters I and II of β subunit and concluded that the difference in sensitivity of MTB and *E. coli* to rifamycins was not due to these regions of MTB RNAP involved in forming the rifamycin binding pocket (*4*). Here, the co-overexpression of MTB and *E. coli* RNAPs allowed for the direct comparison of the sensitivity of these enzymes to rifamycins. The activity of the wild-type and RifR RNAPs of MTB and *E. coli* was assessed in the presence of rifamycins via dose-response studies (Figure II-8). The representative rifamycins evaluated in this study included: RMP (a C3 rifamycin derivative) and RBN and RFX (C3/C4 modified rifamycins). As can be seen from the IC_{50} values in Table II-1, rifamcyins bind tightly to the wild-type MTB and *E. coli* RNAPs and inhibit the enzymes in the 10^{-8} M (10 nM) range. Whereas for the RifR mutants of both MTB and *E. coli,* a dramatic ~10^2-10^5 fold loss of affinity for all four rifamycins was observed where these different mutants were inhibited at much higher concentrations of rifamycins (10^{-4} M range). The three residues mutated in these RifR mutants are among the twelve amino acid residues of the β subunit that directly interact with RMP via hydrogen bonds (*1*). The single amino acid substitutions disrupt critical interactions that contribute to rifamycin binding and potentially change the shape and conformation of the rifamycin-binding site. This leads to the weaker binding of the rifamycins, explaining the decreased susceptibility of the enzyme to inhibition by rifamycins. Even though the C3/C4 modified rifamycins (RBN and RFX) have enhanced

antibacterial activity (*17*), they still inhibit RifR mutant RNAPs only in the 10^{-5} M (1-100 μM) range *in vitro*. Therefore, cross-resistance still exists between these rifamycins for these RifR mutant RNAPs. Our results are similar to what has previously been reported for wild-type *E. coli* RNAP and RMP with IC_{50} values in 10^{-9} M (nM) range; however, our data for resistant mutants indicates lower affinity for RMP, where the values are ~100 fold higher for the mutants (Table II-1) (*2, 5*). Feklistov *et al*. conducted *in vitro* transcription assays using a system containing an *E. coli* holoenzyme (with a sigma factor bound to the *E. coli* core RNAP) and a promoter-containing DNA fragment (*2*). The sigma factor recruits the RNAP to bind to the specific DNA promoter. In our studies, we used the isolated core RNAP and a nanocircle template (a nonnative template without a specific promoter). Even with these differences, Feklistov and colleagues observed a high increase in the IC_{50} value (2000-fold) for RMP with the RifR *E. coli* RNAP (D516V) compared to WT *E. coli* RNAP (*2*).

The MICs were greater than the IC_{50} values reported with these rifamycins for the different RifR mutants, which could be due to permeation, stability, or other factors. The MICs of RMP for wild-type MTB $H_{37}R_V$ strains were determined at the Institute for Tuberculosis Research (ITR/UIC) using Microplate Alamar Blue Assay (MABA) and Low Oxygen-Recovery Assay (LORA), where the latter assay is a model for the latent form of MTB. Williams *et al.* reported the MICs for rifamycins against the wild-type MTB $H_{37}R_V$ strain and the clinical isolates containing the specific prevalent mutations (Table II-2) (*26*). The group also generated recombinant clones with only the specific mutations and obtained similar values as the ones reported with the clinical isolates, which confirmed that any additional mutations that might be present in the clinical

isolates did not affect the MICs of rifamycins. Yang *et al.* conducted a similar study and obtained comparable MICs for these three prevalent mutant isolates and found that 8% of RifR strains are susceptible to RBN (*17*).

Comparing MTB RifR mutants, the most frequently observed mutation in clinical isolates (S450L) had the lowest IC_{50} values for the different rifamycins compared to the other MTB mutants; whereas, H445Y mutant resulted in the highest IC_{50} values (Table II-1). The D435V mutant had intermediate IC_{50} values, but the lowest MIC values among the different mutants. As seen in Table II-2, D435V was the most sensitive to RBN from the MIC data; whereas the other two mutants (H445Y and S450L) were still resistant to these rifamycins. RBN has better antibacterial activity against rifamycin sensitive strains and some rifamycin resistant strains but still exhibit substantial cross resistance *in vitro* (*17, 26*).

Our data are consistent with the structural model for rifamycin binding to RNAP (*1*). In this model, hydrogen bonds are predicted between the rifamycin core and each of the three amino acids probed in this study. Mutations of aspartate 435 and histidine 445 (if it is protonated) would be expected to generate the greatest loss of binding energy due to the loss of a hydrogen bond between a charged moiety and an uncharged moiety. While mutation of serine 450 would be expected to exhibit less loss of binding energy because no charged moieties are involved. The effects of these mutations (*e.g.*, the magnitude of binding energy lost) could be modified depending on the geometry of the hydrogen bonds lost. However, our data does qualitatively correlate with the proposed loss of binding energy as the aspartate and histidine mutants are 6 to 10-fold less sensitive to the rifamycins (Table II-1), consistent with a greater loss of binding energy.

This correlation suggests that the structural model is fairly robust and can help to interpret biochemical data such as in our study. (We should note that a new, complete model for the *E. coli* RNAP has been reported (*27*); however, this report does not discuss the rifamycin-binding pocket. Sequence comparisons indicate that the rifamycin-binding pocket is highly conserved and therefore the thermophilic RNAP structure (*1*) should be a robust model for interpreting our biochemical data.)

It is generally perceived that the differential sensitivities of eubacterial organisms (e.g., *E. coli* vs. MTB) towards rifamycins are not due to changes in the RNAP itself but are due to other factors. Our results, along with those of Zenkin and colleagues with the chimeric (β subunit) *E. coli*/MTB RNAP, provide experimental evidence consistent with this perception. Our results reported herein show that the *E. coli* and MTB RNAPs exhibit similar sensitivities to rifamycins. Therefore, the differential sensitivity must be due to off-target activity or other factor(s). It is well estalblished that efflux pumps (*i.e.*, TolC) are responsible for the active export of antibiotics in Gram-negative bacteria (*28*). Therefore, to experimentally assess the relationship between the *E. coli* TolC protein and the export of rifamycins, the MIC values for wild-type *E. coli* strains (DH5α and TG2) and mutant *E. coli* strain (EC2880-permeable strain with *tolC*$^-$ and *imp*$^-$) were determined for this same set of rifamycins. As reported in Table II-3, the MIC values of these rifamycins are significantly lower for the mutant EC2880 strain compared to the wild-type strains (DH5α and TG2), suggesting that TolC efflux pumps are involved in the export of rifamycins explaining the lower sensitivity of *E. coli* towards rifamycins. The *tolC* knockout leads to retention of rifamycins therefore resulting in lower MICs. The EC2880 MIC values were comparable to what has been reported previously for *E. coli*

D21f/tolC (Table II-3) (*2*) and to the MIC values observed for the wild-type MTB $H_{37}R_V$ strain (Table II-2) (*26*). The wild-type MTB $H_{37}R_V$ strain was more sensitive to C3/C4 modified rifamycins (RBN). Whereas, the wild-type *E. coli* strains had higher MIC values for all rifamycins studied (Table II-3). RMP and RBN had similar MICs in each instance (e.g., wild-type and mutant).

Conclusions

We have developed a system where we can perform *in vitro* inhibition assays using the *M. tuberculosis* RNAP and three Rif-resistant mutants. This system was used to characterize the *in vitro* activity of a series of known rifamycins, with results consistent with MIC data and previous reports. We have also provided experimental evidence that the differential sensitivity of *E. coli* vs MTB organisms to rifamycins results from *E. coli* efflux pump activity, consistent with previous general perceptions.

Notes to Chapter II

We thank Professor Irina Artsimovitch (Ohio State University, Ohio) for generously providing the pVS10 plasmid and also for her helpful suggestions during discussions. We also thank Professor Scott Franzblau (University of Illinois at Chicago) for providing the rifamycin MIC data against MTB $H_{37}R_V$ strains. The avirulent *Mycobacterium tuberculosis* strain ($H_{37}R_a$) was a generous gift from the TB center of Colorado State University. The plasmids containing the individual MTB *rpo* genes (pSR52 (*rpoA*), pJF09 (*rpoB*), pJF10 (*rpoC*)) were a generous gift from Dr. Sébastien Rodrique (MIT). The EC2880 strain (permeable strain with *tolC*$^-$ and *imp*$^-$ mutations) was a generous gift from Dr. Michael Hubband (Pfizer Scientific). We would also like to acknowledge the University of Michigan, College of Pharmacy (Vahlteich and UpJohn Research Funds), Office of the Vice-President for Research, and Rackham Graduate School for funding.

The work described in this chapter was published in *Tuberculosis* (Gill, S. K. and Garcia, G.A. "*In vitro* Investigation of Wild-type and Rifamycin-Resistant Mutants of the *Mycobacterium tuberculosis* RNA Polymerase" *Tuberculosis* (2011) **91** p. 361-369).

Abbreviations used: RMP, rifampin; RNAP, RNA polymerase; WT, wild-type; RifR, Rifamycin-resistant; MTB, *Mycobacterium tuberculosis*; RPN, rifapentine; RBN, rifabutin; RFX, rifaximin; NTP, ribonucleotide triphosphate; ORF, open reading frame; RBS, ribosome binding site; PCR, polymerase chain reaction; IPTG, isopropyl β-D-thiogalactoside; SDS-PAGE, sodium dodecyl sulfate polyacrylamide gel electrophoresis; PMSF, phenylmethylsulfonyl fluoride; EDTA, ethylenediaminetetraacetic acid; DTT, dithiothreitol; RNA, ribonucleic acid; MABA, Microplate Alamar Blue Assay; LORA, Low Oxygen-Recovery Assay; IC_{50}, concentration of rifamycin resulting in 50% inhibition of transcription; MIC_{90}, concentration of rifamycin that results in 90% inhibition of bacterial growth

Appendix II-1

Table II-A1. Plasmids and Bacterial Strains.

	Description
Plasmids	
pVS10[1]	pET21 vector containing *E. coli rpoA, rpoB*, *rpoC*, and *rpoZ* genes encoding the wild-type *E. coli* RNAP subunits
pVS10 (D516V)	pVS10 plasmid containing D516V mutation in *E. coli* β subunit
pVS10 (H526Y)	pVS10 plasmid containing H526Y mutation in *E. coli* β subunit
pVS10 (S531L)	pVS10 plasmid containing D516V mutation in *E. coli* β subunit
pSR52[2]	pET16b vector containing the MTB *rpoA* gene
pJF09[2]	pET16b vector containing the MTB *rpoB* gene
pJF10[2]	pET30a vector containing the MTB *rpoC* gene
pMTBRP-5	Overexpression vector containing MTB *rpoA, rpoB*, *rpoC*, and *rpoZ* genes encoding the wild-type MTB RNAP subunits
pMTBRP-6	pMTBRP-5 plasmid containing D435V mutation in MTB β subunit
pMTBRP-7	pMTBRP-5 plasmid containing H445Y mutation in MTB β subunit
pMTBRP-8	pMTBRP-5 plasmid containing S450L mutation in MTB β subunit
Bacterial Strains	
Mycobacterium tuberculosis $H_{37}R_a$	Avirulent strain
Mycobacterium tuberculosis $H_{37}R_v$	Virulent strain
XL2-Blue Ultracompetent Cells	*endA1 supE44 thi-1 hsdR17 recA1 gyrA96 relA1 lac* [F' *proAB lacI*^{q} *ZΔM15* Tn*10* (Tet^r) Amy Cam^r]
E. coli BL21(DE3)	F$^-$ *ompT gal dcm*$^+$ *hsdS*(r_B^- m_B^-) λ(DE3 [*lacI lacUV5-T7 gene 1 ind1 sam7 nin5*])
E. coli BL21(DE3) CodonPlus-RIPL	B F$^-$ *ompT hsdS*(r_B^- m_B^-) *dcm*$^+$ Tet^r *gal* λ(DE3) *endA* Hte [*argU proL* Cam^r] [*argU ileY leuW* Strep/Spec^r]

[1] Belogurov *et al., Molecular Cell* **26**, 117-129, 2007.
[2] Jacques *et al., FEMS Microbiol Lett* **255**, 140-147, 2006.

Table II-A2. Oligonucleotides Used for Plasmid Construction.

Oligonucleotides	**Primer Sequence (5'-3')**
(MTB PCR Primers)	
NdeI FWD *rpoA*	gaagctCATATGctgatctcacagcgccccaccctgtccg
NcoI REV *rpoA*	gaagctCCATGgctaaagctgttcggtttcggcgtagtcc
AvrII FWD *rpoB*	cagcgaCCTAGGaaccctatggcagattcccgccagagcaaaacagccg
Histag REV *rpoB* (A)	gcgacagctttaATGGTGATGGTGATGGTGcgcaagatcctcgacacttgcgg
BmtI REV *rpoB* (B)	cttGCATGCtagcgggtttagtaattttgcgacagctttaatggtgatgg
AvrII/NheI FWD *rpoC*	cagcgaCCTAGGgtactaGCTAGCgttaggggaaagggagttacatgctcgacgtcaacttcttcgatg
AscI REV *rpoC*	gagctGGCGCGCCtagcggtagtcgctgtagccgtagtcgtcc
AflI FWD *rpoZ*	gaagctCTTAAGgtgagtatctcgcagtccgacgcgtcgttggccg
AflI FWD *rpoZ* (+RBS)	agctCTTAAGaaggagattaagtatgagtatctcgcagtccgacgcgtcgt
NotI REV *rpoZ*	gaagctGCGGCCGCtactcgccctcggtgtgctcgagcag
(B-C Linker) (*NcoI/AvrII/AscI/HindIII*)	aacagaCCATGGatccccgatccgtcgacttgtcagcgagctgaggaacCCTAGGaattggccttaacc ggGGCGCGCCtcaaataacgtaaaaacccgcttcggcgggtttttttatgggggagtttagggaaaga gcatttgtcagaatcAAGCTTcaatga
(MTB Quik-Change Primers)	
rpoB(1) FWD	gacgccggaggagcggctgctgcgtgccatcttcggtgagaaggcccgcg
rpoB(1) REV	cgcgggccttctcaccgaagatggcacgcagcagccgctcctccggcgtc
rpoB(2) FWD (-*StuI*)	gagatggagtgctgggccatgcaggcGtacggtgctgcctacaccctgcag
rpoB(2) REV (-*StuI*)	ctgcagggtgtaggcagcaccgtaCgcctgcatggcccagcactccatctc
rpoC(1) FWD (-*NcoI*)	cggcgagtacttcaccggtgGcatgggcgcggagtcgatcc
rpoC(1) REV (-*NcoI*)	ggatcgactccgcgcccatgCcaccggtgaagtactcgccg
rpoC(4) FWD (-*NcoI*)	gcgtgtgcgcgacctgctacgggcgttcGatggccaccggcaagctggtcg
rpoC(4) REV (-*NcoI*)	cgaccagcttgccggtggccatCgaacgcccgtagcaggtcgcgcacacgc
rpoB(C552R) FWD	gacggtcgcttcgtcgagccgCgcgtgctggtccgccgcaag
rpoB(C552R) REV	cttgcggcggaccagcacgcGcggctcgacgaagcgaccgtc

Table II-A2. (Continued)

Oligonucleotides	**Primer Sequence (5'-3')**
(MTB Quik-Change Primers)	
rpoB(D435V) FWD	cagctgagccaattcatggTccagaacaacccgctgtcggg
rpoB(D435V) REV	cccgacagcgggttgttctggAccatgaattggctcagctg
rpoB(H445Y) FWD	ccgctgtcggggttgaccTacaagcgccgactgtcggcg
rpoB(H445Y) REV	cgccgacagtcggcgcttgtAggtcaaccccgacagcgg
rpoB(S450L) FWD	ccacaagcgccgactgtTggcgctggggcccggcg
rpoB(S450L) REV	cgccgggccccagcgccAacagtcggcgcttgtgg
(*E. coli* Quik-Change Primers)	
rpoB(D516V) FWD	cagctgtctcagtttatggTccagaacaacccgctgtctg
rpoB(D516V) REV	cagacagcgggttgttctggAccataaactgagacagctg
rpoB(H526Y) FWD	caacccgctgtctgagattacgTacaaacgtcgtatctccgcac
rpoB(H526Y) REV	gtgcggagatacgacgtttgtAcgtaatctcagacagcgggttg
rpoB(S531L) FWD	gattacgcacaaacgtcgtatctTGgcactcggcccaggcggtctgac
rpoB(S531L) REV	gtcagaccgcctgggccgagtgcCAagatacgacgtttgtgcgtaatc

Table II-A3. Confirmation of MTB α Subunit by Mass Spectrometry.

N[a]	%Cov[b]	Conf[c]	Prec m/z[d]	Accession[e]	Protein Name[f]	Sequence[g]
1	31.1	99.0	1266.72	sp|P66701|RPOA_ MYCTU	DNA-directed RNA polymerase subunit alpha OS=Mycobacterium tuberculosis (strain ATCC 25177/ H37Ra) GN=rpoA PE=3 SV=1	EGVHTVGELVAR
1	31.1	99.0	1003.56	same as above	same as above	GYVPAVQNR
1	31.1	99.0	1611.93	same as above	same as above	IDGVLHEFTTVPGVK
1	31.1	99.0	1330.79	same as above	same as above	IPVDSIYSPVLK
1	31.1	99.0	2088.15	same as above	same as above	MLISQRPTLSEDVLTDNR
1	31.1	99.0	1954.02	same as above	same as above	SLVVSSEEDEPVTMYLR
1	31.1	99.0	1485.91	same as above	same as above	TLLSSIPGAAVTSIR
1	31.1	99.0	1118.68	same as above	same as above	TLVELFGLAR
1	31.1	99.0	1248.70	same as above	same as above	EGVHTVGELVAR

[a]The rank of the specified protein relative to all other proteins in the list of detected proteins
[b]The number of matching amino acids (from peptides) divided by the total number of amino acids in the sequence (expressed as a percentage)
[c]The confidence for the peptide identification (expressed as a percentage)
[d]The monoisotopic m/z for the ion fragmented in this cycle and experiment, as determined by the instrument
[e]The accession number of the detected protein
[f]The name of the detected protein
[g]The sequence of the peptide with the highest confidence that was identified by the search

Table II-A4. Log IC_{50} Values and Standard Errors of the Fits for Known Rifamycins with RNAP

	Log IC_{50}[1] (standard error of fit[2], Hill slope[3])		
RNAP	**Rifampin**	**Rifabutin**	**Rifaximin**
MTB (WT)	-1.759 (±0.059, 1.41)	-1.639 (±0.059, 1.19)	-2.131 (±0.076, 0.84)
MTB β(D435V)	2.667 (±0.095, 1.13)	2.233 (±0.109, 0.81)	2.704 (±0.101, 0.87)
MTB β(H445Y)	2.785 (±0.496, 1.0)[4]	3.08 (±0.113, 1.06)[4]	2.929 (±0.087, 1.03)
MTB β(S450L)	2.037 (±0.062, 1.35)	1.291 (±0.104, 1.15)[4]	2.053 (±0.075, 1.85)[4]
E. coli (WT)	-1.912 (±0.069, 1.10)	-1.377 (±0.050, 1.34)	-1.239 (±0.061,0.73)
E. coli β(D516V)	2.368 (±0.055, 0.76)	1.111 (±0.039, 1.21)[4]	2.471 (±0.089, 0.68)
E. coli β(H526Y)	3.052 (±0.058, 1.04)	3.133 (±0.513, 0.70)[4]	3.183 (±0.049, 0.88)
E. coli β(S531L)	2.233 (±0.060, 0.82)	0.693 (±0.037, 1.81)[4]	1.931 (±0.098, 0.82)

[1] The log IC_{50} values are such that the IC_{50} values will be in μM. Negative log IC_{50} values reflect IC50 values less than μM (e.g., in the nM range). Values were fit to a four parameter logistic regression model with the top and bottom limits set at 100 and 0 respectively.
[2] The average error is ~10 %, which roughly translates to 20-25% in the IC_{50}.
[3] The average Hill slope is 1.07.
[4] For these IC_{50}s, the regression model was allowed to fit the bottom limit as the data plateaued above zero (see discussion in text).

References

1. E. A. Campbell *et al.*, Structural mechanism for rifampicin inhibition of bacterial RNA polymerase. *Cell* **104**, 901 (2001).

2. A. Feklistov *et al.*, Rifamycins do not function by allosteric modulation of binding of Mg2+ to the RNA polymerase active center. *Proceedings of the National Academy of Sciences of the United States of America* **105**, 14820 (Sep 30, 2008).

3. K. Fujii, H. Saito, H. Tomioka, T. Mae, K. Hosoe, Mechanism of action of antimycobacterial activity of the new benzoxazinorifamycin KRM-1648. *Antimicrob. Agents Chemother.* **39**, 1489 (1995).

4. N. Zenkin, A. Kulbachinskiy, I. Bass, V. Nikiforov, Different Rifampin Sensitivities of Escherichia coli and Mycobacterium tuberculosis RNA Polymerases Are Not Explained by the Difference in the {beta}-Subunit Rifampin Regions I and II. *Antimicrob. Agents Chemother.* **49**, 1587 (April 1, 2005, 2005).

5. D. J. J. a. C. A. Gross, Mapping and Sequencing of Mutations in the *Escherichia coli rpoB* Gene that Lead to Rifampicin Resistance. *Journal of Molecular Biology* **202**, 45 (1988).

6. W. Wehrli, Rifampin: mechanisms of action and resistance. *Reviews of Infectious Diseases* **5**, S407 (1983).

7. R. M. Harshey, T. Ramakrishnan, Purification and properties of DNA-dependent RNA polymerase from Mycobacterium tuberculosis H37Rv. *Biochimica et Biophysica Acta (BBA) - Nucleic Acids and Protein Synthesis* **432**, 49 (1976).

8. H. G. Floss, T.-W. Yu, Rifamycin-mode of action, resistance, and biosynthesis. *Chem. Rev.* **105**, 621 (2005).

9. P. I. A. Telenti, F. Marchesi, D. Lowrie, S.T. Cole, J. Colston, L. Matter, K. Schopfer, and T. Bodmer., Detection of rifampicin-resistance mutation in *Mycobacterium tuberculosis*. *Lancet* **341**, 647 (1993).

10. D. L. Williams *et al.*, Contribution of rpoB mutations to development of rifamycin cross-resistance in Mycobacterium tuberculosis. *Antimicrob. Agents Chemother.* **42**, 1853 (1998).

11. J.-F. Jacques, S. Rodrigue, R. Brzezinski, L. Gaudreau, A recombinant Mycobacterium tuberculosis in vitro transcription system. *FEMS Microbiology Letters* **255**, 140 (Feb, 2006).

12. P. A. Aristoff, G. A. Garcia, P. D. Kirchhoff, and H. D. H. Showalter., Rifamycins-Obstacles and opportunities. *Tuberculosis* **90**, 94 (2010).

13. L. Marsili *et al.*, New rifamycins modified at positions 3 and 4: Synthesis, structure and biological evaluation. *J. Antibiot.* **34**, 1033 (1981).

14. V. Arioli *et al.*, Antibacterial activity of DL 473, a new semisynthetic rifamycin derivative. *J. Antibiot.* **34**, 1026 (1981).

15. P. Bemer-Melchior, A. Bryskier, H. B. Drugeon, Comparison of the in vitro activities of rifapentine and rifampicin against Mycobacterium tuberculosis complex. *J. Antimicrob. Chemother.* **46**, 571 (2000).

16. A. M. Dhople, A. A. Dhople, M. A. Ibanez, Comparative in vitro activities of rifamycin analogues against rifampin-sensitive and rifampin-resistant Mycobacterium tuberculosis. *Internat. J. Antimicrob. Agents* **8**, 209 (1997).

17. B. Yang *et al.*, Relationship between antimycobacterial activities of rifampicin, rifabutin and KRM-1648 and rpoB mutations of Mycobacterium tuberculosis. *J. Antimicrob. Chemother.* **42**, 621 (1998).

18. P. Villain-Guillot, M. Gualtieri, L. Bastide, J.-P. Leonetti, In vitro activities of different inhibitors of bacterial transcription against Staphylococcus epidermidis biofilm. *Antimicrobial Agents & Chemotherapy* **51**, 3117 (Sep, 2007).

19. L. Collins, S. G. Franzblau, Microplate alamar blue assay versus BACTEC 460 system for high- throughput screening of compounds against Mycobacterium tuberculosis and Mycobacterium avium. *Antimicrob Agents Chemother* **41**, 1004 (1997 May, 1997).

20. S. H. W. Cho, S. Wan, B. Hwang, C.H. Pauli, S.G. Franzblau, Low oxygen recovery assay (LORA) for high throughput screening of compounds against non-replicating Mycobacterium tuberculosis. *Antimicrob Agents Chemother* **In Press**, doi:10.1128/AAC.00055 (2007).

21. I. Wiegand, K. Hilpert, R. E. W. Hancock, Agar and broth dilution methods to determine the minimal inhibitory concentration (MIC) of antimicrobial substances. *Nat. Protoc.* **3**, 163 (2008).

22. G. A. Belogurov *et al.*, Structural basis for converting a general transcription factor into an operon-specific virulence regulator. *Mol. Cell* **26**, 117 (Apr, 2007).

23. S. L. Daubendiek, K. Ryan, E. T. Kool, Rolling-Circle RNA Synthesis: Circular Oligonucleotides as Efficient Substrates for T7 RNA Polymerase. *J. Am. Chem. Soc.* **117**, 7818 (1995).

24. Anonymous, Rapidly Screen Bacterial RNA Polymerase Inhibitors Using Innovative Kool™ NC-45™ Technology. *Epicentre Forum Newsletter* **11**, 22 (2004).

25. F. G. Winder, in *The Biology of the Mycobacteria.* (Academic Press, London; New York, 1982), pp. 354-424.

26. D. L. Williams *et al.*, Contribution of rpoB mutations to development of rifamycin cross-resistance in Mycobacterium tuberculosis. *Antimicrobial Agents and Chemotherapy* **42**, 1853 (Jul, 1998).

27. N. Opalka *et al.*, Complete Structural Model of *Escherichia coli* RNA Polymerase from a Hybrid Approach. *PLOS Biology* **8**, 1 (2010).

28. X. Z. Li, H. Nikaido, Efflux-mediated drug resistance in bacteria. *Drugs* **64**, 159 (2004).

CHAPTER III

Synthesis and Structure-Activity Relationships of Novel Substituted 8-amino, 8-thio, and 1,8-pyrazole Congeners of Antituberculars Rifamycin S and Rifampin

Rifamycins have been used to treat tuberculosis (TB) for the past 40 years. Rifampin (RMP), along with other rifamycins, is a potent inhibitor of DNA-dependent RNA polymerase (RNAP), an essential enzyme involved in gene expression (*1-3*). Since first introduced in the 1960's, RMP has been effectively used to treat both forms of TB (active and latent) and has reduced TB treatment from 18 to 9 months (*4-6*). Unfortunately, RMP has a number of shortfalls that include issues of resistance, hepatotoxicity, flu-like syndrome at higher doses, and drug-drug interactions (*1, 7*).

Due to these limiting characteristics of RMP, it is necessary to develop new derivatives that are: 1) successful against resistant strains (MDR and XDR); 2) effective against both forms of TB; 3) able to reduce the length of TB therapy; 4) unable to induce cytochrome P450 (CYP) (*1, 8*). Previously, structure-activity relationship studies have led to the synthesis of numerous rifamycin derivatives; however, only a few rifamycins have been approved in the United States with improved potency and antibacterial activity than RMP (*1, 9*).

Although many rifamycin derivatives have been investigated, the recent availability of crystal structures (RMP bound to *Thermus aquatic* RNAP; rifabutin and rifapentine bound to *Thermus thermophilus* RNAP) provides information on how to

improve the design of rifamycins (*10, 11*). There are twelve β subunit residues that directly interact with RMP via hydrogen bonds and van der Waals interactions (*10*). The most frequently mutated residue in clinical isolates that results in rifamycin-resistant (RifR) RNAP is Ser450, which forms a hydrogen bond with the rifamycin hydroxyl at C-8. Previously, acetylation of the C-8 hydroxyl resulted in an inactive rifamycin derivative; however, this position has not been fully investigated (*1, 12*).

To further investigate the C-8 position, a series of novel rifamycin S (Rif S) and RMP analogues incorporating 8-amino, 8-thio, and 1,8-pyrazole substituents were synthesized (Figure III-1 and III-2). The analogues were screened against the virulent strain, MTB $H_{37}R_V$, to quantify their antitubercular activity under both aerobic and anaerobic conditions. The inhibition of wild-type (WT) *Mycobacterium tuberculosis* (MTB) RNAP and RifR MTB RNAP (S450L) by select C-8 analogues was assessed via an *in vitro* rolling circle transcription assay. The MIC_{90} values were determined for these analogues against *E. coli* strains. Additionally, representative analogues were evaluated in the human pregnane X receptor (hPXR) activation assay. Our goal is to use this information to not only investigate the molecular mechanisms responsible for resistance but also to guide the development of new analogues with potential for enhanced activity against RifR RNAP.

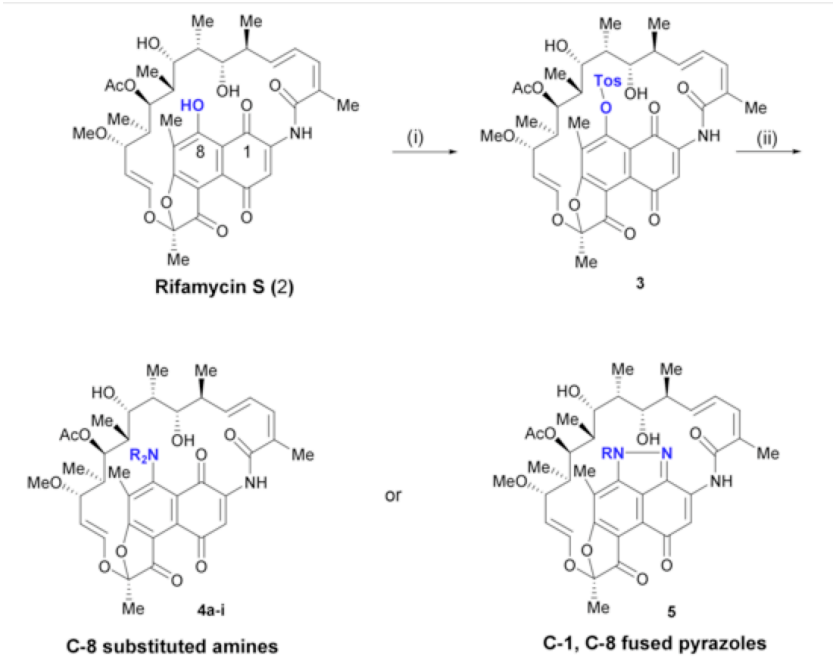

Figure III-1: Synthesis of C-8 analogues of Rifamycin S. (The detailed synthesis of these analogues is described in Appendix III-1)

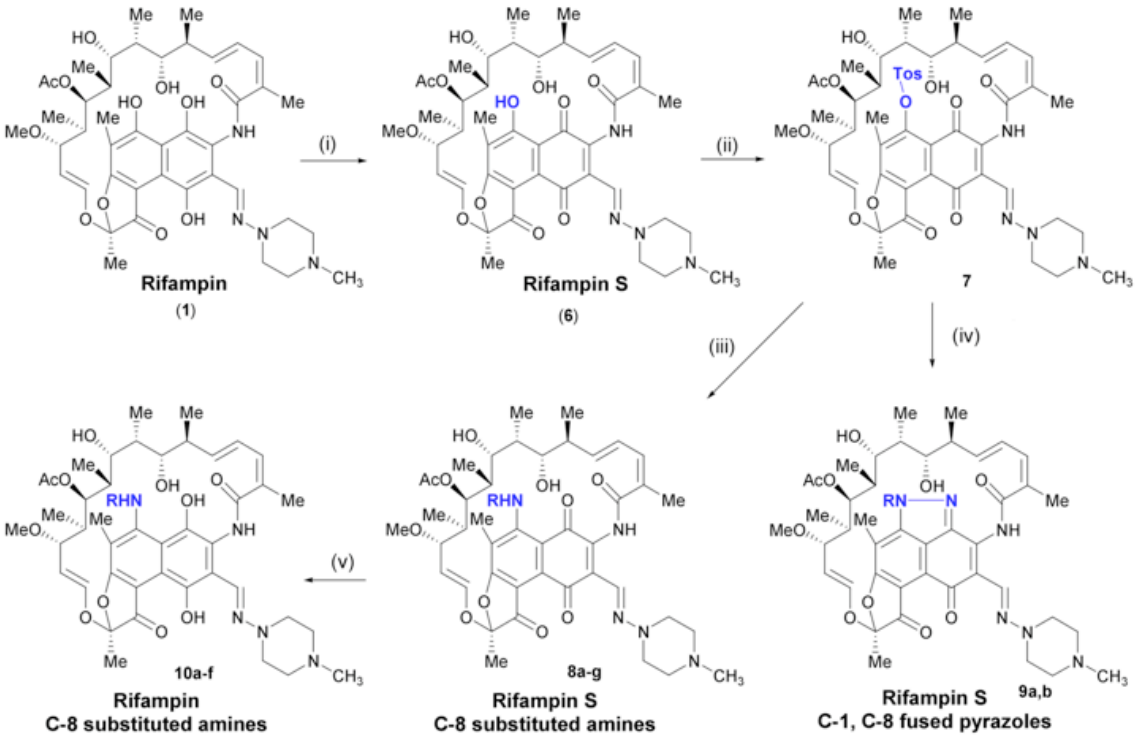

Figure III-2: Synthesis of C-8 analogues of Rifampin and Rifampin S. (The detailed synthesis of these analogues is described in Appendix III-1)

Materials and Methods

Reagents

All of the reagents were the same as the ones specified in Chapter II. The hPXR activation and cell viability in 96-well format assay was from Puracyp, Inc. Rifamycin S was from AAPharmaSyn LLC. Rifampin was from Boche Scientific.

Determination of Minimal Inhibitory Concentration (MIC) of C-8 Analogues Against MTB $H_{37}R_v$ *Strains*

The analogues were screened against the MTB virulent strain ($H_{37}R_v$) under both aerobic and anaerobic conditions (Table III-1). Briefly, the 8-day Microplate Alamar Blue Assay (MABA) (*13*) was used to give an assessment of activity against replicating MTB. The 11-day high-throughput, luminescence-based Low-Oxygen-Recovery Assay (LORA) (*14*) was used to measure activity against bacteria in a non-replicating state that models clinical persistence. Minimum inhibitory concentrations (MIC_{90}) are defined as the lowest compound concentration effecting >90% growth inhibition.

Expression and Purification of WT MTB RNAP and RifR MTB RNAP (Ser450Leu)

Both the WT and RifR MTB RNAP (Ser450Leu) were expressed and purified as described in Chapter II.

Inhibition Studies via Rolling Circle Transcription Assay

The IC_{50} values were determined for RMP (**1**), Rif S (**2**), and RMP S (**6**) and the following C-8 rifamycin analogues: **3, 4a, 4c, 4i, 4j, 7, 9b** (Figures III-1 & III-2, Table III-1). The dose response curves (Figure III-3) were constructed by using the *in vitro* rolling circle transcription assay as described in Chapter II. The assays were performed on Synergy H1 Hybrid Multi-Mode Microplate Reader (BioTek) using 96-well half-area

black plates. Each of the rifamycin analogues was tested in duplicate against the wild-type MTB RNAP and the MTB RNAP (S450L) mutant. The concentration ranges used for the wild-type MTB RNAP were as follows: for **1** (1.56-100 nM); for **2** (3.13-200 nM); for **3** (6.25-400 nM); for **4a** (1.56-100 μM); for **4c** (0.08-5 μM); for **4i** (0.1-800 μM); for **4j** (3.13-200 nM); for **6** (1.56-100 nM); for **7** (25-1600 nM); for **9b** (12.5-800 nM). The concentration ranges used for the MTB RNAP (S450L) mutant were as follows: for **1** (0.02-2.5 mM); for **2** (0.01-2.5 mM); for **3** (0.08-5 mM); for **4a** (0.08-5 mM); for **4c** (0.04-2.5 mM); for **4i** (0.04-2.5 mM); for **4j** (0.01-2.5 mM); for **6** (0.01-2.5 mM); for **7** (0.01-2.5 mM); for **9b** (0.01-2.5 mM). The reaction was allowed to continue for 2 h for WT MTB RNAP or 1.5 h for RifR MTB RNAP (S450L) and aliquots were taken every 30 min and quenched in TE buffer. RiboGreen (an ultrasensitive fluorescent nucleic acid stain) was used to determine the amount of RNA synthesized (λ_{ex}=480 nm; λ_{em}=520 nm). The IC_{50} value for each rifamycins was calculated by non-linear regression as described in Chapter II, and the logIC_{50}s and their standard errors (of the fit) are reported below in Table III-A1 in Appendix III-3.

Minimal Inhibitory Concentration 90% (MIC_{90}) Against E. coli Strains

Initially all analogues were assayed against a WT *E. coli* strain (TG2), a mutant *E. coli* strain (EC2880), and an avirulent strain of *Shigella* (BS103), data not shown. Then the MIC_{90} values of selected rifamycins (reported in Table III-2) were determined for *E. coli* strains DH5α and TG2 (wild-type lab strains) and EC2880 (*tolC*$^-$ mutant, gift of Dr. M. Hubband, Pfizer Inc.). The strains were grown on LB plates. A colony was grown in 2xTY media at 37^{o}C for 3-4 h until the culture reached OD_{625nm} 0.08-0.13. The assays were performed using sterile 96-well polystyrene plates. Each well contained 50 μL

aliquots of culture and 50 μL serial two-fold dilutions of rifamycin analogues (**1, 2, 3, 4a, 4c, 4i, 4j, 6, 7, 9b**). The compounds were initially dissolved in DMSO and then serial dilutions were made in 2xTY media. The concentrations of the rifamycins were 0.049-100 μM for DH5α and TG2 strains and 0.006-12.5 μM for EC2880 strain. The plates were covered and incubated at 37°C for 16-20 h. OD_{600nm} absorbance was measured on Synergy H1 Hybrid Multi-Mode Microplate Reader (BioTek). The error of the reported MIC_{90} values is within one 2-fold dilution.

Human Pregnane X Receptor (hPXR) Activation Assay

The manufacturer's protocol for the hPXR activation and cell viability assay was followed for the 96 well plate assay. Briefly, the DPX2 cells were thawed in a 37°C water bath and mixed thoroughly with culture media. Then 100 μL of cell mixture was transferred into each well and the plate was incubated overnight in a 5% CO_2 incubator at 37°C. The following day, the dosing media was thawed in a 37ºC water bath. The dilutions of rifamycin derivatives (**8a**, **9a**, and **10a**) and RMP (**1**, positive control) were prepared as described in the manual. The 96 well plate was removed from the incubator and liquid from each well was discarded before adding 100 μL of the dilutions to the specific wells. Each dilution of the rifamycin derivative was tested in triplicate. The plate was placed in the 5% CO_2/37ºC incubator again for 24 h. The next day, the CellTiter-Fluor Buffer and CellTiter-Fluor™ were thawed at room temperature before adding 5 μL of CellTiter-Fluor™ to 10 mL of CellTiter-Fluor Buffer. The wells of the 96 well plate were emptied again and 100 μL of CellTiter-Fluor™ reagent was added to each well. The plate was incubated for 1 h in the 5% CO_2/37ºC incubator. The Synergy H1 Hybrid Multi-Mode Microplate Reader (BioTek) was used to measure fluorescence

(λ_{ex}=390 nm; λ_{em}=505 nm). To obtain luminescence readings, the contents of ONE-Glo™ Assay Buffer were added to the ONE-Glo™ Assay Substrate and then 100 µL of mixture was transferred into each well. The plate was read after 5 min where the luminometer was set for 5 sec pre-shake with 5 sec/well read time. The Relative Luminescence Units (RLU) and Relative Fluorescence Units (RFU) were determined as outlined under the "Quantitation of PXR Receptor Activation" section of the manual. The normalized luciferase activity (RLU/RFU) was divided by the normalized DMSO control to represent the data as 'fold activation' relative to the control. The replicate data points were averaged and both the original data points and the average values were plotted as a function of log concentration versus hPXR Activation. The average values were then fit by non-linear regression to a modified four parameter logistic equation using Kaleidagraph (Synergy Software, Essex, VT):

$$y = 1+ [(M3– 1)/(1 + 10^{[(M1-M0)*M2]})],$$

where M3 is the E_{MAX}, and 1 is the lower limit of the assay, M0 is the log of the rifamycin concentration, M1 is the log of the EC_{50}, and M2 is the Hill slope. The data were normalized such that the lower limit was set to 1. M1, M2, and M3 were fit by the regression.

Chemistry and Synthesis of C-8 Analogues

All of the C-8 rifamycin analogues were synthesized by Ms. Yafei Jin and Prof. Hollis Showalter. See Appendix III-1 for details.

Structure-based Modeling Studies

The structure-based modeling was performed by Dr. Paul Kirchhoff. See Appendix III-2 for details.

Results

MIC_{90} values of C-8 Analogues Against MTB $H_{37}R_v$ *Strains*

The antitubercular activity of these C-8 Rif S and RMP analogues was assessed via MABA and LORA (Table III-1). Under aerobic conditions within the Rif S series (MABA), analogues incorporating C-8 amine substituents (**4a** – **4j**) displayed modest MIC_{90} values (1.4 – >5.6 μM) relative to the parent Rif S (**2**) (0.03 μM). A similar pattern of activity was observed under anaerobic conditions (LORA). The LORA MIC_{90} values were ~3 to 16 fold greater than the MABA MIC_{90} values, and only analogue **4c** displayed modest activity (5.4 μM). The thioether derivative (**4j**) within the Rif S series was the only analogue with modest (and essentially equivalent) potency in both MABA and LORA (2.0 μM vs. 1.3 μM, respectively). Amine adducts within the RMP S (**8a** – **8f**) and RMP (**10a** – **10f**) series displayed similar potencies as the Rif S series in the MABA (MIC_{90} values 3.6 – >4.7 μM) and the LORA (MIC_{90} values 13.7 – >19.2 μM), with a 3.5 – > 5 fold differential between the two assays. Core-modified pyrazole analogues within both Rif S (**5**) and RMP S (**9a**, **9b**) series are weakly to moderately active with MIC_{90} values of 3.9 – >5.4 μM in the MABA and >18.6 μM in the LORA. Surprising and especially noteworthy are the potencies of the tosylated intermediates. Rif S tosylate (**3**) exhibited MIC_{90} values of 0.20 μM in the MABA and 3.0 μM in the LORA, and the MIC_{90} values for RMP S tosylate (**7**) were 0.24 μM and 4.8 μM, respectively. To determine if these values were due to a prodrug effect from simple sulfonate hydrolysis to parent compounds **2** and **6**, respectively, we subjected each tosylate to conditions utilized for MIC determinations (2xTY media, 37ºC, 24 h) and the RNAP assay (RNAP 5X reaction buffer, 37ºC, 2 h). At the end of the assay period, the

medium was extracted with ethyl acetate and the organic extract was analyzed by thin-layer chromatography for the presence of either parent phenol or corresponding tosylate. In all cases, only the presence of tosylate was observed.

Table III-1. Screening Results of Rifamycin Analogues vs. MTB

No.	Class	C-8 Substituent	MTB MIC_{90} (μM)[a]	
			MABA	LORA
2	Rif S	hydroxyl	0.03	0.4
3	Rif S	tosyloxy	0.20	3.0
4a	Rif S	amino	1.41	22.2
4b	Rif S	methylamino	> 5.6	20.6
4c	Rif S	dimethylamino	1.8	5.4
4d	Rif S	ethylamino	5.5	21.4
4e	Rif S	methoxyamino	3.8	12.5
4f	Rif S	N-(2-propenyl)amino	5.2	18.3
4g	Rif S	(2-hydroxyethyl)amino	5.32	> 21.7
4h	Rif S	benzylamino	2.4	> 20.4
4i	Rif S	cycloheptylamino	2.2	> 20.2
4j	Rif S	methylthio	2.0	1.3
5	Rif S pyrazole	2-hydroxyethyl	> 5.4	> 21.7
6	RMP S	hydroxyl	0.07	0.5
7	RMP S	tosyloxy	0.24	4.8
8a	RMP S	methylamino	3.64	> 19.2
8b	RMP S	ethylamino	> 4.7	> 18.9
8c	RMP S	N-(2-propenyl)amino	> 4.7	> 18.6
8e	RMP S	(2-hydroxyethyl)amino	> 4.6	> 18.5
8f	RMP S	benzylamino	> 4.4	> 17.6
8g	RMP S	cycloheptylamino	3.9	13.7
9a	RMP S	methyl	> 4.8	> 19.3
9b	RMP S	2-hydroxyethyl	3.9	> 18.6
10a	RMP	methylamino	4.0	> 19.1
10b	RMP	ethylamino	> 4.7	> 18.8
10c	RMP	N-(2-propenyl)amino	> 4.6	> 18.6
10d	RMP	(2-hydroxyethyl)amino	> 4.6	> 18.5
10e	RMP	benzylamino	> 4.4	> 17.5
10f	RMP	cycloheptylamino	3.8	> 17.4
1 (RMP)		hydroxyl	0.13	1.9
Isoniazid		N/A[b]	0.39	> 128
PA824		N/A	0.66	2.3
Moxifloxacin		N/A	0.64	4.3

[a] The MIC_{90} is defined as the minimum concentration of the compound required to inhibit 90% of bacterial growth; [b] N/A = not applicable

Inhibition Studies via Rolling Circle Transcription Assay

The inhibition of WT MTB RNAP and RifR MTB RNAP (S450L) by these novel C-8 rifamycin derivatives was assessed via dose-response studies. Each analogue was tested in duplicate in dilutions ranging in concentrations specified in the Materials and Methods section. The data were plotted (log rifamycin concentration vs. % activity) and then fit by nonlinear regression (Figure III-3), and the apparent IC_{50} values are listed in Table III-2. For the WT MTB RNAP, RMP (**1**), Rif S (**2**), thioether **4j** and RMP S (**6**) show the highest potency with IC_{50} values in the low nM range. The IC_{50} values for RMP (**1**) and Rif S (**2**) were determined to be less than 10 nM. However, the amount of enzyme used in each reaction was 10 nM (the lowest concentration that could be used confidently). Under these conditions, it is possible that a 10 nM IC_{50} value may simply reflect the "titration" of the enzyme by an inhibitor with a much lower true IC_{50} value.

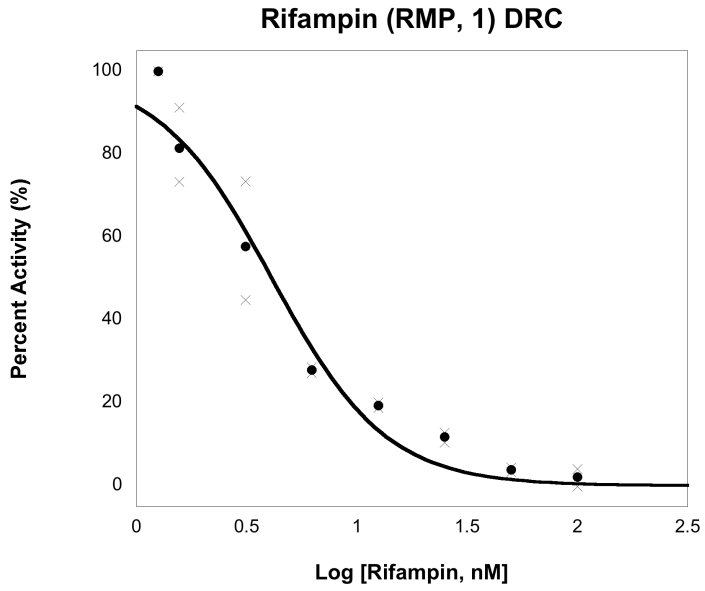

Figure III-3: Example of a Dose-Response Curve. All of the individual data point (x) and the average data points (•) were plotted. The average data were fit by nonlinear regression to determine the IC_{50} values.

Therefore, any IC_{50} value determined to be less than 10 nM was reported simply as "< 0.01" μM.

As mentioned above, the tosylated intermediates **3** & **7** have comparable MTB MIC_{90} values for both MABA and LORA; however, the IC_{50} value with WT MTB RNAP for **7** was ~7-fold greater than that for **3**. The IC_{50} value of **3** (21 nM) was >2-fold greater than the IC_{50} value of Rif S (<10 nM) with the WT MTB RNAP. Owing to the fact that the MABA MIC_{90} value for **3** was 5-fold greater than that for Rif S, a parallel decrease in potency was observed for both the MIC_{90} and IC_{50} values for **3** in comparison with Rif S. However for compound **7**, this trend was not as quantitative. The IC_{50} value with WT MTB RNAP for **7** (142 nM) was more than 10-fold greater than the IC_{50} value for RMP S (13 nM); whereas, the MABA MIC_{90} value of **7** was only ~3-fold greater than that for RMP S. Surprisingly for the MTB RNAP (S450L) mutant, a lower IC_{50} value was observed for **7** (~9 fold lower) than the IC_{50} value of **3**. Within the Rif S series, the amino analogues (**4a, 4c,** and **4i**) that had exhibited modest MIC_{90} values under aerobic conditions have much more variable IC_{50} values (~70-2000 fold greater than Rif S). These analogues have comparable IC_{50} values against the MTB RNAP (S450L) mutant, which are still 3-8 fold greater than Rif S. The thioether derivative (**4j**) also exhibited modest MABA MIC_{90} values, but the IC_{50} values are comparable to the IC_{50} values observed for the controls (**1, 2, 6**) with both WT MTB RNAP and the mutant. Although the pyrazole analogue (**9b**) was weakly active microbiologically with higher MTB MIC_{90} values, the IC_{50} value is comparable to that observed for **7** for WT MTB RNAP (both about 10-20 fold higher than those for RMP, RMP S and Rif S). In general, all rifamycin

analogues have MTB MIC_{90} values that are higher than their IC_{50} values for the MTB RNAP with the exception of **4i**.

Table III-2. Selected Rifamycins vs. MTB RNAP and *E. coli*

No.	IC_{50} (μM)[a] (WT MTB RNAP)	IC_{50} (μM)[a] (MTB RNAP (S450L))	*E. coli* MIC_{90} (μM)[b]		
			TG2	DH5α	EC2880
1	< 0.01	52.1	12.5	12.5	0.1
2	< 0.01	36.0	100	> 100	0.78
3	0.021	982	> 100	> 100	3.125
4a	4.4	186	> 100	> 100	12.5
4c	0.503	270	> 100	> 100	12.5
4i	15.4	127	> 100	> 100	> 12.5
4j	0.015	37.5	> 100	> 100	> 12.5
6	0.013	46.5	12.5	25	0.1
7	0.142	111	> 100	> 100	12.5
9b	0.139	29.9	> 100	> 100	> 12.5

[a] The IC_{50} is defined as the concentration that results in 50% inhibition of transcription. The log IC_{50} values and their standard errors (of the fit) are reported in Table III-A1 in Appendix III-3.
[b] The MIC_{90} is defined as the minimum concentration of the compound required to inhibit 90% of bacterial growth

MIC_{90} values of C-8 Analogues Against E. coli Strains

The MIC_{90} values of a subset of C-8 analogues were determined using WT *E. coli* strains (TG2 and DH5α) and a mutant *E. coli* strain (EC2880-"permeable" strain, *tolC*$^-$ and *imp*$^-$) (Table III-2). The *E. coli* MIC_{90} value for compound **3** was only 4-fold greater than that observed for Rif S, which parallels compound **3**'s IC_{50} value that is 3-4 higher than that for Rif S. Interestingly, the analogues with MTB MABA MIC_{90} values of 1.8 μM or lower had *E. coli* MIC_{90} values of 12.5 μM or less for the mutant strain but no correlation could be made for WT *E. coli* strains.

Human Pregnane X Receptor (hPXR) Activation Assay

To assess the ability of specific rifamycins to activate the human pregnane X receptor (hPXR), the hPXR activation assay system from Puracyp, Inc. was used. The results are shown in Figure III-4 and Table III-3 for analogues **8a**, **9a**, and **10a**.

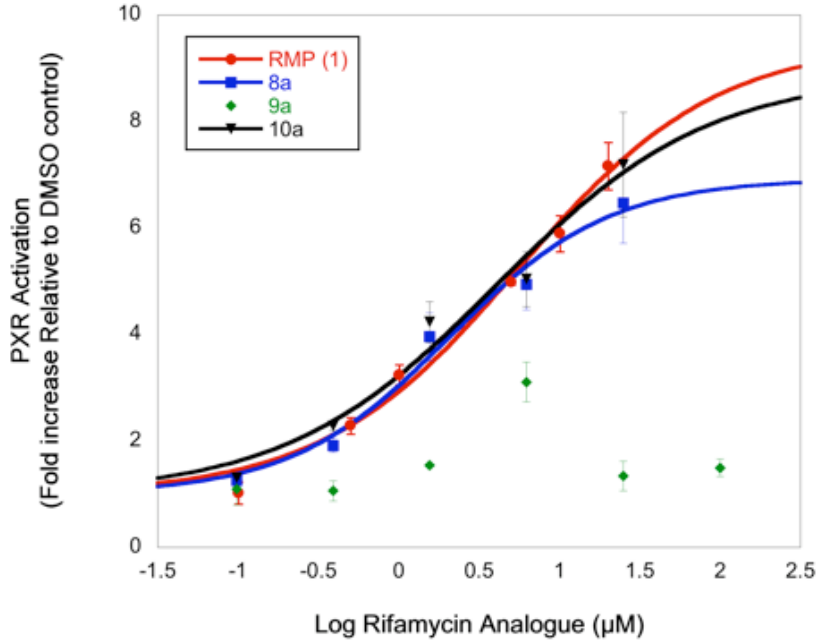

Figure III-4: The hPXR Activation Assay. Concentrations of positive control (RMP, red) and selected rifamycin analogues (**8a**, **9a**, and **10a**, blue, green and black respectively) versus fold PXR activation.

RMP exhibited a high maximal degree of activation (9.5 fold) and an EC_{50} of 5.6 μM (Figure III-4 left). The methylamino derivatives of RMP S (**8a**) and RMP (**10a**) were fit to a dose-response curve that revealed a 6.9 and 8.9-fold maximal activation of hPXR and an EC_{50} of 2.1 and 4.1 μM, respectively (Figure III-4 right; Table III-3). These analogues did exhibit loss of cell viability at 25 μM (such that the 100 μM data point was not used in the dose-response curve fit). The RMP S pyrazole derivative (**9a**) showed ~2 fold hPXR activation at 6.25 μM and dramatic loss of cell viability above 6.25 μM (such

that no hPXR activation was seen). The loss of cell viability could be observed from the lower RFU values obtained from the assay (Table III-4).

Table III-3. PXR Activity of Selected Rifamycin Analogues

No.	EC_{50} (μM)[a]	E_{MAX}[b] (fold increase)
1	5.6	9.5
8a	2.1	6.9
9a	-	-
10a	4.1	8.9

[a] EC_{50} is defined as the half maximal effective concentration.
[b] EC_{MAX} is the maximal effective concentration of the compound.

Table III-4. Mean Relative Fluorescence Units (RFU)[a] for RMP (**1**) and C-8 Analogues (**8a**, **9a**, **10a**) in the hPXR Activation Assay

Conc (μM)	RMP (1) (n=2)	Conc (μM)	8a (n=3)	9a (n=3)	10a (n=3)
20	39860	**100**	10339	5139	4510
10	43506	**25**	29469	6083	20902
5	46648	**6.25**	46186	33527	38109
1	45714	**1.56**	44676	39444	39274
0.5	42223	**0.39**	49578	48660	41326
0.1	46084	**0.098**	48519	47122	44851

[a] RFU is a measure of cell viability in the assay. For controls, 1% DMSO = 46021; Dosing media = 42907.

Structure-based Modeling Studies

Modeled poses were generated by Dr. Kirchhoff for each of the analogues listed in Table III-2. Modeling was based on the 2.5 Å resolution structure of rifabutin complexed with the *Thermus thermophilus* RNAP holoenzyme (PDB ID: 2a68) (*11*) and described more in detail in Appendix III-2. Modeled poses for Rif S (**2**) and amino analogue (**4i**) are shown in Figure III-5. RNAP is shown as a molecular surface within 5 Å of the inhibitors and shaded to indicate areas of lipophilicity (green), hydrogen bonding

(magenta) and mild polar (blue). This figure illustrates how the loss of the C-8 hydroxyl is a potential loss of a hydrogen bond contact with RNAP.

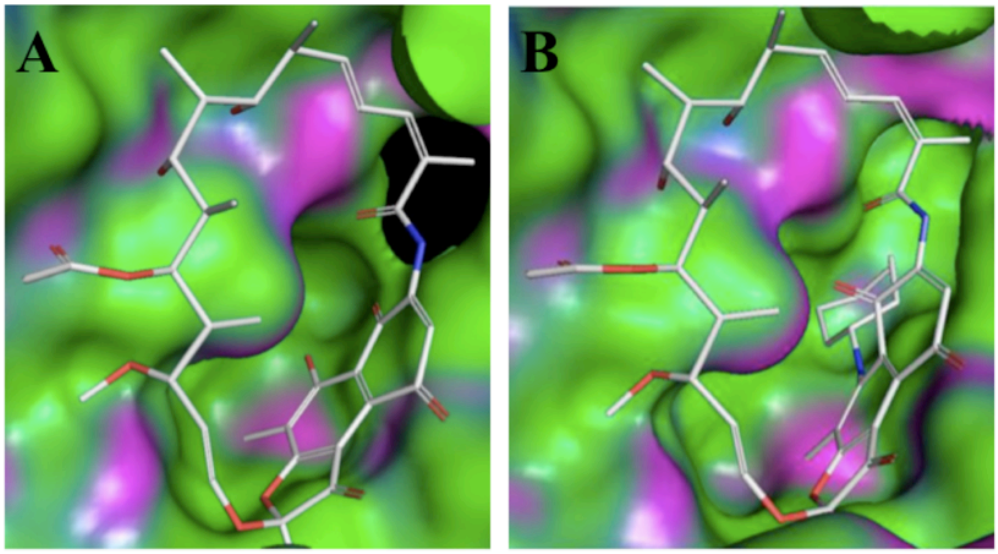

Figure III-5: RNAP is shown as a molecular surface within 5 Å of the inhibitors (carbon atoms shown in gray) and shaded to indicate areas of lipophilicity (green), hydrogen bonding (magenta) and mild polar (blue). (A) Rif S (**2**). (B) Cycloheptylamino analogue (**4i**).

Discussion

Previously, the acetylation of the C-8 hydroxyl has led to an inactive rifamycin derivative (*12*); however, this position has not been fully investigated. No C-8 rifamycin analogues derived from amine or sulfur nucleophiles have been reported other than the synthesis of Rif S ammonia adduct **4a** reported in the patent literature (*15*). Additionally, there is no account of any ring fusions onto the 1,8-carbon positions. Hence the syntheses of pyrazoles **5**, **9a**, and **9b** represent the first reports of such a core modification. Herein, we explore the SAR of the C-8 position by incorporating 8-amino, 8-thio, and 1,8-pyrazole substituents.

The MIC_{90} values of these C-8 analogues against WT MTB $H_{37}R_V$ strains were determined at the Institute for Tuberculosis Research (ITR/UIC) using Microplate Alamar Blue Assay (MABA) and Low Oxygen-Recovery Assay (LORA), where the latter assay is a model for the latent form of MTB. The MIC_{90} values (for both MABA and LORA) were higher for the amine and pyrazole derivatives compared to their parent scaffolds. The unsubstituted NH_2 analogue (compare **4a** vs. **4b** – **4i**) was observed to be the best within this small series, although there is no significant variation from the smallest to the largest substituent. The addition of small polar functionality (e.g., **4e**, **4g**) or bulky lipophilic moieties (e.g., **4h**, **4i**) seemed to impart minimal effect on potency. However, the tosylated (**3** and **7**) and thioether (**4j**) derivatives displayed surprisingly low MIC_{90} values (but still higher than parent scaffolds), which are corroborated by excellent potency toward the target RNAP enzyme. In general, enhanced antitubercular activity was not observed with these C-8 analogues.

From the crystal structure of RMP bound to *Thermus aquaticus* RNAP, it was observed that there are twelve β residues in close proximity that directly interact with RMP (*10*). Mutations of most of these residues lead to RifR RNAPs. The most frequently mutated residue found in MTB clinical isolates is the Ser450 residue, which directly interacts with the C-8 hydroxyl via hydrogen bond (*10, 16*). Therefore, these C-8 rifamycin analogues were screened against both WT MTB RNAP and RifR RNAP (Ser450Leu) via an *in vitro* rolling circle transcription assay. As shown in Table III-2, the control rifamycins (**1**, **2**, and **6**) inhibited WT MTB RNAP in the 10^{-9} M (nM) range; whereas, the IC_{50} values for the RifR MTB RNAP (Ser450Leu) were in the 10^{-6} M (μM) range (consistent with what has been observed previously (*17*)). Unfortunately, no

analogues tested here resulted in a more potent rifamycin derivative against the RifR MTB RNAP (S450L) mutant.

All rifamycin analogues have MTB MIC_{90} values that are higher than their IC_{50} values for the MTB RNAP with the exception of **4i**. This differential between IC_{50} and MTB MIC_{90} may be due in some cases (where the differential is large) to the molecules not equilibrating efficiently across the cell envelop or to the more trivial explanation (in cases where the differential is small) that the IC_{50} is a 50% inhibition point whereas the MIC_{90} is a 90% inhibition point. In the case of **4i**, the analogue has an MTB MIC_{90} that is approximately 8-fold smaller than the IC_{50}. One possibility is that the cycloheptyl moiety of **4i** may help to concentrate the analogue within the MTB cell.

In addition to determining the MTB MIC_{90} values, the MIC_{90} values for WT *E. coli* strains (DH5α and TG2) and mutant *E. coli* strain (EC2880-*tolC* deficient) were determined for select C-8 analogues (Table III-2). The MIC_{90} values were lower for the mutant strain compared to the WT strains, but these values were still higher than the values observed for the control compounds (**1**, **2**, and **6**). This observation is consistent with previous postulates that the lower sensitivity of Gram-negative bacteria to rifamycins is due to the removal of rifamycins from the interior of the cell via TolC-dependent efflux pumps.

One of the clinical liabilities of RMP (**1**) includes its induction of cytochrome P450 3A4 (CYP3A4), which is mediated by the human pregnane X receptor (PXR) (*1, 8*). Activation of hPXR was seen for the representative analogues (**8a**, **9a**, and **10a**) to a certain concentration before cytotoxicity was observed at higher concentrations. From this data, it seems unlikely that any of these analogues are Cyp inhibitors.

To gain better understanding of the SAR, structure-based modeling studies were conducted. Modeling was based on the 2.5 Å resolution structure of rifabutin complexed with the *Thermus thermophilus* RNAP holoenzyme (PDB ID: 2a68) (*11*). Since the rifamycin binding site is highly conserved among bacteria, this structure provides a good foundation for understanding how proposed rifamycin analogues may interact with the MTB RNA polymerase.

Conclusions

In summary, a novel series of rifamycin S and rifampin analogues incorporating substituted 8-amino, 8-thio, and 1,8-pyrazole substituents were synthesized. The compounds were screened for inhibition of WT MTB RNAP and RifR MTB RNAP (S450L) as well as antitubercular effects under both aerobic and anaerobic conditions. The data show that our modification of the C-8 position of the parent scaffolds resulted in diminished activity. The enzymatic and microbiological data are consistent with modeling and computational studies which support the C-8 hydroxyl acts as a hydrogen bond acceptor/donor with S450 and that Rif resistance in the S450L mutant is due to loss of this hydrogen bond.

Notes to Chapter III

We gratefully acknowledge Yafei Jin and Dr. Hollis Showalter for the synthesis and characterization of the C-8 analogues. We thank Dr. Scott Franzblau (Institute for Tuberculosis Research at University of Illinois at Chicago) for providing the antitubercular activity data. We would also like to thank Dr. Paul Kirchhoff for his contribution with the structural studies/models. We acknowledge generous support by the University of Michigan College of Pharmacy, Ella and Hans Vahlteich and UpJohn Research Funds. We would also like to acknowledge additional funding by the University of Michigan, Office of the Vice President for Research, and the Rackham Graduate School. The EC2880 strain (permeable strain with *tolC*$^-$ and *imp*$^-$ mutations) was a generous gift from Dr. Michael Hubband (Pfizer Scientific).

The work described in this chapter was published in *Bioorganic & Medical Chemistry Letters* (Jin, Y., Gill, S.K., Kirchhoff, P.D., Wan, B., Franzblau, S.G., Garcia, G.A., and Showalter, H.D.H. "Synthesis and Structure-Activity Relationships of Novel Substituted 8-Amino-and 1,8-Pyrazole Congeners of the Antituberculars Rifamycin S and Rifampin" *Bioorganic and Medicinal Chemistry Letters* (2011) **21** p. 6094-6099).

Abbreviations used: TB, tuberculosis; RMP, rifampin; RNAP, DNA-dependent RNA polymerase; Rif S, rifamycin S; RMP S, rifampin S; WT, wild-type; RifR, Rifamycin-resistant; MTB, *Mycobacterium tuberculosis*; MDR, multi-drug resistant TB strain; XDR, extensively-drug resistant TB strains; NTP, ribonucleotide triphosphate; IPTG, isopropyl β-D-thiogalactoside; SDS-PAGE, sodium dodecyl sulfate polyacrylamide gel electrophoresis; PMSF, phenylmethylsulfonyl fluoride; EDTA, ethylenediaminetetraacetic acid; DTT, dithiothreitol; RNA, ribonucleic acid; MABA, Microplate Alamar Blue Assay; LORA, Low Oxygen-Recovery Assay; IC_{50}, concentration of rifamycin resulting in 50% inhibition of transcription; MIC_{90}, concentration of rifamycin that results in 90% inhibition of bacterial growth; CYP3A4, cytochrome P450 3A4; hPXR, human pregnane X receptor; EC_{50}, half maximal effective concentration; EC_{MAX}, maximal effective concentration of the compound; RFU, relative fluorescence units; RLU, relative luminescence units

Appendix III-1

Chemistry

Our strategy was to first activate the C-8 peri-phenolic functionality of readily available Rif S (**2**) as a sulfonate ester, and then displace this with selected nitrogen nucleophiles through an addition-elimination mechanism (Figure III-1). Given that the rifamycin framework is embellished with so much functionality, including free hydroxyl groups at C-21 and C-23 (Figure III-5), we first needed to work out conditions for selective functionalization of the C-8 phenolic moiety. Thus, the reaction of Rif S (**2**) with sulfonyl chlorides representing a range of reactivity (*p*-toluenesulfonyl, *p*-chlorosulfonyl, methanesulfonyl) and triflic anhydride was evaluated under different temperature and solvent conditions. Of these, only *p*-toluenesulfonyl and *p*-chlorosulfonyl sulfonate esters formed cleanly under optimum conditions (Hunig's base, acetonitrile, room temperature) with tosylate **3** formed in 84% yield. Subsequent reactions of these with amines and hydrazines indicated that the *p*-chlorosulfonate ester was susceptible to cleavage to Rif S, whereas the *p*-toluenesulfonate ester provided the desired C-O bond displacement. With this finding, condensation of **3** was then carried out with a range of amines to provide adducts **4a**-**4i** in 11-51% yields, and with (2-hydroxyethyl)hydrazine to give annulated pyrazole product **5** in very low (5%) yield. We also tested tosylate displacement with a single thiol (methanethiol sodium salt), which provided analogue **4j** in poor yield. Having developed the chemistry for Rif S, we then applied it toward making related analogues of RMP (**1**, Figure III-2). Thus, oxidation of RMP with potassium ferricyanide provided rifampin S (RMP S, **6**) in 65% yield. Tosylation of the 8-hydroxyl function was conducted as described above to give

key intermediate **7** in nearly quantitative yield. Amination of **7** was then carried out with several of the same amines utilized above to give adducts **8a** – **8f** in 35-60% yields and pyrazoles **9a** (33% yield) and **9b** (40% yield). Disappointingly, an attempt to make the simple unsubstituted pyrazole congener derived from hydrazine was unsuccessful. Similarly, we were unable to secure a highly sought for analogue derived from ammonia displacement of tosylate **7**. Utilizing the same conditions that gave **4a** led to a product in 46% yield that both mass spec and NMR data showed incorporation of the NH_2 function, but without loss of the C-8 tosyloxy moiety. The NMR spectrum was too complex to make a definitive structural assignment. Candidate possibilities include Michael addition of ammonia to the dienone function or to the imino double bond of the side chain hydrazone. The quinone function of each RMP S amine adduct was then reduced with ascorbic acid to the hydroquinone form, providing corresponding RMP C-8 amine congeners **10a** – **10f** in 51 – 93% yield. The full range of synthesized compounds is shown in Table III-1.

No effort was made to optimize the reaction conditions that provided amine, thiol, or pyrazole adducts from tosylates **3** or **7**, and product yields in general represent a single run for each target compound. All compounds were rigorously purified by preparative silica gel chromatography, and their structural assignments were supported by diagnostic peaks in the ^{1}H NMR spectra and by mass spectrometry.

General Chemical Methods.

^{1}H NMR spectra were recorded on Bruker 500 MHz and Varian 300 MHz spectrometers. Chemical shifts are reported in δ (parts per million: ppm), by reference to the hydrogen residues of deuterated solvent as internal standard ($CDCl_3$: δ = 7.28 ppm;

CD_3OD: δ = 3.31). Signals are described as s, d, t, dd, m, and dt for singlet, doublet, triplet, doublet of doublets, multiplet, and doublet of triplets, respectively. All coupling constants (*J*) are given in Hertz (Hz). Mass spectra were recorded on a Micromass LCT time-of-flight instrument utilizing the electrospray ionization mode. Reactions were monitored by thin-layer chromatography (TLC) using pre-coated silica gel 60 F254 plates. Chromatography was performed with silica gel GHLF plates (250 microns). Rifamycin S was obtained from AAPharmaSyn, Ann Arbor, MI, and rifampin from Bosche Scientific. Reagents and monomers were purchased from common vendors and were used without purification. Glassware was oven-dried before use for reactions run under anhydrous conditions.

8-(*p*-Toluenesulfonyloxy)rifamycin S (3)

Into an ice-cold solution of rifamycin S (**2**, 696 mg, 1.0 mmol) in acetonitrile (5 mL) was added diisopropylethylamine (155 mg, 1.2 mmol). Then, *p*-toluenesulfonyl chloride (210 mg, 1.1 mmol) was added to the reaction mixture portion-wise. This resultant mixture was slowly warmed to room temperature. After stirring for 2 h, it was diluted with dichloromethane (40 mL). This solution was washed with 1N aqueous NH_4Cl (3 x 30 mL), followed by saturated brine (30 mL), dried over anhydrous sodium sulfate and evaporated *in vacuo* to dryness to yield **3** as a light brown solid (717 mg, 84%). The compound was utilized without further purification. ESI MS: *m/z* 872.2 ($M+Na^+$). ^1H NMR (500 MHz, $CDCl_3$): δ 8.28 (s, 1H), 7.90 (d, *J* = 8.2 Hz, 2H), 7.84 (s, 1H), 7.41 (d, *J* = 8.1 Hz, 2H), 6.39 (dd, *J* = 10.5, 15.7 Hz, 1H), 6.24 (d, *J* = 10.5 Hz, 1H), 6.15 (dd, *J* = 6.8, 15.3 Hz, 1H), 5.98 (d, *J* = 12.3 Hz, 1H), 5.10 (dd, *J* = 4.8, 12.3 Hz, 1H), 4.95 (d, *J* = 10.3 Hz, 1H), 3.88 (d, *J* = 4.3 Hz, 1H), 3.69 (d, *J* = 9.7 Hz, 1H), 3.37 (br

s, 2H), 3.07 (s, 3H), 3.00 (d, *J* = 7.7 Hz, 1H), 2.50 (s, 3H), 2.34 (m, 1H), 2.18-2.02 (complex pattern), 1.78 (s, 3H), 1.67 (m, 2H), 1.26 (m, 1H), 1.08 (d, *J* = 6.7 Hz, 3H), 0.87 (d, *J* = 6.9 Hz, 3H), 0.68 (d, *J* = 6.8 Hz, 3H), 0.06 (d, *J* = 7.0 Hz, 3H).

8-(Methylamino)rifamycin S (4b)

Methylamine (105 μL of 2 M solution in THF, 0.21 mmol) was added drop-wise to an ice-cold solution of 8-(tosyloxy)rifamycin S (**3**; 170 mg, 0.2 mmol) in acetonitrile (5 mL). The resulting mixture was stirred at room temperature for 18 h before being diluted with dichloromethane (25 mL). This solution was washed with 1 N aqueous NH_4Cl (2 x 15 mL) followed by saturated brine (15 mL), dried over anhydrous sodium sulfate and concentrated to yield a crude black solid (150 mg). Purification by preparative TLC (1:3 hexanes / ethyl acetate, v/v) afforded **4b** as a dark purple solid (57 mg, 40 %). ESI MS *m/z* 709.1 ($M+H^+$). ^1H NMR (300 MHz, $CDCl_3$): δ 10.02 (m, 1H), 8.55 (s, 1H), 7.74 (s, 1H), 6.41 (dd, *J* = 10.6, 15.6 Hz, 1H), 6.24 (m, 2H), 6.02 (dd, *J* = 6.6, 15.4 Hz, 1H), 5.06 (dd, *J* = 7.6, 8.3 Hz, 1H), 4.72 (d, *J* = 10.5 Hz, 1H), 3.88 (d, *J* = 4.3 Hz, 1H), 3.65 (d, *J* = 9.7 Hz, 1H), 3.55 (s, 1H), 3.37 (d, *J* = 5.4 Hz, 3H), 3.13 (s, 3H), 3.00 (m, 1H), 2.53 (s, 3H), 2.39 (m, 1H), 2.13 (m, 1H), 2.07 (s, 3H), 2.05-1.90 (complex pattern), 1.79 (m, 3H), 1.71 (s, 3H), 1.64-1.49 (complex pattern), 1.03 (d, *J* = 7.0 Hz, 3H), 0.86 (d, *J* = 6.9 Hz, 3H), 0.69 (d, *J* = 6.9 Hz, 3H), 0.28 (d, *J* = 7.1 Hz, 3H).

Prepared in similar fashion were the following rifamycin S analogues:

8-Aminorifamycin S (4a)

From 7N ammonia in methanol, crude product was obtained as a deep red solid. Purification by preparative TLC (1:1 hexanes / ethyl acetate) gave **4a** as an orange solid (15 mg, 11%). ESI MS: *m/z* 717.3 ($M+Na^+$). ^1H NMR (300 MHz, $CDCl_3$): δ 8.62 (s,

1H), 7.79 (s, 1H), 6.40 (dd, *J* = 10.2, 15.6 Hz, 1H), 6.25 (d, *J* = 10.4 Hz, 1H), 6.20 (d, *J* = 12.4 Hz, 1H), 6.01 (dd, *J* = 6.7, 15.5 Hz, 1H), 5.07 (dd, *J* = 7.1, 12.4 Hz, 1H), 4.71 (d, *J* = 10.8 Hz, 1H), 3.81 (d, *J* = 3.7 Hz, 1H), 3.65 (m, 2H), 3.39 (dd, *J* = 2.5, 7.6 Hz, 1H), 3.11 (s, 3H), 2.99 (m, 3H), 2.40-1.59 (complex pattern), 1.03 (d, *J* = 6.9 Hz, 3H), 0.87 (d, *J* = 6.9 Hz, 3H), 0.69 (d, *J* = 6.8 Hz, 3H), 0.24 (d, *J* = 7.0 Hz, 3H).

8-(Dimethylamino)rifamycin S (4c)

From dimethylamine (5.6M in ethanol), crude material was obtained as a purple solid. Purification by preparative TLC (1:1 hexanes / ethyl acetate) gave **4c** as a purple-red solid (29 mg, 80%). ESI MS: *m/z* 723.0 ($M+H^+$). ^{1}H NMR (300 MHz, CD_3Cl): δ 8.59 (s, 1H), 7.76 (s, 1H), 6.53 (dd, *J* = 11.9, 15.8 Hz, 1H), 6.26 (d, *J* = 12.1 Hz, 1H), 6.23 (dd, *J* = 6.9, 15.8 Hz, 1H), 6.10 (d, *J* = 12.3 Hz, 1H), 5.10 (dd, *J* = 5.1, 12.3 Hz, 1H), 5.00 (d, *J* = 10.3 Hz, 1H), 4.03 (d, *J* = 4.1 Hz, 1H), 3.74 (d, *J* = 9.6 Hz, 1H), 3.60 (s, 1H), 3.51 (m, 1H), 3.11 (s, 3H), 3.05 (s, 6H), 3.01 (m, 1H), 2.37 (s + m, 3H + 1H), 2.09 (s, 3H), 2.08 (s, 3H), 1.83-1.69 (complex pattern), 1.03 (d, *J* = 7.0 Hz, 3H), 0.91 (d, *J* = 6.9 Hz, 3H), 0.71 (d, *J* = 6.8 Hz, 3H), 0.20 (d, *J* = 7.0 Hz, 3H).

8-(Ethylamino)rifamycin S (4d)

From ethylamine, crude product was obtained as a purple solid. Three purifications by preparative TLC (1:1 hexanes / ethyl acetate) gave **4d** as a deep red solid (46.4 mg, 29 %). ESI MS: *m/z* 723.1 ($M+H^+$). ^{1}H NMR (300 MHz, CD_3OD): δ 7.60 (s, 1H), 6.32 (m, 1H), 6.31 (s, 1H), 6.27 (d, *J* = 11.9 Hz, 1H), 6.02 (m, 1H), 5.22 (dd, *J* = 6.5, 11.2 Hz, 1H), 5.08 (d, *J* = 10.8 Hz, 1H), 4.95 (d, *J* = 6.5 Hz, 1H), 4.83 (s, 1H), 3.82 (m, 4H), 3.33 (m, 2H), 3.14 (m, 1H), 3.10 (s, 3H), 2.51 (s, 3H), 2.35 (m, 1H), 2.12 (m, 1H), 2.05 (s, 3H), 1.99 (s, 3H), 1.85-1.56 (complex pattern), 1.36 (tr, d = 7.1 Hz, 3H),

1.02 (d, *J* = 7.1 Hz, 3H), 0.90 (d, *J* = 6.9 Hz, 3H), 0.72 (d, *J* = 6.9 Hz, 3H), 0.16 (d, *J* = 7.1 Hz, 3H).

8-(Methoxyamino)rifamycin S (4e)

From methoxylamine hydrochloride and N,N-diisopropylethylamine, crude product was obtained as a deep red solid. Purification by preparative TLC (1:1 hexanes / ethyl acetate) gave **4e** as a deep red solid (9 mg, 27 %). ESI MS: *m/z* 725.0 ($M+H^+$). ^1H NMR (500 MHz, $CDCl_3$): δ 11.86 (s, 1H), 8.50 (s, 1H), 7.78 (s, 1H), 6.42 (dd, *J* = 10.0, 15.6 Hz, 1H), 6.28 (d, *J* = 10.0 Hz, 1H), 6.23 (d, *J* = 12.5 Hz, 1H), 6.01 (dd, *J* = 6.6, 15.6 Hz, 1H), 5.10 (dd, *J* = 7.5, 12.3 Hz, 1H), 4.74 (d, *J* = 10.4 Hz, 1H), 4.25 (m, 1H), 3.86 (s, 3H), 3.72 (m, 3H), 3.63 (m, 2H), 3.50 (m, 1H), 3.39 (m, 1H), 3.14 (s, 3H), 3.01 (m, 1H), 2.50 (s, 3H), 2.37 (m, 1H), 2.10-1.27 (complex pattern), 1.04 (d, *J* = 6.9 Hz, 3H), 0.87 (d, *J* = 6.9 Hz, 3H), 0.70 (d, *J* = 6.8 Hz, 3H), 0.25 (d, *J* = 7.0 Hz, 3H).

8-(Allylamino)rifamycin S (4f)

From allylamine, 120 mg of crude deep brown solid was obtained. Purification by preparative TLC (1:1 hexanes / ethyl acetate) gave **4f** as a deep red solid (19 mg, 13 %). ESI MS: *m/z* 735.1 ($M+H^+$). ^1H NMR (300 MHz, $CDCl_3$): δ 9.99 (m, 1H), 8.53 (s, 1H), 7.76 (s, 1H), 6.44 (dd, *J* = 10.3, 15.6 Hz, 1H), 6.26 (d, *J* = 9.1 Hz, 1H), 6.18 (d, *J* = 12.4 Hz, 1H), 6.02 (m, 2H), 5.35 (dd, *J* = 10.4, 16.8 Hz, 2H), 5.05 (dd, *J* = 7.1, 12.4 Hz, 1H), 4.77 (d, *J* = 10.3 Hz, 1H), 4.31 (m, 1H), 3.89 (d, *J* = 4.3 Hz, 1H), 3.67 (d, *J* = 9.8 Hz, 1H), 3.56 (s, 1H), 3.41 (dd, *J* = 1.8, 6.7 Hz, 1H), 3.19 (m, 1H), 3.10 (s, 3H), 3.05 (m, 2H), 2.46 (s, 3H), 2.37 (m, 3H), 2.19-1.50 (complex pattern), 1.02 (d, *J* = 7.0 Hz, 3H), 0.87 (d, *J* = 6.9 Hz, 3H), 0.69 (d, *J* = 6.9 Hz, 3H), 0.25 (d, *J* = 7.1 Hz, 3H).

8-((2-Hydroxyethyl)amino)rifamycin S (4g)

From (2-hydroxyethyl)amine, 150 mg of crude deep red solid was obtained. Purification by preparative TLC (1:1 hexanes / ethyl acetate) gave **4g** as a deep red solid (70 mg, 48 %). ESI MS: *m/z* 739.1 ($M+H^+$). ^1H NMR (300 MHz, $CDCl_3$): δ 10.19 (m, 1H), 8.56 (s, 1H), 7.73 (s, 1H), 6.32 (dd, *J* = 10.5, 15.8 Hz, 1H), 6.21 (m, 2H), 6.00 (dd, *J* = 6.8, 15.8 Hz, 1H), 5.10 (dd, *J* = 6.0, 12.3 Hz, 1H), 4.74 (d, *J* = 10.5 Hz, 1H), 3.87 (m, 5H), 3.67 (d, *J* = 9.5 Hz, 1H), 3.48 (m, 1H), 3.56 (s, 1H), 3.40 (dd, *J* = 2.4, 7.5 Hz, 1H), 3.12 (s, 3H), 3.03 (m, 2H), 2.50 (s, 3H), 2.34 (m, 1H), 2.19-1.50 (complex pattern), 1.03 (d, *J* = 7.0 Hz, 3H), 0.86 (d, *J* = 6.9 Hz, 3H), 0.69 (d, *J* = 6.8 Hz, 3H), 0.25 (d, *J* = 7.0 Hz, 3H).

8-(Benzylamino)rifamycin S (4h)

From benzylamine hydrochloride and N,N-diisopropylethylamine, 130 mg of crude black solid was obtained. Purification by preparative TLC (1:1 mixture of hexanes / ethyl acetate) afforded **4h** as a deep red solid (80 mg, 51 %). ESI MS: *m/z* 785.2 ($M+H^+$). ^1H NMR (300 MHz, $CDCl_3$): δ 10.28 (m, 1H), 8.48 (s, 1H), 7.76 (s, 1H), 7.37 (m, 5H), 6.38 (dd, *J* = 10.2, 15.6 Hz, 1H), 6.24 (d, *J* = 10.3 Hz, 1H), 6.15 (d, *J* = 12.4 Hz, 1H), 6.06 (dd, *J* = 7.0, 15.4 Hz, 1H), 5.06 (dd, *J* = 6.6, 12.4 Hz, 1H), 4.93-4.81 (m, 2H), 3.96 (d, *J* = 4.3 Hz, 1H), 3.69 (d, *J* = 9.8 Hz, 1H), 3.61 (s, 1H), 3.44 (dd, *J* = 1.6, 6.5 Hz, 1H), 3.12 (s, 3H), 3.06 (m, 2H), 2.46 (s, 3H), 2.35 (m, 3H), 2.20-1.61 (complex pattern), 1.05 (d, *J* = 7.2 Hz, 3H), 0.87 (d, *J* = 6.9 Hz, 3H), 0.71 (d, *J* = 6.8 Hz, 3H), 0.25 (d, *J* = 7.1 Hz, 3H).

8-(Cycloheptylamino)rifamycin S (4i)

From cycloheptylamine, 160 mg of crude deep red solid was obtained. Purification by preparative TLC (1:1 hexanes / ethyl acetate) gave **4i** as a deep red solid (70 mg, 44%). ESI MS: *m/z* 791.2 ($M+H^+$). ^1H NMR (300 MHz, $CDCl_3$): δ 10.03 (d, *J* = 8.5 Hz, 1H), 8.51 (s, 1H), 7.74 (s, 1H), 6.46 (dd, *J* = 10.6, 15.8 Hz, 1H), 6.26 (d, *J* = 9.8 Hz, 1H), 6.15 (dd, *J* = 6.8, 15.7 Hz, 1H), 6.10 (d, *J* = 11.9 Hz, 1H), 5.06 (dd, *J* = 5.9, 12.4 Hz, 1H), 4.90 (d, *J* = 10.6 Hz, 1H), 4.17 (m, 1H), 3.90 (d, *J* = 4.2 Hz, 1H), 3.73 (d, *J* = 9.3 Hz, 1H), 3.56 (s, 1H), 3.46 (dd, *J* = 1.9, 6.6 Hz, 1H), 3.11 (s, 3H), 3.01 (m, 2H), 2.41 (s, 3H), 2.36 (m, 2H), 2.18-1.52 (complex pattern), 1.03 (d, *J* = 7.0 Hz, 3H), 0.88 (d, *J* = 6.9 Hz, 3H), 0.70 (d, *J* = 6.8 Hz, 3H), 0.17 (d, *J* = 7.0 Hz, 3H).

8-Methylthiorifamycin S (4j)

From reaction with sodium methanethiol in place of an amine. Purification by preparative TLC (7:3 hexanes / ethyl acetate) gave **4j** as an orange solid (5 mg, 13%). ESI MS: *m/z* 726.3 ($M+H^+$). ^1H NMR (500 MHz, $CDCl_3$): δ 8.46 (s, 1H), 7.83 (s, 1H), 6.41 (dd, *J* = 9.9, 15.8 Hz, 1H), 6.25 (d, *J* = 9.6 Hz, 1H), 6.16 (d, *J* = 12.4 Hz, 1H), 6.06 (dd, *J* = 7.4, 15.7 Hz, 1H), 5.11 (dd, *J* = 6.4, 12.4 Hz, 1H), 4.75 (d, *J* = 10.3 Hz, 1H), 3.73 (d, *J* = 4.1 Hz, 1H), 3.58 (m, 2H), 3.45 (d, *J* = 6.5 Hz, 1H), 3.12 (s, 3H), 2.98 (m, 1H), 2.65 (s, 3H), 2.49 (s, 3H), 2.36-1.58 (complex pattern), 1.02 (d, *J* = 7.0 Hz, 3H), 0.88 (d, *J* = 6.9 Hz, 3H), 0.69 (d, *J* = 6.8 Hz, 3H), 0.21 (d, *J* = 7.1 Hz, 3H).

1-(2-Hydroxyethyl)-1*H*-benzo[*cd*]indazol-5-one congener of rifamycin S (5)

From (2-hydroxyethyl)hydrazine hydrochloride and N,N-diisopropylethylamine, 158 mg of crude deep orange solid was obtained. Two purifications by preparative TLC (8:92 methanol / dichloromethane) gave **5** as an orange solid (7 mg, 5 %). ESI MS: *m/z*

736.2 ($M+H^+$). ^1H NMR (500 MHz, $CDCl_3$): δ 8.12 (s, 1H), 7.33 (s, 1H), 6.35 (dd, *J* = 10.5, 15.5 Hz, 1H), 6.26 (d, *J* = 10.5 Hz, 1H), 6.06 (m, 2H), 4.98 (dd, *J* = 7.1, 12.4 Hz, 1H), 4.77 (m, 1H), 4.69 (m, 1H), 4.45 (d, *J* = 9.7 Hz, 1H), 4.42 (m, 1H), 4.23 (m, 1H), 3.64 (br s, 1H), 3.52 (d, *J* = 10.0 Hz, 1H), 3.28 (dd, *J* = 2.1, 6.9 Hz, 1H), 3.18 (br s, 1H), 3.03 (s, 3H), 2.90 (d, *J* = 9.6 Hz, 1H), 2.76 (s, 3H), 2.34 (m, 1H), 2.19 (s, 2H), 2.15 (s, 3H), 2.05 (m, 2H), 2.00 (s, 3H), 1.79 (s, 3H), 1.78-1.60 (complex pattern), 1.27 (m, 4H), 0.99 (d, *J* = 7.0 Hz, 3H), 0.85 (d, *J* = 6.9 Hz, 3H), 0.55 (d, *J* = 6.9 Hz, 3H), -0.30 (d, *J* = 7.0 Hz, 3H).

Rifampin S (6)

To a solution of rifampin (**1**; 200 mg, 0.24 mmol) in ethyl acetate (4 mL) was added aqueous 0.1 M sodium phosphate buffer (pH = 7.4, 4 mL) followed by potassium ferricyanide (400 mg, 1.2 mmol). The suspension was stirred vigorously at room temperature for 1.5 h, and then diluted with dichloromethane (50 mL). This solution was washed with phosphate buffer (3 x 30mL) followed by saturated brine (30 mL), dried over anhydrous sodium sulfate and concentrated *in vacuo* to dryness to give **6** as a purple black solid (128 mg, 65%). The compound was pure enough to be utilized directly in the next step. ESI MS: *m/z* 821.1 ($M+H^+$). ^1H NMR (500 MHz, $CDCl_3$): δ 12.77 (br s, 1H), 10.56 (br s, 1H), 7.80 (s, 1H), 7.23 (m, 1H), 6.84 (m, 1H), 6.39 (d, *J* = 10.8 Hz, 1H), 6.10 (d, *J* = 12.0 Hz, 1H), 5.94 (dd, *J* = 5.8, 15.0 Hz, 1H), 5.15 (d, *J* = 9.2 Hz, 1H), 5.08 (dd, *J* = 5.3, 12.0 Hz, 1H), 3.97 (br s, 1H), 3.89 (d, *J* = 7.8 Hz, 1H), 3.44 (s, 1H), 3.29 (m, 3H), 3.10 (s, 3H), 3.02 (m, 4H), 2.58 (s, 3H), 2.44 (m, 2H), 2.37 (s, 3H), 2.30 (s, 3H), 2.11-1.34 (complex pattern), 1.06 (d, *J* = 7.0 Hz, 3H), 0.89 (d, *J* = 7.0 Hz, 3H), 0.56 (d, *J* = 6.7 Hz, 3H), 0.16 (d, *J* = 6.5 Hz, 3H).

8-(*p*-Toluenesulfonyloxy)rifampin S (7)

This compound was prepared from **6** by the same procedure described above to make 8-(*p*-toluenesulfonyloxy)rifamycin S (**3**). The product (194 mg, quantitative yield) was a deep brown solid and pure enough to use directly in the next step. ESI MS: *m/z* 997.2 ($M+Na^+$). ^1H NMR (500 MHz, $CDCl_3$): δ 11.11 (s, 1H), 8.11 (d, *J* = 7.5 Hz, 2H), 7.82 (s, 1H), 7.41 (d, *J* = 7.9 Hz, 2H), 6.81 (dd, *J* = 11.3, 15.4 Hz, 1H), 6.46 (d, *J* = 10.9 Hz, 1H), 6.05 (d, *J* = 12.3 Hz, 1H), 5.96 (dd, *J* = 5.2, 15.8 Hz, 1H), 5.09 (dd, *J* = 5.3, 12.5 Hz, 1H), 5.03 (d, *J* = 10.1 Hz, 1H), 3.81 (d, *J* = 9.5 Hz, 1H), 3.45 (d, *J* = 4.1 Hz, 1H), 3.20 (m, 4H), 3.04 (s, 3H), 2.99 (d, *J* = 7.5 Hz, 1H), 2.56 (br s, 4H), 2.49 (s, 3H), 2.39 (br s, 4H), 2.35 (s, 3H), 2.10-1.84 (complex pattern), 1.80 (s, 3H), 1.67 (m, 1H), 1.64 (m, 1H), 1.36 (m, 1H), 1.02 (d, *J* = 6.8 Hz, 3H), 0.84 (d, *J* = 6.8 Hz, 3H), 0.53 (d, *J* = 6.6 Hz, 3H), -0.01 (d, *J* = 6.7 Hz, 3H).

The following compounds were prepared in similar fashion to that described for 8-(methylamino)rifamycin S **(4b)** described above:

8-(Methylamino)rifampin S (8a)

From methylamine, 180 mg of crude red-purple solid was obtained. Purification by preparative TLC (8:92 methanol / dichloromethane) gave **8a** as a deep red solid (100 mg, 60 %). ESI MS: *m/z* 834.2 ($M+H^+$). ^1H NMR (500 MHz, $CDCl_3$): δ 10.77 (s, 1H), 9.37 (s, 1H), 7.79 (s, 1H), 6.82 (dd, *J* = 11.4, 15.0 Hz, 1H), 6.34 (d, *J* = 11.0 Hz, 1H), 6.12 (d, *J* = 12.5 Hz, 1H), 5.90 (dd, *J* = 4.7, 15.7 Hz, 1H), 5.18 (d, *J* = 10.1 Hz, 1H), 5.09 (dd, *J* = 5.9, 12.4 Hz, 1H), 3.98 (d, *J* = 7.9 Hz, 1H), 3.40 (d, *J* = 5.7 Hz, 1H), 3.32 (d, *J* = 5.4 Hz, 3H), 3.25 (m, 4H), 3.10 (s, 3H), 2.98 (d, *J* = 10.3 Hz, 1H), 2.60 (br s, 4H), 2.51 (m, 1H), 2.47 (s, 3H), 2.37 (br s, 4H), 2.12 (s, 3H), 2.09 (s, 3H), 1.81 (m, 1H), 1.78 (s,

1H), 1.73 (m, 1H), 1.46-1.25 (complex pattern), 1.06 (d, *J* = 6.9 Hz, 3H), 0.94 (d, *J* = 6.5 Hz, 3H), 0.52 (d, *J* = 6.8 Hz, 3H), 0.27 (d, *J* = 7.0 Hz, 3H).

8-(Ethylamino)rifampin S (8b)

From ethylamine, 170 mg of crude purple solid was obtained. Two purifications by preparative TLC (7.5:92.5 methanol / dichloromethane) gave 8b as a purple-black solid (80 mg, 47.0 %). ESI MS: *m/z* 848.1 ($M+H^+$). ^1H NMR (500 MHz, $CDCl_3$): δ 10.69 (s, 1H), 9.21 (s, 1H), 7.78 (s, 1H), 6.81 (dd, *J* = 11.2, 15.9 Hz, 1H), 6.32 (d, *J* = 10.6 Hz, 1H), 6.13 (d, *J* = 12.5 Hz, 1H), 5.90 (dd, *J* = 4.8, 16.0 Hz, 1H), 5.18 (d, *J* = 9.8 Hz, 1H), 5.08 (dd, *J* = 6.0, 12.5 Hz, 1H), 4.05 (d, *J* = 4.6 Hz, 1H), 3.98 (d, *J* = 8.3 Hz, 1H), 3.59 (s, 1H), 3.38 (d, *J* = 5.8 Hz, 2H), 3.24 (m, 4H), 3.09 (s, 3H), 2.98 (dd, *J* = 5.8, 10.5 Hz, 1H), 2.59 (m, 4H), 2.52 (m, 1H), 2.43 (s, 3H), 2.36 (s, 3H), 2.13 (s, 3H), 2.09 (s, 3H), 1.80 (m, 1H), 1.75 (s, 3H), 1.69 (m, 1H), 1.46-1.27 (complex pattern) 1.36 (t, *J* = 7.1 Hz, 3H), 1.06 (d, *J* = 6.9 Hz, 3H), 0.87 (d, *J* = 7.2 Hz, 3H), 0.51 (d, *J* = 6.8 Hz, 3H), 0.27 (d, *J* = 7.0 Hz, 3H).

8-(Allylamino)rifampin S (8c)

From allylamine, 170 mg of crude purple-red solid was obtained. Purification by preparative TLC (7.5:92.5 methanol / dichloromethane) gave **8c** as a purple-black solid (60 mg, 35 %). ESI MS: *m/z* 860.2 ($M+H^+$). ^1H NMR (500 MHz, $CDCl_3$): δ 10.73 (s, 1H), 9.35 (s, 1H), 7.79 (s, 1H), 6.80 (dd, *J* = 11.4, 15.6 Hz, 1H), 6.33 (d, *J* = 10.7 Hz, 1H), 6.13 (d, *J* = 12.5 Hz, 1H), 6.00 (m, 1H), 5.90 (dd, *J* = 5.8, 16.0 Hz, 1H), 5.37 (d, *J* = 17.1 Hz, 1H), 5.29 (d, *J* = 10.3 Hz, 1H), 5.18 (d, *J* = 9.9 Hz, 1H), 5.09 (dd, *J* = 6.0, 12.5 Hz, 1H), 4.04 (d, *J* = 4.5 Hz, 1H), 3.98 (d, *J* = 8.4 Hz, 1H), 3.57 (br s, 1H), 3.39 (d, *J* = 6.0 Hz, 2H), 3.25 (m, 4H), 3.09 (s, 3H), 2.98 (dd, *J* = 3.6, 10.6 Hz, 1H), 2.59 (m, 4H),

2.52 (m, 1H), 2.41 (s, 3H), 2.37 (s, 3H), 2.12 (s, 3H), 2.09 (s, 3H), 1.82 (m, 1H), 1.75 (s, 3H), 1.69 (m, 1H), 1.46-1.27 (complex pattern), 1.06 (d, *J* = 6.9 Hz, 3H), 0.94 (d, *J* = 7.1 Hz, 3H), 0.52 (d, *J* = 6.8 Hz, 3H), 0.27 (d, *J* = 7.0 Hz, 3H).

8-((2-Hydroxyethyl)amino)rifampin S (8d)

From (2-hydroxyethyl)amine, 180 mg of crude deep purple solid was obtained. Two purifications by preparative TLC (7.5:92.5 methanol / dichloromethane) gave **8d** as a purple-black solid (72 mg, 41%). ESI MS: *m/z* 864.1 ($M+H^+$). ^1H NMR (500 MHz, $CDCl_3$): δ 10.90 (s, 1H), 8.66 (m, 1H), 7.77 (s, 1H), 6.79 (dd, *J* = 10.9, 15.8 Hz, 1H), 6.35 (d, *J* = 10.8 Hz, 1H), 6.19 (dd, *J* = 0.9, 12.5 Hz, 1H), 5.91 (dd, *J* = 5.1, 15.9 Hz, 1H), 5.18 (d, *J* = 9.9 Hz, 1H), 5.15 (dd, *J* = 6.3, 12.5 Hz, 1H), 3.99 (d, *J* = 5.8 Hz, 2H), 3.74 (m, 1H), 3.68 (m, 1H), 3.63 (m, 2H), 3.41 (d, *J* = 6.5 Hz, 2H), 3.26 (m, 4H), 3.07 (s, 3H), 2.98 (dd, *J* = 5.1, 10.4 Hz, 1H), 2.60 (m, 4H), 2.55 (m, 1H), 2.37 (br s, 6H), 2.14 (s, 3H), 2.08 (s, 3H), 1.80 (m, 1H), 1.76 (s, 3H), 1.37 (m, 1H), 1.06 (d, *J* = 7.0 Hz, 3H), 0.96 (d, *J* = 7.2 Hz, 3H), 0.50 (d, *J* = 6.8 Hz, 3H), 0.27 (d, *J* = 7.0 Hz, 3H).

8-(Benzylamino)rifampin S (8e)

From benzylamine hydrochloride and N,N-diisopropylethylamine, 180 mg of crude black solid was obtained. Purification by preparative TLC (7.5:92.5 methanol / dichloromethane) gave **8e** as a purple-black solid (84 mg, 42 %). ESI MS: *m/z* 910.2 ($M+H^+$). ^1H NMR (500 MHz, $CDCl_3$): δ 10.71 (s, 1H), 9.61 (m, 1H), 7.79 (s, 1H), 7.38 (m, 4H), 7.31 (m, 1H), 6.88 (dd, *J* = 10.8, 15.1 Hz, 1H), 6.33 (d, *J* = 10.7 Hz, 1H), 6.09 (dd, *J* = 1.0, 12.5 Hz, 1H), 5.92 (dd, *J* = 4.9, 15.9 Hz, 1H), 5.18 (d, *J* = 10.1 Hz, 1H), 5.07 (dd, *J* = 5.8, 12.5 Hz, 1H), 4.81 (m, 2H), 4.09 (d, *J* = 4.6 Hz, 2H), 4.01 (d, *J* = 8.2 Hz, 1H), 3.64 (br s, 1H), 3.39 (d, *J* = 5.7 Hz, 2H), 3.25 (m, 4H), 3.07 (s, 3H), 3.00 (dd, *J* =

4.6, 10.1 Hz, 1H), 2.59 (m, 4H), 2.53 (m, 1H), 2.40 (s, 3H), 2.37 (s, 6H), 2.11 (s, 3H), 2.09 (s, 3H), 1.83 (m, 1H), 1.74 (s, 3H), 1.41 (m, 1H), 1.07 (d, *J* = 6.9 Hz, 3H), 0.95 (d, *J* = 7.1 Hz, 3H), 0.54 (d, *J* = 6.8 Hz, 3H), 0.21 (d, *J* = 7.0 Hz, 3H).

8-(Cycloheptylamino)rifampin S (8f)

From cycloheptylamine, 180 mg of deep red solid was obtained. Two purifications by preparative TLC (7.5:92.5 methanol / dichloromethane) gave **8f** as a purple-black solid (80 mg, 44 %). ESI MS: *m/z* 938.4 ($M+Na^+$). ^1H NMR (500 MHz, $CDCl_3$): δ 10.59 (s, 1H), 9.35 (d, *J* = 8.6 Hz, 1H), 7.78 (s, 1H), 6.84 (dd, *J* = 10.6, 15.6 Hz, 1H), 6.33 (d, *J* = 10.5 Hz, 1H), 6.15 (d, *J* = 12.5 Hz, 1H), 5.90 (dd, *J* = 5.0, 15.9 Hz, 1H), 5.17 (d, *J* = 9.8 Hz, 1H), 5.09 (dd, *J* = 6.1, 12.5 Hz, 1H), 4.03 (d, *J* = 4.5 Hz, 1H), 3.99 (d, *J* = 9.0 Hz, 1H), 3.58 (br s, 1H), 3.38 (d, *J* = 5.9 Hz, 1H), 3.24 (m, 4H), 3.09 (s, 3H), 2.98 (dd, *J* = 3.6, 10.1 Hz, 1H), 2.59 (m, 4H), 2.52 (m, 1H), 2.38 (s, 3H), 2.37 (s, 3H), 2.09 (s, 3H), 2.06 (s, 3H), 2.04 (m, 4H), 1.82 (m, 1H), 1.76 (s, 3H), 1.69 (m, 1H), 1.73-1.23 (complex pattern), 1.06 (d, *J* = 6.9 Hz, 3H), 0.94 (d, *J* = 7.4 Hz, 3H), 0.51 (d, *J* = 6.8 Hz, 3H), 0.26 (d, *J* = 7.1 Hz, 3H).

1-Methyl-1*H*-benzo[*cd*]indazol-5-one congener of rifampin S (9a)

From methylhydrazine hydrochloride and N,N-diisopropylethylamine, a crude deep brown was obtained. Two purifications by preparative TLC (8:92 methanol / dichloromethane) gave **9a** as a black solid (27 mg, 33%). ESI MS: *m/z* 831.2 ($M+H^+$). ^1H NMR (500 MHz, $CDCl_3$): δ 13.06 (s, 1H), 8.27 (s, 1H), 6.96 (dd, *J* = 11.8, 15.4 Hz, 1H), 6.62 (d, *J* = 11.3 Hz, 1H), 6.17 (d, *J* = 12.5 Hz, 1H), 6.02 (dd, *J* = 5.2, 15.6 Hz, 1H), 5.09 (dd, *J* = 5.9, 12.6 Hz, 1H), 4.91 (d, *J* = 10.6 Hz, 1H), 4.43 (s, 3H), 3.84 (d, *J* = 9.9 Hz, 1H), 3.63 (m, 1H), 3.51 (s, 1H), 3.42 (m, 1H), 3.15 (m, 4H), 3.04 (s, 3H), 3.00 (m,

1H), 2.78 (s, 3H), 2.56 (m, 4H), 2.41 (m, 1H), 2.35 (s, 3H), 2.12 (s, 3H), 2.05 (s, 3H), 1.82 (s, 3H), 1.73-1.53 (complex pattern), 1.04 (d, *J* = 6.9 Hz, 3H), 0.90 (d, *J* = 7.0 Hz, 3H), 0.52 (d, *J* = 6.8 Hz, 3H), -0.53 (d, *J* = 6.9 Hz, 3H).

1-(2-Hydroxyethyl)-1*H*-benzo[*cd*]indazol-5-one congener of rifampin S (9b)

From (2-hydroxyethyl)hydrazine hydrochloride and N,N-diisopropylethylamine, 200 mg of crude black solid was obtained. Two purifications by preparative TLC (8:92 methanol / dichloromethane) gave **9b** as a black solid (76 mg, 40 %). ESI MS: *m/z* 861.2 ($M+H^+$). ^{1}H NMR (500 MHz, $CDCl_3$): δ 13.11 (s, 1H), 8.26 (s, 1H), 6.92 (dd, *J* = 11.5, 15.4 Hz, 1H), 6.59 (d, *J* = 11.1 Hz, 1H), 6.17 (d, *J* = 12.6 Hz, 1H), 6.03 (dd, *J* = 5.3, 15.3 Hz, 1H), 5.09 (dd, *J* = 6.0, 12.5 Hz, 1H), 4.89 (d, *J* = 10.3 Hz, 1H), 4.79 (m, 2H), 3.85 (d, *J* = 9.5 Hz, 1H), 3.64 (m, 1H), 3.51 (m, 1H), 3.41 (d, *J* = 5.6 Hz, 2H), 3.08 (m, 4H), 3.03 (s, 3H), 3.00 (m, 1H), 2.78 (s, 3H), 2.56 (m, 4H), 2.41 (m, 1H), 2.35 (s, 3H), 2.09 (s, 3H), 2.05 (s, 3H), 1.82 (s, 3H), 1.80-1.52 (complex pattern), 1.03 (d, *J* = 7.0 Hz, 3H), 0.90 (d, *J* = 7.0 Hz, 3H), 0.52 (d, *J* = 6.8 Hz, 3H), -0.54 (d, *J* = 7.0 Hz, 3H).

8-(Methylamino)rifampin (10a)

Ascorbic acid (74 mg, 0.42 mmol) was added to a solution of 8-(methylamino)rifampin S (**8a**; 35 mg, 0.04 mmol) in methanol (1.5 mL). The resulting mixture was stirred at room temperature for 2 h and then diluted with dichloromethane (15 mL). This solution was washed with 0.2 N aqueous NH_4Cl (3 x 10 mL) followed by saturated brine (10 mL), dried over anhydrous sodium sulfate and evaporated *in vacuo* to dryness to give **10a** as an orange solid (18 mg, 51%). ESI MS: *m/z* 858.3 ($M+Na^+$). ^{1}H NMR (500 MHz, $CDCl_3$): δ 12.91 (s, 1H), 12.78 (s, 1H), 12.00 (s, 1H), 10.15 (s, 1H), 8.36 (s, 1H), 6.68 (dd, *J* = 11.4, 14.9 Hz, 1H), 6.41 (d, *J* = 10.8 Hz, 1H), 6.18 (d, *J* = 12.5

Hz, 1H), 5.93 (dd, *J* = 4.7, 15.2 Hz, 1H), 5.10 (dd, *J* = 6.3, 12.5 Hz, 1H), 4.98 (d, *J* = 10.4 Hz, 1H), 3.81 (d, *J* = 9.3 Hz, 1H), 3.31 (d, *J* = 5.0 Hz, 3H), 3.27 (m, 4H), 3.07 (s, 3H), 3.01 (m, 1H), 2.71 (br s, 4H), 2.42 (m, 4H), 2.38 (s, 3H), 2.37 (m, 1H), 2.09 (s, 3H), 1.42-1.27 (complex pattern), 1.04 (d, *J* = 6.9 Hz, 3H), 0.94 (d, *J* = 7.0 Hz, 3H), 0.61 (d, *J* = 6.8 Hz, 3H), -0.17 (d, *J* = 6.9 Hz, 3H).

Prepared in similar fashion were the following rifampin analogues:

8-(Ethylamino)rifampin (10b)

From 8-(ethylamino)rifampin S (**8b**), **10b** was obtained as an orange solid (41 mg, 84 %). ESI MS: *m/z* 872.3 ($M+Na^+$). ^1H NMR (500 MHz, $CDCl_3$): δ 12.90 (br s, 1H), 12.80 (s, 1H), 12.01 (s, 1H), 10.11 (s, 1H), 8.37 (s, 1H), 6.68 (dd, *J* = 11.9, 15.5 Hz, 1H), 6.41 (d, *J* = 11.1 Hz, 1H), 6.18 (d, *J* = 12.6 Hz, 1H), 5.94 (dd, *J* = 4.8, 15.5 Hz, 1H), 5.09 (dd, *J* = 6.5, 12.6 Hz, 1H), 4.98 (dd, *J* = 10.5 Hz, 1H), 3.82 (m, 2H), 3.72 (m, 1H), 3.57 (m, 1H), 3.51 (d, *J* = 6.4 Hz, 2H), 3.25 (m, 4H), 3.06 (s, 3H), 3.01 (m, 1H), 2.72 (m, 4H), 2.47 (s, 3H), 2.41 (m, 1H), 2.35 (m, 3H), 2.08 (m, 6H), 1.79 (s, 3H), 1.74 (m, 1H), 1.61-1.27 (complex pattern) 1.35 (t, *J* = 7.1 Hz, 3H), 1.04 (d, *J* = 6.9 Hz, 3H), 0.90 (d, *J* = 7.0 Hz, 3H), 0.62 (d, *J* = 6.8 Hz, 3H), -0.17 (d, *J* = 6.9 Hz, 3H).

8-(Allylamino)rifampin (10c)

From 8-(allylamino)rifampin S (**8c**), **10c** was obtained as an orange solid (24 mg, 89%). ESI MS: *m/z* 884.3 ($M+Na^+$). ^1H NMR (500 MHz, $CDCl_3$): δ 12.95 (br s, 1H), 12.69 (s, 1H), 12.04 (s, 1H), 10.17 (s, 1H), 8.36 (s, 1H), 6.67 (dd, *J* = 11.4, 15.6 Hz, 1H), 6.41 (d, *J* = 10.8 Hz, 1H), 6.19 (d, *J* = 12.6 Hz, 1H), 5.99 (m, 1H), 5.94 (dd, *J* = 5.0, 16.3 Hz, 1H), 5.39 (d, *J* = 17.4 Hz, 1H), 5.28 (d, *J* = 10.3 Hz, 1H), 5.10 (dd, *J* = 6.4, 12.6 Hz, 1H), 4.99 (d, *J* = 10.3 Hz, 1H), 4.34 (m, 1H), 3.82 (d, *J* = 9.6 Hz, 1H), 3.70 (br s, 1H),

3.51 (d, *J* = 5.2 Hz, 2H), 3.20 (m, 4H), 3.07 (s, 3H), 3.02 (m, 1H), 2.66 (m, 4H), 2.42 (m, 1H), 2.34 (s, 3H), 2.08 (m, 6H), 2.04 (m, 1H), 1.80 (s, 3H), 1.75-1.22 (complex pattern), 1.04 (d, *J* = 6.8 Hz, 3H), 0.91 (d, *J* = 6.6 Hz, 3H), 0.62 (d, *J* = 6.4 Hz, 3H), -0.17 (d, *J* = 6.7 Hz, 3H).

8-(2-Hydroxyethylamino)rifampin (10d)

From 8-((2-hydroxyethyl)amino)rifampin S (**8d**), **10d** was obtained as an orange solid (14 mg, 82 %). ESI MS: *m/z* 888.4 ($M+Na^+$). ^1H NMR (500 MHz, $CDCl_3$): δ 12.77 (m, 2H), 11.95 (s, 1H), 10.34 (s, 1H), 8.37 (s, 1H), 6.65 (dd, *J* = 11.4, 15.3 Hz, 1H), 6.38 (d, *J* = 11.2 Hz, 1H), 6.16 (d, *J* = 12.6 Hz, 1H), 5.90 (dd, *J* = 4.6, 15.4 Hz, 1H), 5.09 (dd, *J* = 6.4, 12.6 Hz, 1H), 4.97 (d, *J* = 9.9 Hz, 1H), 3.91 (m, 2H), 3.86 (m, 1H), 3.79 (m, 1H), 3.72 (m, 2H), 3.49 (d, *J* = 6.2 Hz, 2H), 3.37 (m, 4H), 3.05 (s, 3H), 3.01 (m, 1H), 2.86 (m, 4H), 2.56 (s, 3H), 2.42 (m, 1H), 2.35 (s, 3H), 2.07 (m, 6H), 1.79 (s, 3H), 1.72 (m, 1H), 1.56 (m, 1H), 1.43-1.26 (complex pattern) 1.03 (d, *J* = 6.9 Hz, 3H), 0.87 (d, *J* = 6.9 Hz, 3H), 0.61 (d, *J* = 6.7 Hz, 3H), -0.20 (d, *J* = 6.8 Hz, 3H).

8-(Benzylamino)rifampin (10e)

From 8-(benzylamino)rifampin S (**8e**), **10e** was obtained as an orange solid (26 mg, 93 %). ESI MS: *m/z* 934.4 ($M+Na^+$). ^1H NMR (500 MHz, $CDCl_3$): δ 12.90 (s, 1H), 12.70 (s, 1H), 12.00 (s, 1H), 10.46 (m, 1H), 8.36 (s, 1H), 7.35 (m, 5H), 6.65 (dd, *J* = 11.3, 15.4 Hz, 1H), 6.38 (d, *J* = 11.1 Hz, 1H), 6.19 (d, *J* = 12.6 Hz, 1H), 5.92 (dd, *J* = 4.7, 15.5 Hz, 1H), 5.10 (dd, *J* = 6.5, 12.6 Hz, 1H), 4.99 (d, *J* = 10.5 Hz, 1H), 4.91 (m, 2H), 3.81 (d, *J* = 9.4 Hz, 1H), 3.74 (br s, 1H), 3.51 (d, *J* = 6.5 Hz, 1H), 3.24 (m, 4H), 3.06 (s, 3H), 3.03 (m, 1H), 2.70 (m, 4H), 2.44 (s, 3H), 2.40 (m, 1H), 2.37 (s, 3H), 2.08 (s, 3H),

2.06 (s, 3H), 1.79 (s, 3H), 1.73 (m, 1H), 1.04 (d, *J* = 6.7 Hz, 3H), 0.90 (d, *J* = 6.8 Hz, 3H), 0.62 (d, *J* = 6.6 Hz, 3H), -0.16 (d, *J* = 6.6 Hz, 3H).

8-(Cycloheptylamino)rifampin (10f)

From 8-(cycloheptylamino)rifampin S (**8f**), **10f** was obtained as an orange solid (19 mg, 87 %). ESI MS *m/z* 918.2 ($M+H^+$). ^{1}H NMR (500 MHz, $CDCl_3$): δ 12.90 (br s, 1H), 12.80 (s, 1H), 12.00 (s, 1H), 10.30 (d, *J* = 8.3 Hz, 1H), 8.37 (s, 1H), 6.67 (dd, *J* = 11.4, 15.5 Hz, 1H), 6.41 (d, *J* = 11.1 Hz, 1H), 6.18 (d, *J* = 12.6 Hz, 1H), 5.94 (dd, *J* = 4.9, 15.4 Hz, 1H), 5.09 (dd, *J* = 6.4, 12.5 Hz, 1H), 4.97 (d, *J* = 10.5 Hz, 1H), 4.09 (m, 1H), 3.82 (d, *J* = 9.3 Hz, 1H), 3.71 (br s, 1H), 3.50 (d, *J* = 6.3 Hz, 1H), 3.24 (m, 4H), 3.06 (s, 3H), 3.00 (m, 1H), 2.71 (m, 4H), 2.46 (m, 1H), 2.40 (m, 3H), 2.30 (s, 3H), 2.10 (s, 3H), 2.08 (s, 3H), 2.05 (m, 2H), 1.89 (m, 2H), 1.80 (m, 1H), 1.79-1.27 (complex pattern), 1.04 (d, *J* = 6.9 Hz, 3H), 0.90 (d, *J* = 6.9 Hz, 3H), 0.61 (d, *J* = 6.8 Hz, 3H), -0.18 (d, *J* = 6.9 Hz, 3H).

Appendix III-2

Structure-based Modeling Studies

To gain better understanding of the SAR, we carried out structure-based modeling studies. Modeling was based on the 2.5 Å resolution structure of rifabutin complexed with the *Thermus thermophilus* RNAP holoenzyme (PDB ID: 2a68) (*11*). Since the rifamycin binding site is highly conserved among bacteria, this structure provides a good foundation for understanding how proposed rifamycin analogues may interact with the MTB RNA polymerase. Preparation of the structure before modeling was conducted using MOE.

Given the size of the rifamycins, size of the binding site, and the flexibility of the ansa ring, accurate docking of these inhibitors to the RNAP complex would be challenging using standard docking approaches. Since most of the rifamycin structure remains unchanged, modeled poses of the analogues were generated by mutating rifamycin to the analogue and then relaxing the complex through a series of energy minimizations as described in the Supplementary Material.

Modeled poses were generated for each of the structures listed in Table III-2. A QSAR model (not shown) using interaction energies between the inhibitor and RNAP complex and two other ligand descriptors produced a very good R^2 of 0.90 and a cross validation R^2 of 0.79. The good fit of the QSAR model based on energies from the structure-based modeling supports the accuracy of the latter. The robustness of our structure-based modeling has also been supported by experimental studies where sensitivity to rifamycins against binding site mutants qualitatively correlates with our models (*17*).

Preparation for the 2a68 structure before modeling

All water molecules and metal ions more than 12 Å from rifamycin were removed. Residues with missing atoms were rebuilt. Residues which were not resolved in the structure were distant from the binding site and were not modeled in. All N and C termini (either real or as a result of missing residues) were acetylated and amidated respectively. Bond orders were checked for the rifabutin and hydrogen atoms added to it and the complex.

A series of energy minimizations were then used to relax the structure. The positions of the hydrogen atoms were relaxed with energy minimization using the MMFF94x forcefield. Hydrogen atoms, rebuilt residues and termini except for carbon alpha atoms were relaxed with energy minimization. All protein and rifamycin heavy atoms were fixed and positions of all hydrogen atoms and water molecules relaxed. Positions of the rifamycin atoms were then relaxed. Finally all atoms within 12 Å from rifamycin were relaxed with energy minimization.

Generation of binding complexes for the analogues

Rifamycin was modified to form the analogue structure. A series of energy minimizations were then used to relax the structure. The positions of the hydrogen atoms were relaxed with energy minimization using the MMFF94x forcefield. Atoms added or modified to create the analogue and positions of hydrogen atoms were relaxed with energy minimization. Positions of water molecules and hydrogen atoms were relaxed. Protein side chains within 12 Å from rifamycin, water molecules and hydrogen atoms were relaxed. Finally all atoms within 12 Å from original rifamycin were relaxed with energy minimization.

Appendix III-3

Table III-A1. Log IC_{50} Values and Standard Errors of the Fits for C-8 Rifamycins with MTB RNAPs

No.	**Log IC_{50}[1] (standard error of fit[2], Hill slope[3])**	
	(WT MTB RNAP)	**(MTB RNAP (S450L))**
1	-2.3986 (0.037, 1.54)	1.7166 (0.026, 1.52)
2	-2.1734 (0.049, 1.4)	1.5566 (0.082, 1.73)
3	-1.6795 (0.028, 1.04)	2.9922 (0.086, 1.11)
4a	0.6441 (0.054, 1.39)	2.2706 (0.103, 0.73)
4c	-0.2984 (0.027, 1.54)	2.4317 (0.109, 0.61)
4i	1.1879 (0.076, 1.26)	2.1042 (0.113, 1.45)
4j	-1.8199 (0.092, 0.74)	1.5742 (0.064, 1.46)
6	-1.8767 (0.107, 1.45)	1.6672 (0.034, 1.11)
7	-0.8462 (0.043, 0.94)	2.0451 (0.075, 0.90)
9b	-0.85567 (0.061, 0.96)	1.4751 (0.065, 0.98)

[1] The log IC_{50} values are such that the IC_{50} values will be in μM. Negative log IC_{50} values reflect IC50 values less than μM (e.g., in the nM range). Values were fit to a four parameter logistic regression model with the top and bottom limits set at 100 and 0 respectively.
[2] The average error is ~10 %, which roughly translates to 20-25% in the IC_{50}.
[3] The average Hill slope is 1.193.

References

1. P. A. Aristoff, G. A. Garcia, P. D. Kirchhoff, H. D. H. Showalter, Rifamycins-Obstacles and Opportunities. *Tuberculosis* **90**, 94 (2010).

2. S. A. Darst, New inhibitors targeting bacterial RNA polymerase. *Trends in Biochemical Sciences* **29**, 159 (Apr, 2004).

3. W. Wehrli, J. Nuesch, F. Knusel, M. Staehelin, Action of rifamycins on RNA polymerase. *Biochim. Biophys. Acta* **157**, 215 (1968).

4. D. A. Mitchison, The search for new sterilizing anti-tuberculosis drugs. *Frontiers in Bioscience* **9**, 1059 (2004).

5. P. Sensi, History of the development of rifampin. *Rev. Infectious Dis.* **5**, S402 (1983).

6. G. Binda *et al.*, Rifampin, a general review. *Arzneimittel-Forschung* **21**, 1907 (1971).

7. R. J. O'Brien, M. Spigelman, New drugs for tuberculosis: Current status and future prospects. *Clin. Chest Med.* **26**, 327 (Jun, 2005).

8. M. W. Sinz, Pregnane X receptor: prediction and attenuation of human CYP3A4 enzyme induction and drug-drug interactions. *In Annual Reports in Medicinal Chemistry* **43**, 405 (2008).

9. S. Riva, Silvestr.Lg, RIFAMYCINS - GENERAL VIEW. *Annu. Rev. Microbiol.* **26**, 199 (1972).

10. E. A. Campbell *et al.*, Structural mechanism for rifampicin inhibition of bacterial RNA polymerase. *Cell* **104**, 901 (2001).

11. I. Artsimovitch *et al.*, Allosteric modulation of the RNA polymerase catalytic reaction is an essential component of transcription control by rifamycins. *Cell* **122**, 351 (Aug 12, 2005).

12. W. Wehrli, M. Staehelin, The rifamycins-relation of chemical structure and action on RNA polymerase. *Biochim. Biophys. Acta* **182**, 24 (1969).

13. L. Collins, S. Franzblau, Microplate alamar blue assay versus BACTEC 460 system for high- throughput screening of compounds against Mycobacterium tuberculosis and Mycobacterium avium. *Antimicrob. Agents Chemother.* **41**, 1004 (May 1, 1997, 1997).

14. S. H. Cho *et al.*, Low-Oxygen-Recovery Assay for High-Throughput Screening of Compounds against Nonreplicating Mycobacterium tuberculosis. *Antimicrob. Agents Chemother.* **51**, 1380 (April 1, 2007, 2007).

15. E. Marchi, L. Montecchi, Rifamycin derivatives and process for their preparation. *United States Patent*, (1980) (4,200,574).

16. A. Telenti *et al.*, DETECTION OF RIFAMPICIN-RESISTANCE MUTATIONS IN MYCOBACTERIUM-TUBERCULOSIS. *Lancet* **341**, 647 (Mar, 1993).

17. S. K. Gill, G. A. Garcia, Rifamycin inhibition of WT and Rif-resistant Mycobacterium tuberculosis and Escherichia coli RNA polymerases in vitro. *Tuberculosis* **91**, 361 (Sep, 2011).

CHAPTER IV

Structure-based Design of Novel Benzoxazinorifamycins with Potent Binding Affinity to Wild-type and Rifampin-resistant Mutant *Mycobacterium tuberculosis* RNA polymerases

The emergence of multi-drug resistant TB (MDR-TB) has become of main concern with approximately half a million new cases reported in 2008 (*1*). MDR-TB strains are resistant to rifampin (**1**, RMP, Figure IV-1) and isoniazid, the two most effective TB drugs. The treatment of MDR-TB consists of a combination of three or four second-line anti-TB drugs that includes a fluoroquinolone (*2, 3*). These second-line bacteriostatics have more serious side effects and need to be taken for an extended period of time (at least 2 years) (*2, 3*). Furthermore, TB strains resistant to these agents along with RMP and isoniazid are classified as the virtually untreatable extensively drug-resistant TB (XDR-TB) (*1*). Therefore, agents that are non-toxic, well tolerated, effective against drug-susceptible and drug-resistant TB, and that will result in shortened TB therapy are needed urgently (*4-7*).

Benzoxazinorifamycins, a new generation of rifamycin derivatives with a four ring structure, have shown improved antimicrobial activity against *Mycobacterium tuberculosis* (MTB) (*8, 9*). Amongst the benzoxazinorifamycin derivatives, rifalazil (**2a**, RLZ, Figure IV-1) was selected as the most promising due to its excellent potency (both *in vivo* and *in vitro*), high tissue affinity, long elimination time from tissues and its

relative lack of toxicity in early rodent studies (*8-11*). RLZ is an exceedingly potent rifamycin derivative being 16 - 256 times more potent than RMP (*8, 9, 12-14*). RLZ is effective against most rifamycin-resistant (RifR) MTB strains but not all (*13, 15-18*). In addition to being active against RifR MTB strains, RLZ also has potent activity against several other clinically important bacterial pathogens (*19-21*)

One major downside of rifamycins is their many drug-drug interactions. RMP and other rifamycins induce the expression of cytochrome P450 3A4 (CYP3A4), a drug-metabolizing enzyme responsible for eliminating 36% of clinically important drugs, by activating the human pregnane X receptor (hPXR) (*22*). However, RLZ does not induce the expression of CYP3A4 (presumably due to lack of activation of hPXR). Unfortunately, RLZ was seen to be quite toxic in a series of phase I (*23, 24*) and phase II (*12, 23-25*) clinical trials with most adverse effects associated with a flu-like syndrome and leucopenia even at lower dose levels. Hence, its development as a treatment for TB has been suspended (*26*).

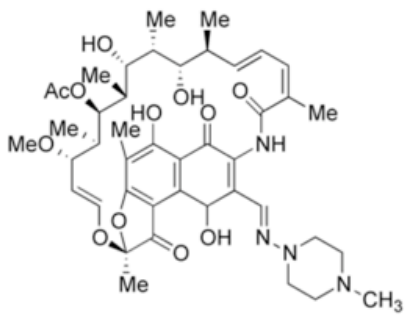

Rifampin (RMP; 1)

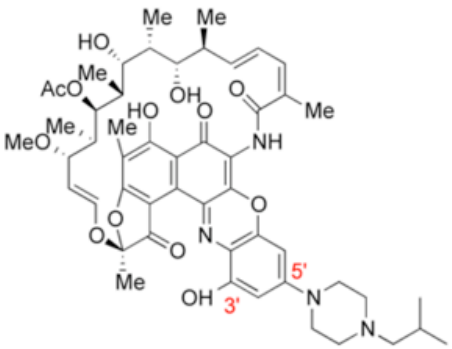

Rifalazil (RLZ; 2a)

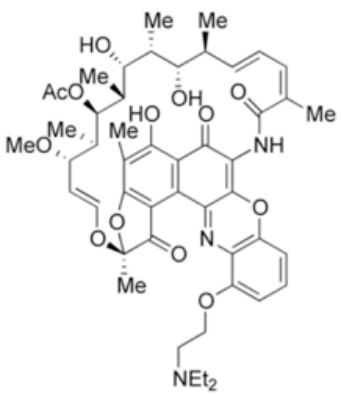

2b

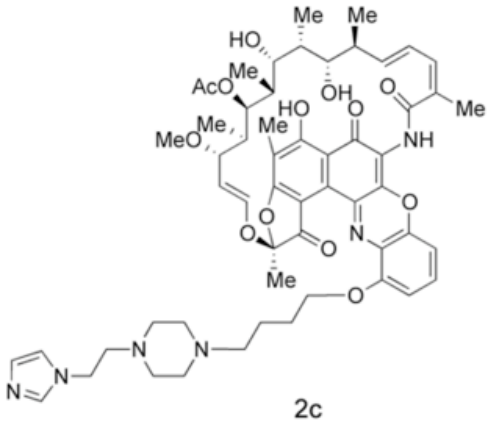

2c

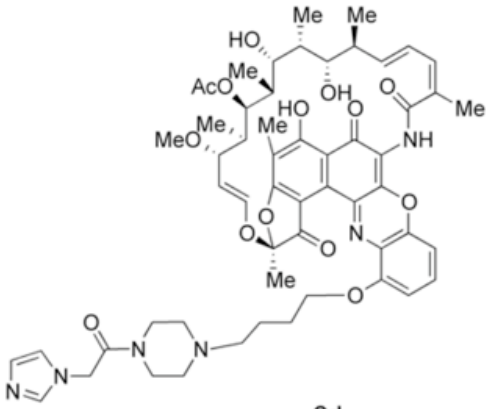

2d

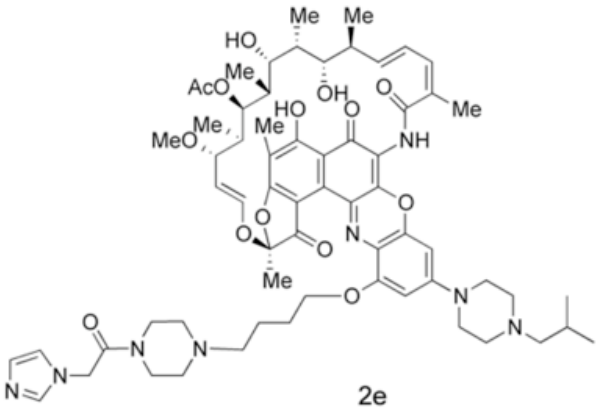

2e

Figure IV-1: Structures of reference agents (**1**, **2a**) and novel benzoxazinorifamycins (**2b**-**2e**)

Due to the overall favorable properties of RLZ, benzoxazinorifamycin derivatives (**2b** – **2e**; Figure IV-1) where ether tethers had been installed off the 3'-position of the "southeastern" part of the benzoxazinorifamycin template were synthesized. The design of these derivatives was based upon the three-dimensional X-ray structures of rifamycins bound to RNA polymerase (RNAP) (*27, 28*) and the human pregnane X receptor (hPXR) (*22*) in order to obtain an analogue with equal or better potency than RLZ against WT and RifR mutants of RNA polymerase (RNAP), the multi-subunit target of the rifamycins, with potential of making additional interactions with the other RNAP subunits. Furthermore, these analogues were expected to display lowered affinity for and therefore lowered activation of the hPXR. These studies demonstrate proof of principle for this subclass of rifamycins and support further expansion of structure-activity relationships (SAR) toward uncovering analogues with development potential.

Materials and Methods

Reagents

Chemistry

All reagents were commercially available and used without further purification. Melting points were determined in open capillary tubes on a Laboratory Devices Mel-Temp apparatus and are uncorrected. ^{1}H and ^{13}C NMR spectra were obtained on Bruker 500 MHz spectrometers with $CDCl_3$ or d_6-DMSO as solvent and chemical shifts are reported relative to the residual solvent peak in δ (ppm). Mass spectrometry analysis was performed using a Waters LCT time-of-flight mass spectrometry instrument. High resolution mass spectrometry (HRMS) analysis was performed on an Agilent Q-TOF system. Analytical HPLC was performed on a Perkin Elmer Series 200 system with an

Agilent Eclipse plus C18 (4.6 + 7.5 mm, 3.5 mm particle size) column. The mobile phase was a 15 min binary gradient of acetonitrile (containing 0.1 % TFA) and water (20–90%). Thin-layer chromatography (TLC) was performed on silica gel GHLF plates (250 microns) purchased from Analtech. Extraction solutions were dried over $MgSO_4$ prior to concentration. (The chemistry scheme and synthesis described in Figure IV-A2 in Appendix IV-2.)

Biochemistry

All the reagents were the same as specified in Chapter II. The hPXR activation and cell viability in 96-well format assay was from Puracyp, Inc. Rifamycin S was from AAPharmaSyn LLC. Rifampin was from Boche Scientific.

Computational Modeling of Rifamycin•RNAP Complexes.

Initially, the rifabutin (RBN) bound to *Thermus thermophilus* RNAP complex was modified (described in Figure IV-A1 in Appendix IV-1). The proposed analogues were then generated using the modified RBN complex where all of the water molecules present in the structure were removed. All residues that did not have one or more atoms within approximately 20 Å of the RBN were deleted. The remaining atoms of RBN, which were not modified in the generation of the proposed analogue, were initially fixed in space and treated as part of the RNAP holoenzyme. A LowModeMD (*29*) conformational search algorithm with energy minimization was then employed to generate plausible poses (conformations) of the modified portions of RBN. The LowModeMD search was conducted in MOE (*30*) using default settings. Hydrogen atoms, modified portions of RBN and protein side chains within ~16 Å of the modified portions were allowed to move during the conformational search and energy

minimizations. Generated poses were ranked by interaction energies and duplicate poses based on a RMSD cutoff removed. The lowest energy pose was then selected and the truncated RNAP complex soaked with water to a surrounding distance of 6 Å. A series of energy minimizations were then conducted using the MMFF94x force field to relax the complex. First, hydrogen atoms and then the water molecules were allowed to relax while the entire analogue and all of the RNAP atoms were held fixed. Second, the modified portions of RBN and side chains of RNAP within 16 Å were also allowed to relax with the water molecules and hydrogen atoms. Finally, the entire analogue molecule, residues of RNAP within 16 Å, and the water molecules and hydrogen atoms were allowed to relax. The relaxed complexes were then examined to determine how the proposed analogue may interact with the sigma factor or other portions of RNAP (specifically the β and β` subunits).

Synthesis of Analogues 2a – 2e

The synthetic route utilized to make our target "one-armed" compounds **2b-2d** is shown in Figure IV-A2 in Appendix IV-2. A "two-armed" RLZ congener (**2e**) was also synthesized to assess the effect of the additional side chain on biological activity. The complete synthesis is described in Appendix IV-A2.

Expression and Purification of MTB RNAP (WT and RifR mutants)

The WT and RifR mutants were prepared as described in Chapter II from the co-expression vectors (pMTBRP-5, 6, 7, 8) with minor alterations. For cell lysis, the sonication method (used to prepare *E. coli* RNAPs in Chapter II) was preferred over the freeze/thaw method. For the remainder of the purification steps, the protocol outlined in Chapter II was followed.

Cloning, Expression and Purification of MTB sigma factor (SigA)

The pAvitag vector (modified pMSCG7 vector with an Avitag introduced between *BglII* and *KpnI* sites) was linearized with SspI at 37°C for 1 h and the reaction product was purified using the Qiagen PCR kit. The linearized pAvitag vector (1.6-2.0 µg) was treated with T4 DNA polymerase in 10X T4 polymerase buffer, 5 mM DTT, 4 mM dGTP in a final reaction volume of 60 µL. The reaction was incubated for 30 min at 22°C and then for 20 min at 75°C before being stored at -20°C. PCR primers were designed to amplify the Rv2703/*sigA* gene encoding SigA from pSR01 (*31*). The primers included an overhang sequence that complemented the vector Ligation Independent Cloning (LIC) overhangs. The *sigA* gene was purified via Qiagen PCR kit. The purified PCR product (0.2 pmol) was incubated with T4 DNA polymerase, 5 mM DTT, 4 mM dCTP, 10X T4 DNA polymerase in a final reaction volume of 20 µL. The reaction was incubated for 30 min at 22°C and then for 20 min at 75°C and stored at -20°C. The treated *sigA* was incubated with treated pAvitag vector (~0.2 pmol) for 10 min at 22°C. Then 6.25 mM EDTA was added followed by incubation at 22°C for 5 min before reducing the temperature to 4°C. The annealed pAvitag vector containing *sigA* was transformed into BL21(DE3) CodonPlus RIPL cells.

For the expression of SigA protein in BL21(DE3) CodonPlus RIPL cells, the cells were grown in 500 mL of 2xTY liquid cultures containing 100 µg/mL carbenicillin and 30 µg/mL chloramphenicol at 37°C with vigorous shaking until cell density reached OD_{600nm}=0.5-0.6. The protein was induced by the addition of IPTG to a final concentration of 1 mM. The cultures were allowed to incubate for an additional 20-24 hours at 19°C. The cells were harvested by centrifugation (6000xg, 15 min, 4°C). The

cell pellet of each 500 mL culture was re-suspended in 10 mL of Ni^{2+}-NTA bind buffer (300 mM NaCl, 50 mM NaH_2PO_4, 10 mM imidazole, pH 8.0). The freeze/thaw method was followed to lyse the cells, and it was repeated a total of three times. The sample was supplemented with 10 µL of Lysonase™ Bioprocessing Reagent and 100 µM of PMSF, and then the resulting lysate was cleared by centrifugation (21,000xg, 30 min, 4°C). All further purification steps were performed at 4°C. The lysate was incubated with 2 mL Ni^{2+}-NTA His•Bind Resin overnight with gentle shaking. Each supernatant-resin mixture was applied to individual columns. The columns were washed twice with 4 mL of Ni^{2+}-NTA wash buffer (300 mM NaCl, 50 mM NaH_2PO_4, 20 mM imidazole, pH 8.0), and the protein was then eluted in 6 mL of Ni^{2+}-NTA elute buffer (300 mM NaCl, 50 mM NaH_2PO_4, 250 mM imidazole, pH 8.0). The protein was concentrated to a final volume of ~500 µL and then sterile-filtered with 0.22-µm syringe before being applied to a HiPrep 16/60 Sephacryl S-200 HR (GE Healthcare) column and the running buffer was RNAP storage buffer (10 mM Tris-HCl (pH 7.9), 0.1 mM EDTA, 0.1 mM DTT, 0.1 M NaCl). The fractions containing SigA were pooled together and concentrated to a final volume of ~500 µL using Amicon Centrifugal Filter Units (MWCO=10 kDa). SigA was mixed with one volume of 100% glycerol and stored in liquid nitrogen. The final concentration of SigA was determined via Bradford assay using the Bio-Rad Protein Assay Kit.

In vitro Transcriptional Activity of MTB RNAPs and Dose Response Curves

Dose response studies with RLZ (**2a**) and analogues (**2b-2e**) were performed via rolling circle transcription assay to determine the IC_{50} values. Each of the compounds was tested in duplicate (n=2). The concentration range used for the wild-type MTB RNAP (+/- SigA) was 1.56-100 nM for RLZ and analogues (**2b-2e**). The concentration ranges used for MTB RNAP (D435V) with SigA were as follows: for **2a** and **2e** (39.1-2500 μM); for **2b-2d** (1.25-80 μM). The concentration ranges used for MTB RNAP (H445Y) with SigA were as follows: for **2a** and **2e** (20.5-5000 μM); for **2b-2d** (8.2-2000 μM). The concentration ranges used for MTB RNAP (S450L) with SigA were as follows: for **2a** (8.2-2000 μM); for **2b** (3.3-800 μM); for **2c** and **2d** (1.64-400 μM); for **2e** (6.55-1600 μM). The final concentration of the wild-type MTB RNAP was 10 nM, whereas the final concentration of the RifR RNAPs was 100 nM in the reactions. The core RNAP and SigA were incubated for 30 min on ice in 1X RNAP reaction buffer (40 mM Tris-HCl (pH 8.0), 50 mM KCl, 10 mM $MgCl_2$, 0.01% Triton X-100) before adding the test compound and DNA nanocircle template (80 nM). The reactions were set up as outlined in Chapter II. The IC_{50} values were determined by non-linear regression and, the logIC_{50}s and their standard errors (of the fit) are reported in Table IV-A2 in Appendix IV-3).

Determination of Minimal Inhibitory Concentration (MIC) Against MTB **$H_{37}R_v$** ***Strains***

All compounds were evaluated for MIC_{90} vs. MTB $H_{37}R_V$ using the microplate Alamar Blue assay (MABA) as previously described (*32*) except that 7H12 media was used (replacing 7H9 + glycerol + casitone + OADC). The use of this and other redox

reagents such as MTT have shown excellent correlation with colony-forming unit (CFU)-based and radiometric analyses of mycobacterial growth in many laboratories. The MIC is defined as the lowest concentration effecting a reduction in fluorescence (or luminescence) of 90% relative to controls. Isoniazid and rifampin are included as positive quality control compounds with expected MIC ranges of 0.025-0.1 and 0.06-0.125 μg/mL, respectively.

The Low Oxygen Recovery (LORA) *in vitro* assay (*33*) is designed to detect compounds which may have the potential for shortening the duration of therapy through (more) efficient killing of the non-replicating persistor (NRP) population. The assay involves (1) adaptation of MTB to low oxygen through gradual, monitored, self-depletion of oxygen during culture in a sealed fermenter, (2) exposure for 10 days of the low-oxygen adapted culture to test compounds in microplates that are maintained under an anaerobic environment, thus precluding growth and (3) subsequent evaluation of MTB viability as determined by the ability to recover. Recovery/viability is determined either by (a) (aerobic) subculture onto solid, drug-free media and determination of colony forming units or (b) by the extent to which a luciferase-expressing strain can recover the ability to produce luminescence. Compounds such as isoniazid and ethambutol, which are considered to be devoid of "sterilizing activity", are inactive in this assay while the rifamycins and the more potent fluoroquinolones, which do appear to eliminate some proportion of the persistor population and thus can affect treatment duration, are active, albeit at concentrations higher than the MICs for replicating cultures. Correlation between the CFU and luminescence readout has been good with the exception of the

fluoroquinolone class for which luminescence underestimates absolute activity but not relative activity.

Computational Modeling of Rifamycin•hPXR Complexes

A 2.8 Å resolution crystal structure of hPXR in complex with rifampin is available from the Protein Data Bank (PDB ID: 1skx) (*22*). Unfortunately, the 1-amino-4-methylpiperazine tail of RMP and three hPXR loops adjacent to the binding pocket (residues 178-209, 229-235, and 310-317) are disordered and unresolved in the structure. The missing residues in this and other published hPXR structures make accurate modeling of the hPXR and the tails of rifamycins difficult. Figure IV-4 was created by overlaying the naphthalene portions of the four rifamycins generated from the 2a68 structure onto the naphthalene portion of RMP in complex with hPXR structure 1skx. The relative location of synthetic branch point for the analogues described in Figure IV-1 is also indicated in Figure IV-4. In addition to the complex with RMP, four other relatively complete hPXR structures are available. The hPXR apo structure (PDB ID: 1ilg) (*34*) and hPXR complexes with SR12813 (PDB ID: 1ilh) (*34*) hyperforin (PDB ID: 1m13) (*35*) and colupulone (PDB ID:2qnv) (*36*) were obtained from the Protein Data Bank. These four hPXR complexes were superimposed onto the hPXR structure of 1skx containing the four modeled in rifamycins. Coordinates were not relaxed with energy minimization due to the many missing residues.

Human Pregnane X Receptor Activation Assay

To assess the ability of specific rifamycins to activate the hPXR, the hPXR activation assay system from Puracyp, Inc. was used. The manufacturer's protocol was followed for the 96 well plate assay. Briefly, the DPX2 cells were thawed in a 37°C

water bath and mixed thoroughly with culture media. Then 100 µL of cell mixture was transferred into each well and the plate was incubated overnight in a 5% CO_2 incubator at 37 °C. The following day, the dosing media was thawed in a 37ºC water bath. The dilutions of RLZ (**2a**) and analogues (**2b-2e**) and RMP (**1**, positive control) were prepared as described in the manual. The 96 well plate was removed from the incubator and liquid from each well was discarded before adding 100 µL of the dilutions to the specific wells. Each dilution of the rifamycin derivative was tested in duplicate. The plate was placed in the 5% CO_2/37ºC incubator again for 24 h. The next day, the CellTiter-Fluor Buffer and CellTiter-Fluor™ were thawed at room temperature before adding 5 µL of CellTiter-Fluor™ to 10 mL of CellTiter-Fluor Buffer. The wells of the 96 well plate were emptied again and 100 µL of CellTiter-Fluor™ reagent was added to each well. The plate was incubated for 1 h in the 5% CO_2/37ºC incubator. A Synergy H1 Hybrid Multi-Mode Microplate Reader (BioTek) was used to measure fluorescence (λ_{ex}=390 nm; λ_{em}=505 nm). To obtain luminescence readings, the contents of ONE-Glo™ Assay Buffer were added to the ONE-Glo™ Assay Substrate and then 100 µL of mixture was transferred into each well. The plate was read after 5 min where the luminometer was set for 5 sec pre-shake with 5 sec/well read time. The Relative Luminescence Units (RLU) and Relative Fluorescence Units (RFU) were determined as outlined under the "Quantitation of PXR Receptor Activation" section of the manual. The normalized luciferase activity (RLU/RFU) was divided by the normalized DMSO control to represent the data as 'fold activation' relative to the control. The replicate data points were averaged and both the original data points and the average values were plotted as a function of log concentration versus PXR activation. The average values

were then fit by non-linear regression to a modified four parameter logistic equation using Kaleidagraph (Synergy Software, Essex, VT),

$$y = 1+ [(M3– 1)/(1 + 10^{[(M1-M0)*M2]})]$$

where M3 is the EC_{MAX}, and 1 is the lower limit of the assay, M0 is the log of the rifamycin concentration, M1 is the log of the EC_{50}, and M2 is the Hill slope. The data were normalized such that the lower limit was set to 1. M1, M2, and M3 were fit by the regression.

Microsome stability and Pharmacokinetic (PK) studies

Microsome stability and pharmacokinetics studies were performed in the Institute for Tuberculosis Research, University of Illinois, Chicago (see Appendix IV-4).

Results

Analogue Design and Synthesis

Modeling was based on the 2.5 Å resolution structure of RBN in complex with the *Thermus thermophilus* RNAP holoenzyme (PDB ID: 2a68) (*28*). From this structure and a related complex (PDB ID: 2a69; rifapentine in complex with the *T. thermophilus* RNAP holoenzyme), it was observed that the sigma factor hairpin loop might exist in two distinct physiologically relevant conformations, at least in the free holoenzyme. The modeled RLZ/RNAP complex without bound water molecules is shown in Figure IV-2. RLZ (**2a**) is shown with bright green carbon atoms and the different molecular surfaces of the RNAP are shown as follows: β subunit surface is colored white and light blue, β' subunit is brown, and the sigma factor is dark green. The interaction surfaces at 4.5 Å between the tail of analogue **2b** and surrounding RNAP are shown in Figure IV-3. (Similar poses for RLZ and analogues **2c** – **2e** are shown in Figure IV-A1 (A-D) in

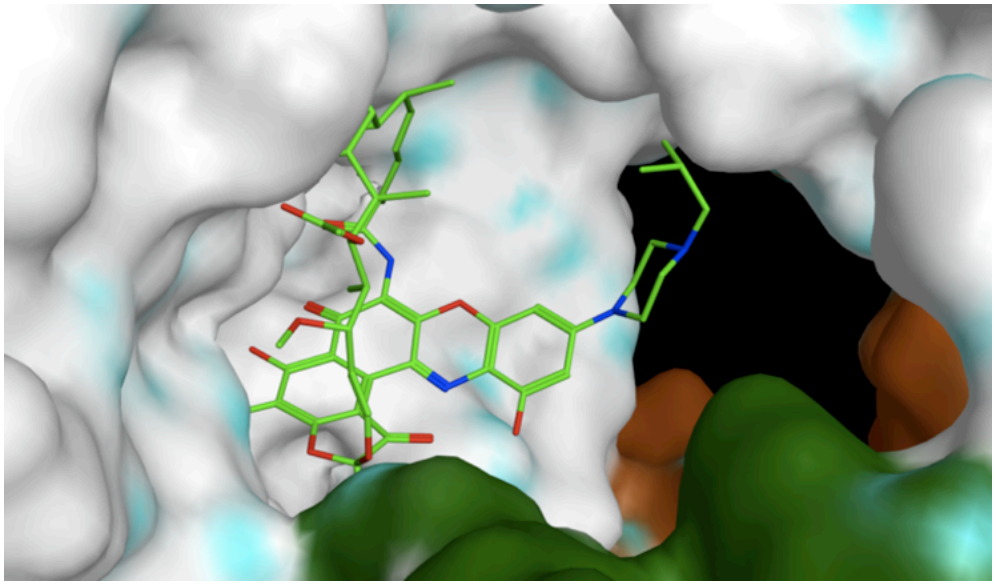

Figure IV-2: The modeled RLZ/RNAP complex without bound water molecules. RLZ (**2a**) is shown with bright green carbon atoms. The RNAP molecular surface is shown with β colored white and light blue, β' in brown, and the sigma factor in dark green.

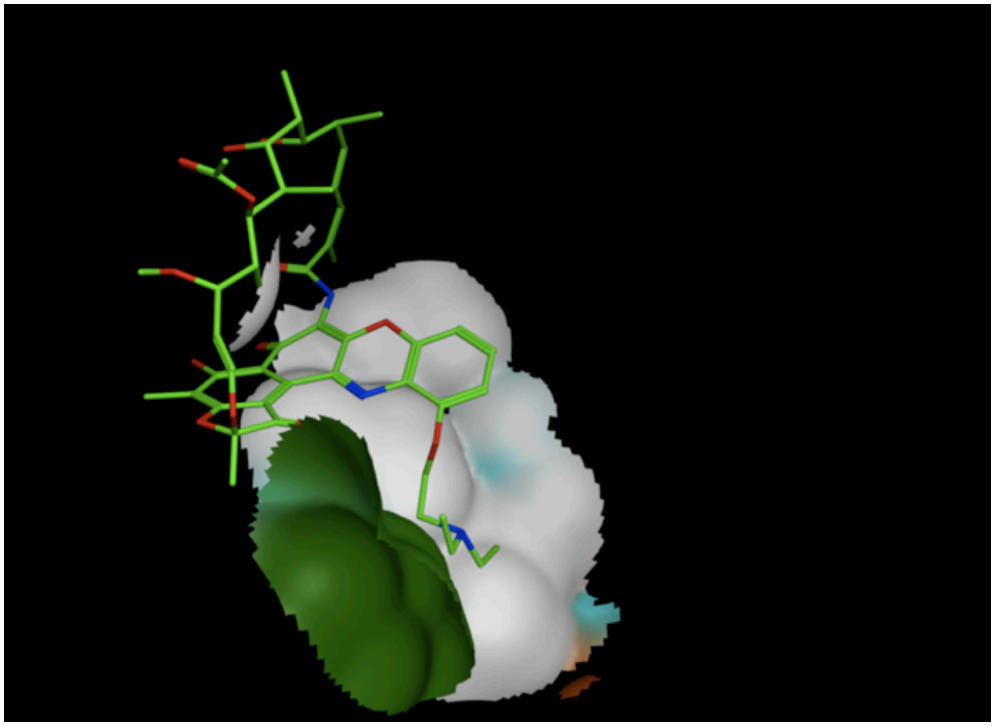

Figure IV-3: Interaction surfaces at 4.5 Å between the compound tail and surrounding RNAP for benzoxazinorifamycin **2b**, in the same coloring scheme as Figure IV-2.

Appendix IV-1.) These representative analogues **2a** – **2e** were then synthesized (the synthesis is described in Appendix IV-2).

In vitro Inhibition of Wild-type and RMP-resistant Mutant MTB RNAPs

The inhibition constants of the wild-type and three RifR mutants of the MTB RNAP by RLZ (**2a**) and analogues (**2b** – **2e**) were determined via dose-response studies where each compound was tested in duplicate at the specified concentrations in Materials and Methods section. To assess the additional binding of these analogues to the sigma factor, the MTB sigma factor (SigA) was expressed and purified and then incubated with the core enzyme for 30 minutes on ice to form a holoenzyme before initiating the assay. The band corresponding to SigA was observed on the SDS-PAGE after gel filtration of the preincubated sample of the core MTB RNAP and SigA, suggesting that the SigA did bind to form the holoenzyme (data not shown). (The IC_{50} values for these analogues with the core RifR RNAPs were not evaluated due to the very low activity observed after 30 min incubation of enzyme on ice.) The data were plotted (% activity vs. log benzoxazinorifamycin concentration) and then fitted by nonlinear regression. The logIC_{50} values and their standard errors (of the fit) are reported, with these roughly translating into a 20-25% error in the IC_{50} values (Table IV-A2 in Appendix IV-3). The apparent IC_{50} values are listed in Table IV-1. All of the benzoxazinorifamycins (**2a** – **2e**) inhibit the wild-type MTB RNAP in the 10^{-9} M (nM) range. The IC_{50} values for RLZ (**2a**) against the RifR mutants of MTB were much higher, in the 10^{-4} M (~100 μM) range. The most frequently observed MTB RifR mutant in clinical isolates, S450L, (*18, 37*) was inhibited at 2 to 5-fold lower concentrations of **2b**, **2c** & **2e** relative to RLZ with **2d** being essentially the same as RLZ. The MTB D435V mutant was inhibited at 5 to 50-

fold lower concentrations of **2b**, **2c, 2d** & **2e** relative to RLZ. For the H445Y mutant, Rlz and **2b** similar IC_{50} values; whereas, the other analogues (**2c**, **2d**, **2e**) were inhibited at 2.5-6 fold higher concentrations.

Table IV-1: *In vitro* RNAP IC_{50} Values (μM)[a] for RLZ (**2a**) and Analogues (**2b** – **2e**)

	2a (RLZ)	**2b**	**2c**	**2d**	**2e**
WT RNAP (-σ^A)	0.0115	< 0.01	< 0.01	< 0.01	0.017
WT RNAP (+σ^A)	< 0.01	< 0.01	< 0.01	< 0.01	0.021
D435V (+σ^A)	541	20	9	13	112
H445Y (+σ^A)	172	171	437	574	1074
S450L (+σ^A)	117	16	18	122	78

[a] IC_{50} is the concentration of rifamycin resulting in 50% inhibition of transcription. Errors of the logIC_{50} values are reported as described in the Material and Method Section. As a control the mutant RNAPs (D435V, H445Y, and S450L) without SigA were tested against RMP where the IC_{50} values are as follows: 313 μM (D435V), 830 μM (H445Y), and 126 μM (S450L). The standard errors of the logIC_{50} values roughly translate into a 20-25% error in the IC_{50} values.

Activity against M. tuberculosis ($H_{37}R_V$) in Cell Culture

Under aerobic conditions (MABA), all newly synthesized compounds **2b** – **2e** display superior activities (MIC_{90} values of 0.02 – 0.08 μM) relative to RMP (0.13 μM), but are less potent (5 to 40-fold) than RLZ (< 0.004 μM). Under anaerobic conditions (LORA), activity for "one armed" compounds **2b** – **2d** (MIC_{90} values 0.35 – 0.40 μM) is essentially equivalent to RMP (0.46 μM), and these range from 4 – 18.5 fold higher than in the MABA. Relative to RLZ, LORA potency for analogues **2b** – **2d** is lower (at least 20-fold) with **2e** strikingly poor, being essentially inactive (MIC_{90} > 6.72 μM).

Table IV-2: MIC_{90} Values (μM)[a] of RMP (**1**) and Benzoxazinorifamycins **2a** – **2e** vs. MTB

	1 (RMP)	**2a (RLZ)**	**2b**	**2c**	**2d**	**2e**
MABA	0.13	< 0.004	0.02	0.08	0.07	0.08
LORA	0.46	< 0.017	0.37	0.35	0.40	> 6.72

[a] The MIC_{90} is defined as the minimum concentration of the compound required to inhibit 90% of bacterial growth. Isoniazid (MABA: 0.24, LORA: >128), moxifloxacin (MABA: 0.46), streptomycin (MABA: 0.46), and PA824 (LORA: 2.53).

Human Pregnane X Receptor

RMP (**1**) is one of, if not the most, potent activators of hPXR (*22*). RMP fills the ligand-binding pocket very well. In Figure IV-4, four known rifamycins (RMP, rifapentine, RBN, and RLZ) were modeled in the hPXR binding site with spatial relation to resolved hPXR residues. In particular, there are seven hPXR residues, namely Phe-237, Ser-238, Leu-239, Leu-240, Pro-241, His-242 and Met-243, in very close proximity to the synthetic branch point for our synthesized analogues. These residues are resolved in each of the five hPXR structures and other than one of the Phe-237 rings, have fairly conserved relative coordinates. This, along with the presence of Pro-241, would suggest a more rigid region of the hPXR ligand-binding pocket.

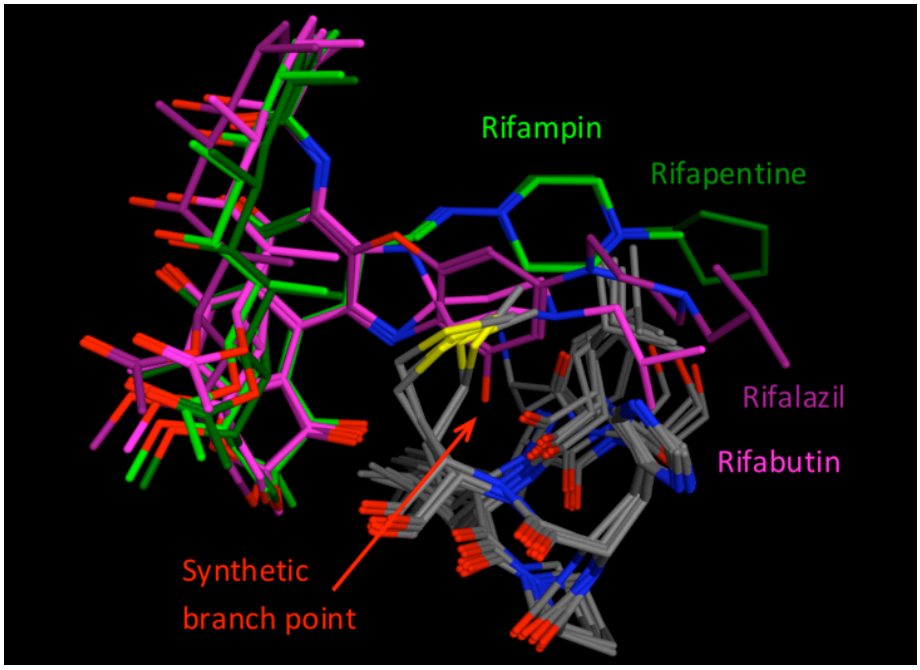

Figure IV-4: Clinical rifamycins modeled into the hPXR binding pocket.

To probe for hPXR activation, the commercially available *in vitro* assay for hPXR activation (Puracyp, Inc.) was used. The dose-response plots for the hPXR assay are shown in Figure IV-5. RMP exhibited a high maximal degree of activation (~12-fold) and an EC_{50} value of ~2 μM. RLZ did not display hPXR activation at concentrations as high as 25 μM. But RLZ did show ~2-fold receptor activation along with ~2-fold loss of cell viability at 100 μM. Analogue **2d** was fit to a dose-response curve that revealed a 6-fold maximal activation of hPXR and an EC_{50} of ~6 μM. Analogue **2d** also started to exhibit loss of cell viability at 25 μM; therefore, the 100 μM data point was not used in the dose-response curve fit (Figure IV-6 and Table IV-A3 in Appendix IV-3). Analogue **2e** shows hPXR activity very similar to that of RLZ, with no activation or loss of cell viability below 25 μM and ~3-fold activation and ~25% loss of cell viability at 100 μM. Analogues **2b** and **2c** were essentially identical with ~3-fold hPXR activation at 6.25 μM

and dramatic loss of cell viability above 6.25 µM (such that no hPXR activation was seen).

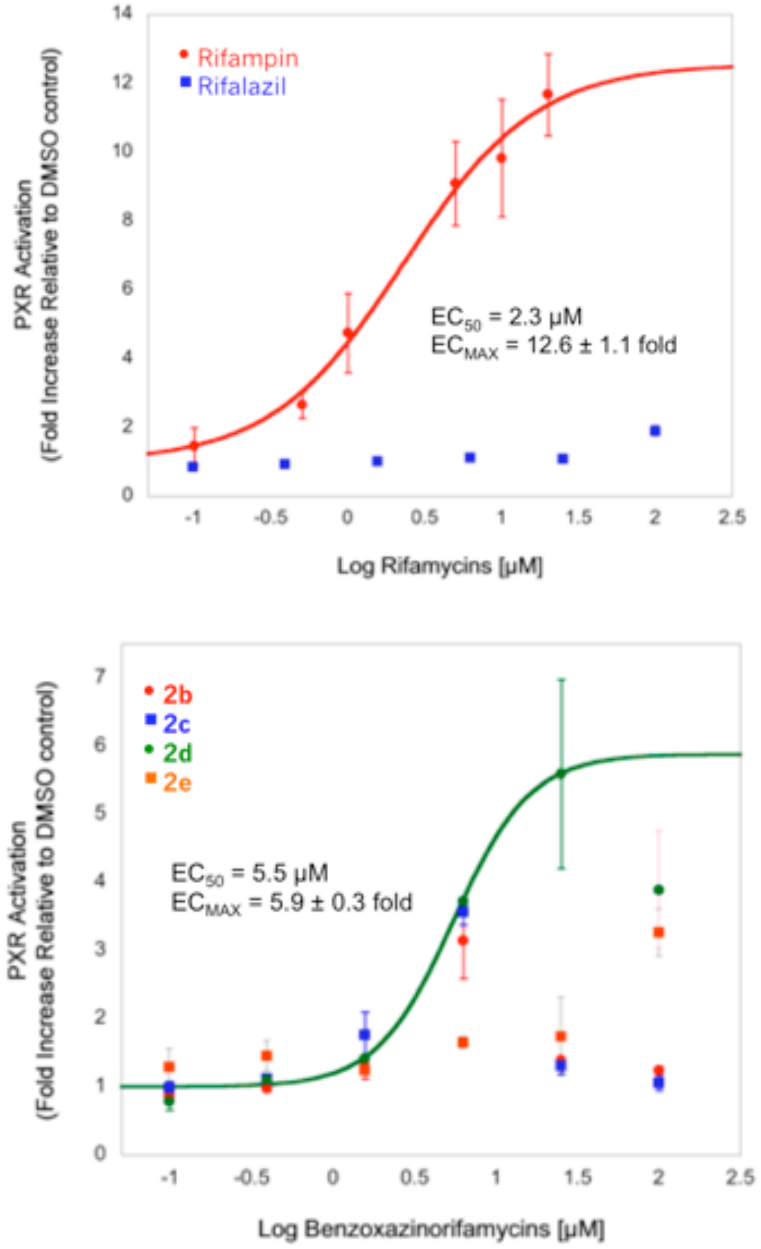

Figure IV-5: Plots from the hPXR activation assay.

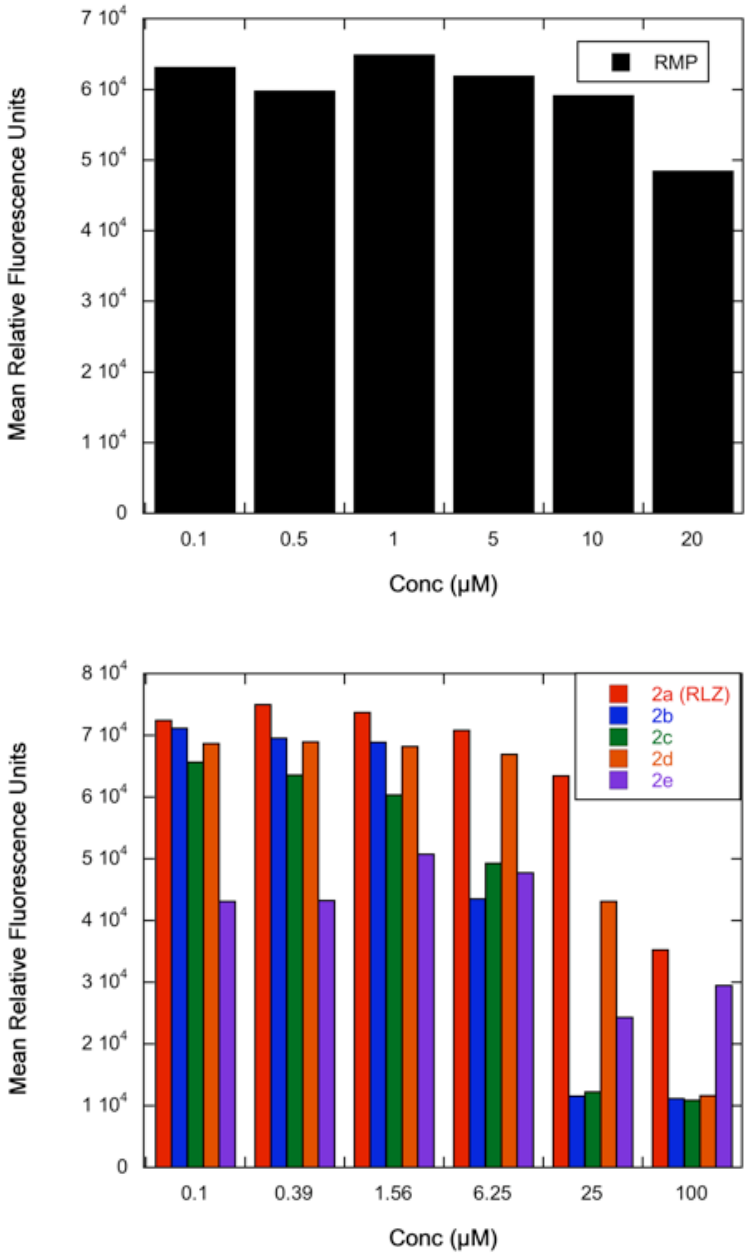

Figure IV-6: Effect of Rifampin (top) and Benzoxazinorifamycins (bottom) on DPX2 cell growth as measured by CellTiter-Fluor™.

Microsome Stability and Pharmacokinetics (PK)

RLZ (**2a)** and analogue **2b** were evaluated for metabolic stability in human microsomes. Both were relatively stable with estimated half-lives of 65 and 54 min,

respectively (Table IV-3). Similarly, the estimated half-life of **2a** in mouse microsomes was 53 min while that of **2b** was 141 min.

Table IV-3: Half-life of Selected Benzoxazinorifamycins in Human and Mouse Microsomes

	% Remaining compound after 30 min incubation in microsomes		$t_{1/2}$ (min)	
Compound	**Mouse**	**Human**	**Mouse**	**Human**
2a (RLZ)	67	73	53	65
2b	86	68	141	54

The PK of analogue **2b** was assessed using a suspension prepared in carboxymethylcellulose (0.05% CMC). In the single dose study, **2b** was detected in the blood but the signal was below the lower limit of quantitation. The C_{max} was 0.0185 μM at a T_{max} of 1 h. However, analogue **2b** appeared to accumulate in the blood of mice that were dosed once daily for 5 consecutive days with a C_{max} of 1.74 μM at a T_{max} of 2 h, which is 100-fold higher than that observed after a single oral dose (Figure IV-A4 in Appendix IV-4). In the lung tissue of these mice, **2b** was also detected at a concentration of 1.79 ug/g (around 0.4 μM), but only exceeded the MIC of 0.02 μM for ~4 h (Figure IV-A4).

Discussion

Recent determinations of the three-dimensional structures of rifamycins bound to RNAP provide a conceptual framework for structure-based discovery of improved rifamycins (*27, 28*). In addition, the design of these novel analogues was based on benzoxazinorifamycins that have shown improved antimicrobial activity against MTB (*8, 9*). Previously, C-5' benzoxazinorifamycin and C-3' hydroxy derivatives have been synthesized where RLZ was selected as the most promising derivative (*9*). Apart from an

obscure report on the synthesis of a small series of simple benzoxazinorifamycin C-3' monoethers (*38*), there are no examples of more elaborate ethers that have been incorporated onto a rifamycin S scaffold utilizing the strategy outlined here. These analogues are the first example (as far as we know) where structure-based design has been utilized to elaborate the ansa-napthalene core in a novel way that would lead to enhanced binding affinity to both WT MTB RNAP and RifR mutants.

Although modeling was based on *Thermus thermophilus* RNAP, the rifamycin binding site is highly conserved among prokaryotes (*27, 39*); therefore, this structure provides a good foundation for understanding how proposed rifamycin analogues may interact with the MTB RNAP. The designed analogues ranged in size, flexibility, and spatial variation with the likelihood of increasing potency by one or more of the following: (a) making additional contacts with the sigma factor, β, and/or β' regions of the RNAP and (b) interfering with the binding of the sigma factor and/or further occluding the channel. The modeled complexes seen in Figure IV-3 and Figure IV-A1 (A-D) illustrate that the benzoxazinorifamycins have the potential to interact with different regions of RNAP.

Previously, the effect of RLZ on *E. coli* and *Mycobacterium avium* RNAPs was examined and compared to RMP. The IC_{50} value of RLZ was higher than RMP for both RNAPs (*E. coli*: RLZ, 0.138 μM; RMP, 0.122 μM; *M. avium*: RLZ, 0.213 μM; RMP 0.085 μM). Therefore, it was concluded that the greater antibacterial activity of RLZ (a more hydrophobic compound) is due to greater permeability into the cell (*40*). Here, the IC_{50} values of RLZ and analogues **2b** – **2d** were determined for the WT and the three RifR mutants (Table IV-1). The lower limit of detection of the rolling circle transcription

assay is an IC_{50} value of ~5 nM, so it is quite possible that these analogues have true IC_{50} values that are much lower; therefore, a more sensitive assay needs to be developed to determine the very low IC_{50} values. RLZ and all other analogues inhibit the WT MTB RNAP at 10^{-9} M (nM) range with and without SigA. The IC_{50} values for RLZ with the RifR mutants of MTB were much higher, in the 10^{-4} M (~100 μM) range. Increasing the concentration of RifR RNAPs to 100 nM and the binding of SigA seemed to stabilize the MTB RNAPs, which allowed the IC_{50} values of each analogue to be determined and compared to the one another. Here the IC_{50} values of RLZ with RifR RNAPs were similar to those observed for RMP (listed underneath Table IV-1). Previously, RLZ has been reported to be active against RifR strains including the D435V mutant, but RifR MTB strains with mutations at His445 and Ser450 (major mutation sites) were still resistant to RLZ (*13, 15-18*). However, our data indicates that RLZ has a higher apparent IC_{50} value for the D435V mutant than the other two RifR mutants (Table IV-1). The results from this very limited series of analogues provide proof of principle that the potency of rifamycins towards RifR MTB RNAPs can be substantially improved and the range of inhibition by the analogue depends on the type of RifR mutation.

RLZ was the most potent under both MABA and LORA conditions. The MABA MIC_{90} value was comparable to what has been reported previously for MTB $H_{37}R_V$ strain (MIC_{90} value 0.004 μM) (*16*). Analogues **2b** – **2e** had improved antimicrobial activity compared to RMP but were less potent than RLZ. However analogue **2e** had a much higher LORA MIC_{90} value (> 6.72 μM) where the addition of the RLZ side chain into the 5'-position of **2e** introduces another basic moiety, which may impede its transport across the cell membrane of the non-replicating bacterial strain of the LORA.

In addition to designing analogues that might be more potent against WT and RifR RNAPs, these novel compounds were also expected to reduce Cyp450 induction effects. Cyp450 induction effects (due to activation of the hPXR) decrease with a progression from the RMP (hydroquinone core) to the RLZ (markedly modified quinone core) scaffold. The relative potency of CYP3A4 induction is RMP > rifapentine > rifabutin > RLZ (*41, 42*). Within this same order of structural subclasses, there is also a trend of RLZ possessing increased potency against drug-susceptible isolates of slow-growing mycobacteria and better *in vivo* efficacy in mice (*14*). Analysis of a recent structure of RMP (**1**) bound to the hPXR suggests that these elaborations may have the significant added benefit of reducing the affinity of the analogues for hPXR, thereby reducing CYP450 induction activity (*22*). The hPXR ligand-binding pocket is large, flexible, and capable of adapting itself to bind a large variety of ligands (*22*). It appears the tails of these benzoxazinorifamycins may prevent binding to hPXR by projecting into rigid, sterically encumbered regions of hPXR. Therefore, the diminished binding to hPXR would then presumably reduce induction of CYP450s.

The activation of hPXR by these novel analogues was then assessed. RLZ as reported previously does not activate the hPXR (*41*). Unfortunately, the other analogues did exhibit hPXR activation up to a certain concentration before cell toxicity was observed (Figure IV-6). The apparent toxicities (in this cell line) of **2b** and **2c** is currently unexplained. Further studies in this and other cell lines are needed to confirm this toxicity and to probe the responsible mechanism. The lower toxicities of **2d** and **2e** show that improved rifamycin analogues are possible. It seems likely that the flexible side chains may allow for the side chains to adopt a conformation that minimizes the

clash with the hPXR ligand binding pocket. The observation that **2e** is very similar to RLZ in hPXR activation is consistent with this hypothesis since **2e** is a very close analogue of RLZ and has both sides chains, thereby reducing their degrees of freedom. It should be noted that at least for the wild-type RNAP, there is ~1000 fold difference between the RNAP IC_{50} and the threshold for apparent cytotoxicity. Nevertheless, the lower toxicity of and hPXR activation by **2e** shows that novel rifamycin analogues with improved side effects can be made.

Mouse and human microsomal studies of analogue **2b** show it to have excellent metabolic stability relative to RLZ (**2a**). The pharmacokinetics of **2b** showed accumulation of the compound in plasma after multiple dosing with an apparent half-life of ~1-2 h, suggesting that compound levels are above the MIC ~7-8 h if the decay is linear. This is corroborated by studies in lung tissue where levels of **2b** exceeded the MIC of 0.02 μM for only ~4 h. These studies suggest non-optimal pharmacokinetics for this compound, and that further SAR will be necessary to find a compound to take to *in vivo* efficacy studies.

Conclusions

We have utilized recent determinations of the three-dimensional structures of rifamycins bound to RNAP to design and synthesize a novel subclass of benzoxazinorifamycins (**2b** – **2e**), possessing a range of size, flexibility, and spatial variation to interact with the sigma hairpin loop and other regions of the RNAP complex. Relative to RLZ (**2a**), these analogues generally displayed superior affinity toward WT and RifR mutants of the MTB RNAP but lower antitubercular activity in cell culture (under both aerobic and anaerobic conditions). We have also utilized information from

the crystal structure of RMP (**1**) bound to hPXR as part of our design strategy toward analogues **2b** – **2e**, and have determined that analogue **2e** displays lowered affinity for hPXR relative to RMP (**1**) and similar to RLZ (**2a**), thereby suggesting a potential for reduced CYP450 induction activity. Mouse and human microsomal studies of analogue **2b** show it to have excellent metabolic stability; mouse pharmacokinetics in plasma and lung show accumulation of **2b**, but with a half-life suggesting non-optimal pharmacokinetics.

Notes to Chapter IV

We gratefully acknowledge Hao Xu and Dr. Hollis Showalter for the synthesis of the rifalazil and benzoxazinorifamycin analogues. We thank Dr. Scott Franzblau (Institute for Tuberculosis Research at University of Illinois at Chicago) for providing the antitubercular activity, microsomal stability and pharmacokinetics data. We would also like to thank Dr. Paul Kirchhoff for his contribution with the structural studies/models. We acknowledge generous support by the University of Michigan College of Pharmacy Ella and Hans Vahlteich and UpJohn Research Funds. We would also like to acknowledge additional funding by the University of Michigan Office of the Vice President for Research, and the Rackham Graduate School.

The work described in this chapter has been accepted in the *Journal of Medicinal Chemistry* (Gill, S.K., Hao, X., Kirchhoff, P.D., Wan, B., Zhang, N., Peng, K.-W., Franzblau, S.G., Garcia, G.A., and Showalter, H.D.H. Structure-based Design of Novel Benzoxazinorifamycins with Potent Binding Affinity to Wild-type and Rifampin-resistant Mutant *Mycobacterium tuberculosis* RNA Polymerases *Journal of Medicinal Chemistry* (2012) **DOI: 10.1021/jm201716n**). Due to poor purity and NMR results, the data for benzoxazinorifamycin analogue (**2e**) was not published.

Abbreviations used: TB, tuberculosis; RNAP, DNA-dependent RNA polymerase; SigA, MTB housekeeping sigma factor A; WT, wild-type; RifR, Rifamycin-resistant; MTB, *Mycobacterium tuberculosis*; MDR, multi-drug resistant TB strain; XDR, extensively-drug resistant TB strains; RMP, rifampin; RLZ, rifalazil; RBN, rifabutin; SAR, structure-activity relationship; NTP, ribonucleotide triphosphate; IPTG, isopropyl β-D-thiogalactoside; SDS-PAGE, sodium dodecyl sulfate polyacrylamide gel electrophoresis; PMSF, phenylmethylsulfonyl fluoride; EDTA, ethylenediaminetetraacetic acid; DTT, dithiothreitol; RNA, ribonucleic acid; MABA, Microplate Alamar Blue Assay; LORA, Low Oxygen-Recovery Assay; IC_{50}, concentration of rifamycin resulting in 50% inhibition of transcription; MIC_{90}, concentration of rifamycin that results in 90% inhibition of bacterial growth; CYP3A4, cytochrome P450 3A4; hPXR, human pregnane X receptor; EC_{50}, half maximal effective concentration; EC_{MAX}, maximal effective concentration of the compound; RFU, relative fluorescence units; RLU, relative luminescence units; HRMS, high resolution mass spectrometry; TLC, thin layer chromatography; LIC, ligation independent cloning

Appendix IV-1

Structural Modeling

The structure of 2a68 was used as the starting point in our modeling studies (*28*). In brief, modifications made to the structure prior to its use in the modeling were as follows. All water molecules and metals greater than 12 Å from RBN were removed. Four magnesium ions within 12 Å were converted to water molecules. Partially missing residues were repaired. Connection points for completely missing residues were greater than 35 Å from RBN, and were kept fixed in space during the energy minimizations. All N and C termini, either real or as a result of missing residues, were acetylated and amidated respectively. RBN was removed from the complex. Hydrogen atoms were added to the proteins and the force field set to AMBER99 and charged. Modifications were made to the RBN structure to produce the proposed analogue while keeping the unmodified atoms of RBN fixed in relation to the RNAP complex.

A series of energy minimizations were then conducted to relax the positions of the modified atoms using the AMBER99 force field to gradients of 0.01. Positions of hydrogen atoms were first relaxed with energy minimization. Repaired residues except for their C alpha atoms, termini, and hydrogen atoms were then relaxed. Lastly, the complete repaired residues, termini, and hydrogen atoms were relaxed. Resulting confirmations of the repaired residues and termini were checked. Bond orders for RBN were corrected, hydrogen atoms added, and the force field set to MMFF94x and charged. Positions of hydrogen atoms were relaxed with energy minimization using the MMFF94x force field to a gradient of 0.01. RBN was returned to the complex in its original pose.

A second series of energy minimizations were then conducted using the MMFF94x force field to gradients of 0.01. Positions of hydrogen atoms were first relaxed followed by positions of hydrogen atoms and all water molecules. Atoms of the RBN were then included in the minimizations. Lastly, positions of all RBN, water, and hydrogen atoms and protein residues having one or more atoms within 12 Å from RBN were relaxed with energy minimization. The naphthalene ring of RBN drifted approximately 1 Å toward the cleft of the complex from their crystallographic positions with relatively minor movements of the protein residues well within the 2.5 Å resolution of the starting structure.

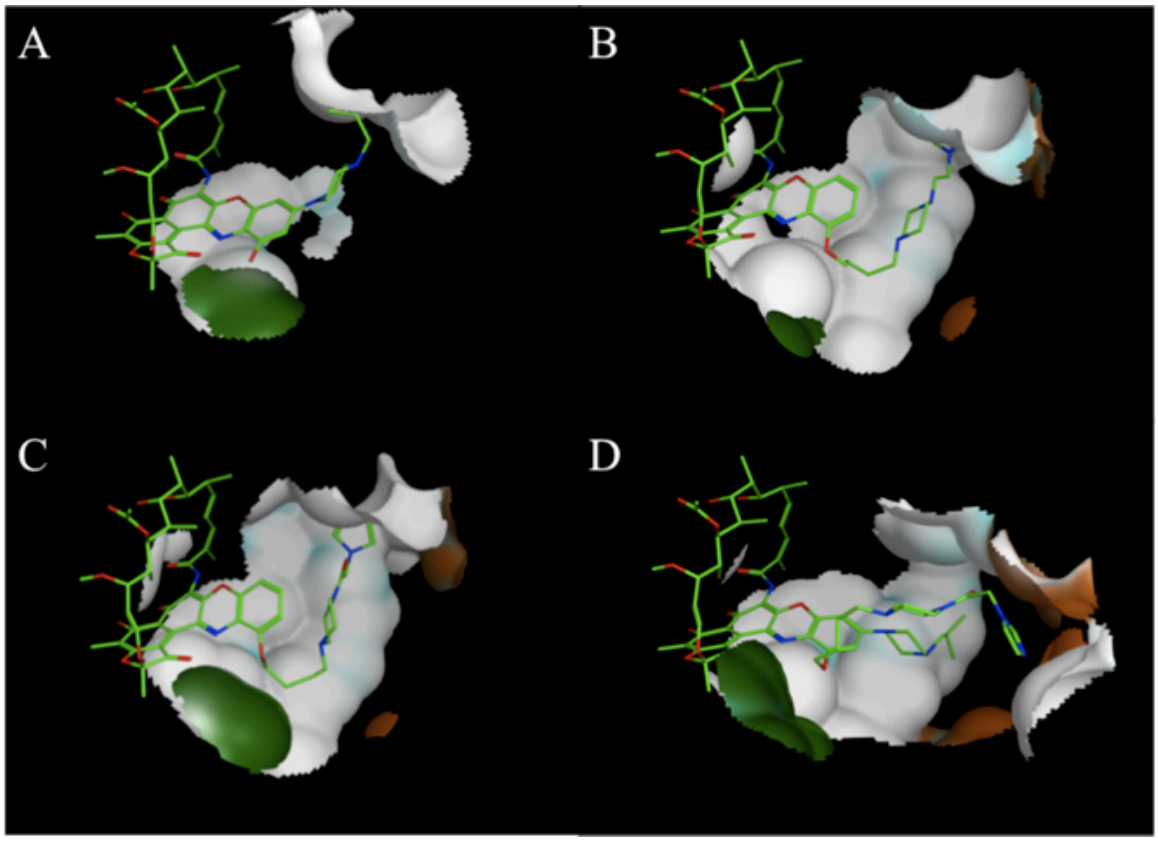

Figure IV-A1 (A-D): Interaction surfaces at 4.5 Å between the compound tail and surrounding RNAP for benzoxazinorifamycins **2a** and **2c-e** in the same coloring scheme as Figure IV-2.

Appendix IV-2

Chemistry and Synthesis

The RLZ literature (*43*) suggested a strategy of annulating the benzoxazino moiety onto rifamycin S (**12**) with a suitably protected monoether (e.g., TBS) of 2-aminoresorcinol, followed by ether deprotection and then side chain installation off the nascent phenol by any number of alkylation methodologies. This was investigated, but yields were very poor and the scope of alkylation possibilities was quite limited (data not shown). We opted instead to annulate a fully tethered 2-aminoresorcinol monoether onto the rifamycin S framework in a single step. This allowed us to consider a wide range of tethers off the "southeastern" part of the rifalazil-type template, and more importantly, minimized difficult synthetic transformations and product purifications involving the complex rifamycin S core to a single last step. Thus, we set our sights initially on developing a robust procedure to intermediate **5**, which would serve as a key starting material for introduction of our chosen tethers. While there are two reports for the synthesis of this compound (*44, 45*) neither was deemed practical for our needs. Instead, we pursued a two-step procedure. Accordingly, dialkylation of 2-nitroresorcinol (**3**), similar to the literature procedure (*46*), gave a 95% yield of dibenzyl ether **4** which was then cleanly mono-debenzylated to nitrophenol **5** (*44*) in 82% yield. With **5** now in hand, we were ready to install our target tethers. Phenolic alkylation with 2-(diethylaminoethyl)ethyl chloride hydrochloride under standard conditions provided **6** in 87% yield. Hydrogenation of **6** utilizing Pearlman's catalyst simultaneously reduced the nitro function and hydrogenolyzed the benzyl protecting group to give the 2-aminoresorcinol ether **7** in 81% yield. A similar sequence of reactions was followed to

provide ethers **11a**, **11b**. Alkylation of **5** with 1,4-dibromobutane gave **8** in 93% yield, which was subsequently aminated with two mono-substituted piperazines to afford compounds **9a** and **9b** in 68% and 99% yields, respectively. *t*-Boc deprotection of **9b** followed by acylation of **9c** with 2-(1*H*-imidazol-1-yl)acetic acid provided **10**, the amide congener of **9a**, in 72% yield. Hydrogenation of **9a** and **10** was conducted as described for **6** to provide the remaining 2-aminoresorcinol ethers **11a** and **11b**, respectively, in nearly quantitative yields. Each 2-aminoresorcinol ether (**7**, **11a**, **11b**) was then annulated onto rifamycin S (**12**) to provide target compounds **2b** – **2d** in 35 – 74% yields following a two-stage purification utilizing medium pressure and then preparative plate silica gel chromatography. No effort was made to optimize the condensation reaction with rifamycin S, but we feel that this has the potential to be an efficient transformation.

Having achieved the synthesis of our desired "one-armed" target molecules, we decided to make a single proto-type "two-armed" RLZ congener (**2e**) to test the chemistry of its synthesis and the effect of the additional side chain on biological activity. Thus, condensation of **2d** with *N*-isobutylpiperazine under oxidative conditions as described for the synthesis of RLZ (**2a**) (*43*) gave a 74% yield of **2e** following rigorous purification. The structural assignments of **2b** – **2e** were supported by diagnostic peaks in the ^{1}H NMR spectra and by chemical ionization (CI) and high resolution (HR) mass spectrometry.

Figure IV-A2: Synthesis of **2b** – **2e**[a]

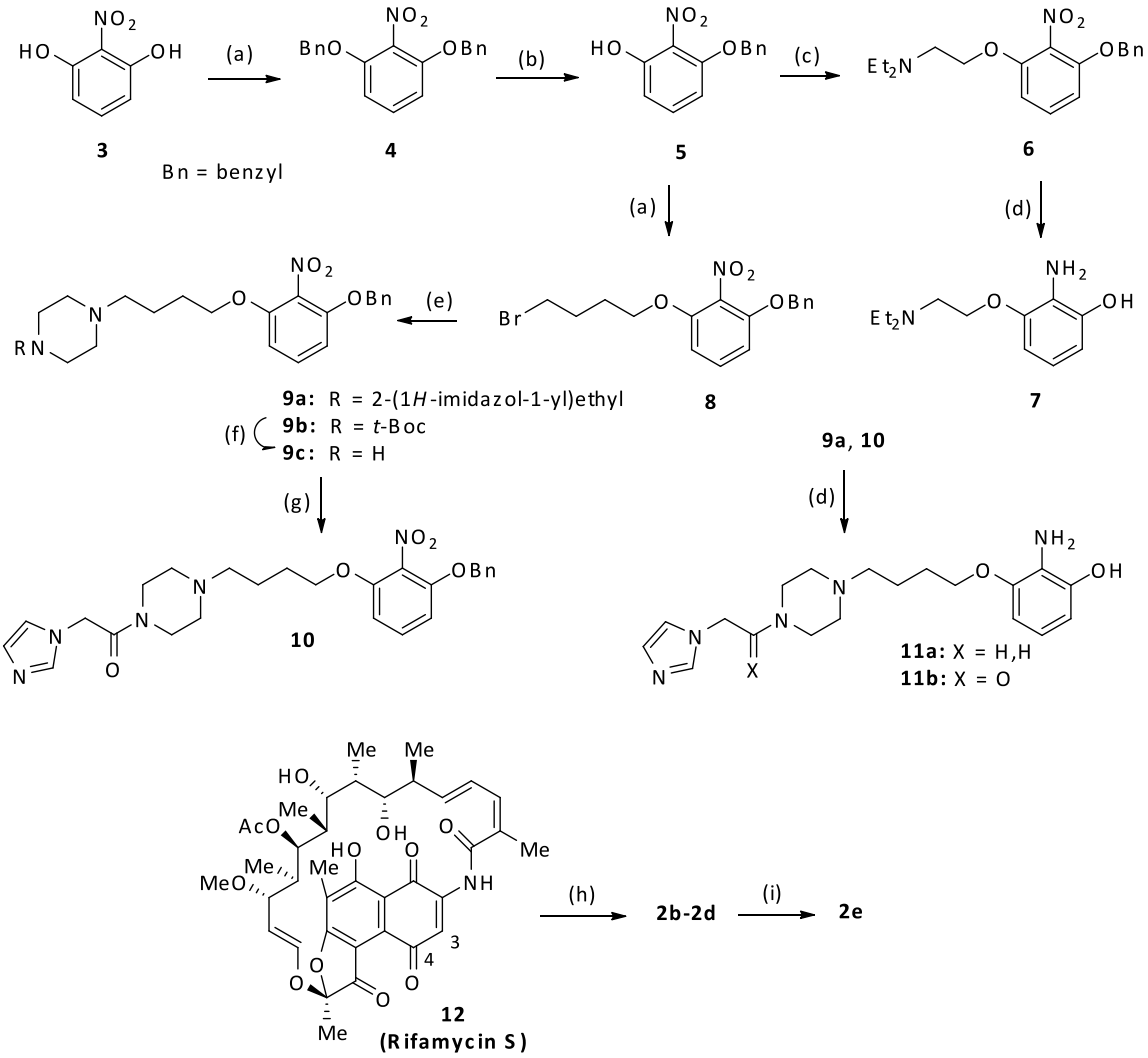

[a]Reagents and conditions: (a) benzyl bromide (for **3**) and 1,4-dibromobutane (for **5**), Cs_2CO_3, DMF, 25 °C, 12-16 h, 93-95%; (b) BCl_3, DCM, -78 °C, 1 h, 82%; (c) $Et_2NCH_2CH_2Cl \cdot HCl$, Cs_2CO_3, acetone, 50 °C, 3 h, 93% (d) 20% Pd/C, H_2 (40 psi), 25 °C, 20-40 h, MeOH:HOAc (9:1) for **6**; MeOH:10% aq HCl (9:1) for **9a**,**10**; 81 – 98%; (e) 1-[2-(1*H*-imidazol-1-yl)ethyl]piperazine or 1-Boc-piperazine, DIPEA, CH_3CN, reflux, 12-18 h, 68-99%; (f) TFA, DCM, 25 °C, 3 h; (g) 2-(1*H*-imidazol-1-yl)acetic acid, DIPEA, EDC·HCl, HOBT, DMF, 25 °C, 16 h, 72% from **9b**; (h) **7**, **11a**, or **11b**; *p*-dioxane or 1,2-DCE, MnO_2, 25 °C – reflux, 35 – 74%; (i) for **2d**, 1-(2-methylpropyl)piperazine, DMSO, MnO_2, 2 h, 74%.

Synthesis of RLZ and analogues

(((2-Nitro-1,3-phenylene)bis(oxy))bis(methylene))dibenzene (4)

A mixture of 2-nitroresorcinol (**3**; 2.0 g, 12.9 mmol), Cs_2CO_3 (10.5 g, 32.2

mmol), benzyl bromide (3.39 ml, 28.4 mmol) and DMF (35 mL) was stirred at room temperature for 12 h. The mixture was diluted with ethyl acetate and washed sequentially with 1% aq HCl and brine. The organic phase was dried and concentrated to leave a yellow oil, which was diluted with 2-propanol to precipitate pure product. The solids were collected to leave **4** (4.35 g, 95%) as light yellow crystals: mp 87.5 - 88° C (lit(*46*) 80° C); R_f 0.26 (hexanes : ethyl acetate, 5 : 1); ^{1}H NMR ($CDCl_3$) δ 7.3 (m, 10 H), 7.23 (t, *J* = 8.5 Hz, 1 H), 6.64 (d, *J* = 8.5, 2 H), 5.16 (s, 4 H); ^{13}C NMR ($CDCl_3$) δ 150.9, 135.6, 130.9, 128.7, 128.2, 127.0, 106.2, 71.0; MS (ES^+) *m/z* 358.1 $(M+Na)^+$.

*3-(Benzyloxy)-2-nitrophenol (**5**)*

A solution of dibenzyl ether **4** (3.0 g, 8.95 mmol) in dichloromethane (80 mL) at -78° C was treated drop-wise with boron trichloride (13 mL, 1M in heptane) during which the color changed to dark purple. The reaction was monitored by TLC and stirred at -78° C until all starting material was consumed (1 h). Methanol (5 mL) was added drop-wise and the mixture was brought to room temperature, cautiously diluted with 5% aq sodium bicarbonate, and then extracted with dichloromethane (2x). The combined extracts were dried and concentrated to an orange oil that was purified by flash silica gel chromatography eluting with hexanes : ethyl acetate (5 : 1). Product fractions were pooled and concentrated to give **5** (1.79 g, 82%) as a bright yellow solid: mp 67 - 67.5 ° C; R_f 0.24 (hexanes : ethyl acetate, 5 : 1); ^{1}H NMR ($CDCl_3$) δ 10.18 (brs, 1 H), 7.4 (m, 2 H), 7.3 (m, 4 H), 6.72 (d, *J* = 8.5 Hz, 2 H), 6.6 (d, *J* = 8.5 Hz, 2 H), 5.21 (s, 2 H); ^{13}C NMR ($CDCl_3$) δ 155.7, 154.7, 135.6, 135.4, 128.7, 128.2, 126.9, 111.0, 105.1, 71.4; MS (ES^+) *m/z* 268.0 $(M+Na)^+$.

*2-(3-(Benzyloxy)-2-nitrophenoxy)-N,N-diethylethanamine (**6**)*

A mixture of nitrophenol **5** (1.31 g, 5.4 mmol), 2-(diethylaminoethyl)ethyl chloride hydrochloride (1.2 g, 7 mmol), Cs_2CO_3 (4.37 g, 13.4 mmol) and acetone (20 mL) was stirred at 50° C for 3 h. The mixture was filtered and the filtrate was concentrated to a residue that purified by flash silica gel chromatography eluting with hexanes : ethyl acetate (5 : 1). Product fractions were pooled and concentrated to leave **6** (1.71 g, 93%) as a light yellow oil: R_f = 0.22 (CH_2Cl_2 : methanol, 95 : 5); ^{1}H NMR ($CDCl_3$) δ 7.3 (m, 6 H), 6.62, (dd, J_1 = 3.6 Hz, J_2 = 14.1 Hz, 2 H), 5.16 (s, 2 H), 4.1 (t, J = 10.5 Hz, 2 H), 2.8 (t, J = 10.5 Hz, 2 H), 2.6 (q, J = 11.9 Hz, 4 H), 1.0 (t, J = 11.9 Hz, 6 H); ^{13}C NMR ($CDCl_3$) δ 151.2, 150.8, 135.6, 130.9, 128.6, 128.2, 127.0, 105.9, 105.6, 70.9, 68.5, 51.2, 47.9, 11.9; MS (ES^+) *m/z* 245.1 $(M+H)^+$.

*2-Amino-3-(2-(diethylamino)ethoxy)phenol (**7**)*

2-(Diethylamino)ethyl ether **6** (1.8 g, 5.2 mmol) was dissolved in 10% acetic acid in methanol (50 mL) in a 250 mL Parr hydrogenation bottle. Catalyst (20% $Pd(OH)_2$/C, 0.1 g) was added and the mixture was hydrogenated at 40 psi H_2 for ~20 h. The reaction mixture was rapidly filtered over Celite®, and the filtrate was concentrated and diluted with ethyl acetate. The solution was washed with 5% aq sodium carbonate, dried, and concentrated to a brown solid that was triturated in hot hexanes. The solids were collected and dried to leave **7** (0.95 g, 81%): mp 91 - 91.5° C; R_f 0.21 (CH_2Cl_2 : methanol, 85 : 15); ^{1}H NMR ($CDCl_3$) δ 6.55 (t, J = 7.7 Hz, 1 H), 6.4 (m, 2 H), 4.07 (t, J = 5.8 Hz, 2 H), 2.91 (t, J = 5.8 Hz, 2 H), 2.7 (m, 4 H), 1.1 (t, J = 7.1 Hz, 6 H); ^{13}C NMR ($CDCl_3$) δ 148.0, 145.3, 124.9, 117.8, 109.0, 104.4, 66.5, 51.9, 47.4, 11.1; MS (ES^+) *m/z* 225.1 $(M+H)^+$.

*1-(Benzyloxy)-3-(4-bromobutoxy)-2-nitrobenzene (**8**)*

To a mixture of DMF (5 mL), 1,4-dibromobutane (5 mL) and Cs_2CO_3 (1.66 g, 5.1 mmol) was added slowly a solution of nitrophenol **5** (0.5 g, 2.0 mmol) in DMF (5 mL). The mixture was stirred at room temperature for 16 h, and then DMF was removed *in vacuo* to leave an oil that was distributed between 1% aq HCl and ethyl acetate. The organic phase was dried and concentrated to a light yellow oil that was purified by flash silica gel chromatography eluting with hexanes : ethyl acetate (6 : 1). Product fractions were pooled and concentrated to give **8** (0.702 g, 93%) as a light yellow oil: R_f 0.45 (hexanes : ethyl acetate, 2 : 1); ^{1}H NMR ($CDCl_3$) δ 7.36 (m, 5 H), 7.26 (m, 1 H), 6.61 (m, 2 H), 5.16 (s, 2 H), 4.08 (t, *J* = 5.8 Hz, 2 H), 3.46 (t, *J* = 6.3 Hz, 2 H), 2.02 (m, 2 H), 1.92 (m, 2 H); ^{13}C NMR ($CDCl_3$) δ 151.1, 150.9, 135.6, 131.0, 128.7, 128.2, 127.0, 106.1, 105.6, 70.9, 68.4, 33.4, 28.9, 27.5; MS (ES^+) *m/z* 401.9, 403.9 $(M+Na)^+$.

*1-(2-(1H-Imidazol-1-yl)ethyl)-4-(4-(3-(benzyloxy)-2-nitrophenoxy)butyl)piperazine (**9a**)*

A solution of bromobutyl ether **8** (1.0 g, 2.6 mmol), 1-[2-(1*H*-imidazol-1-yl)ethyl]piperazine (0.52 g, 2.9 mmol; Oakwood Products Inc.), *N*,*N*-diisopropylethylamine (5 mL) and acetonitrile (18 mL) was heated at reflux overnight. The solution was concentrated and the residue was distributed between dichloromethane and 5% aq sodium carbonate. The organic phase was dried and concentrated to an orange oil that was purified by flash silica gel chromatography eluting with dichloromethane : methanol : NH_4OH (90 : 10 : 0.5). Product fractions was pooled and concentrated to leave **9a** (0.86 g, 68%) as an oil: ^{1}H NMR ($CDCl_3$) δ 7.53 (s, 1 H), 7.36-7.22 (m, 6 H), 7.03 (s, 1 H), 6.97 (d, *J* = 1.1 Hz, 1 H), 6.61 (m, 1 H), 5.15 (s, 1 H), 4.05 (t, *J* = 6.3 Hz, 2 H), 4.01 (t, *J* = 6.5 Hz, 2 H), 2.67 (t, *J* = 6.5 Hz, 2 H), 2.48 (bs, 8 H), 2.36 (t, *J* = 6.5 Hz, 2

H), 1.79 (m, 2 H), 1.61 (m, 2 H); ^{13}C NMR ($CDCl_3$) δ 151.3, 150.8, 137.4, 135.6, 132.8, 130.9, 129.2, 128.7, 128.2, 127.0, 119.3, 105.8, 105.6, 70.9, 69.3, 58.6, 57.8, 53.3, 53.0, 44.7, 26.9, 23.1; MS (ES^+) *m/z* 480.1 $(M+H)^+$.

*tert-Butyl 4-(4-(3-(benzyloxy)-2-nitrophenoxy)butyl)piperazine-1-carboxylate (**9b**)*

A solution of bromobutyl ether **8** (0.4 g, 1.05 mmol), 1-Boc-piperazine (0.282 g, 1.514 mmol) *N*,*N*-diisopropylethylamine (4 mL) and acetonitrile (10 mL) was heated at reflux for 12 h. The solution was concentrated and distributed between ethyl acetate and brine. The organic phase was dried and concentrated to residue that was purified by flash silica gel chromatography eluting with ethyl acetate. Product fractions were pooled and concentrated to leave **9b** (0.505 g, 99%): ^{1}H NMR ($CDCl_3$) δ 7.36 (m, 4H), 7.31 (m, 1 H), 7.24 (m, 1 H), 6.61 (m, 2 H), 5.16 (s, 2 H), 4.06 (t, *J* = 6.2 Hz, 2 H), 3.41 (t, *J* = 7.0 Hz, 4 H), 2.36 (t, *J* = 7.0 Hz, 4 H), 1.80 (m, 2 H), 1.62 (m, 2 H), 1.46 (s, 9 H), 1.26 (t, *J* = 7.2 Hz, 2 H); ^{13}C NMR ($CDCl_3$) δ 154.9, 151.5, 150.9, 135.8, 131.0, 128.8, 128.3, 127.1, 106.0, 105.7, 79.7, 71.1, 69.4, 60.5, 58.1, 53.1, 28.6, 27.0, 23.2, 21.2, 14.3; MS (ES^+) *m/z* 486.1 $(M+H)^+$.

*1-(4-(4-(3-(Benzyloxy)-2-nitrophenoxy)butyl)piperazin-1-yl)-2-(1H-imidazol-1-yl)ethanone (**10**)*

Trifluoroacetic acid (2 mL) was added dropwise to a solution of **9b** (0.505 g, 1.04 mmol) in dichloromethane (8 mL), and the resultant mixture was stirred at room temperature for 3 h. The solution was concentrated to leave **9c** (0.52 g, quantitative) as the crystalline trifluoroacetate salt. This was then dissolved into DMF (10 mL) and *N*,*N*-diisopropylethylamine (3 mL), and the mixture was stirred at room temperature for 10 min followed by treatment with 1-ethyl-3-[3-dimethylamino propyl]carbodiimide

hydrochloride (EDC·HCl; 0.22 g, 1.14 mmol), *N*-hydroxybenzotriazole (HOBt; 0.175 g, 1.14 mmol) and 2-(1*H*-imidazol-1-yl)acetic acid (0.197 g, 1.56 mmol; Tokyo Chemical Industry Co. Ltd.) After stirring under N_2 for 16 h, DMF was removed *in vacuo* and the residue was distributed between dichloromethane and 5% aq sodium carbonate. The organic phase was dried and concentrated to an oil that was purified by flask silica gel chromatography eluting with dichloromethane : methanol : NH_4OH (95 : 5 : 0.5). Product fractions were pooled and concentrated to give **10** (0.37 g, 72%) as a yellow oil: ^{1}H NMR ($CDCl_3$) δ 7.49 (s, 1 H), 7.36 (m, 5 H), 7.26 (m, 1 H), 7.09 (s, 1 H), 6.95 (s, 1 H), 6.61 (m, 1H), 5.16 (s, 2 H), 4.75 (s, 2 H), 4.07 (t, *J* = 5.9 Hz, 2 H), 3.62 (m, 2 H), 3.44 (m, 2 H), 2.42 (t, *J* = 4.9 Hz, 4 H), 2.39 (t, *J* = 7.2 Hz, 2 H), 1.81 (m, 2 H), 1.62 (m, 2 H); ^{13}C NMR ($CDCl_3$) δ 164.4, 151.3, 150.8, 138.0, 135.6, 131.0, 129.5, 128.7, 128.2, 127.0, 120.1, 105.9, 105.5, 70.9, 69.1, 57.6, 52.6, 47.9, 45.1, 42.3, 26.7, 22.9; MS (ES^+) *m/z* 494.1 $(M+H)^+$.

*3-(4-(4-(2-(1H-Imidazol-1-yl)ethyl)piperazin-1-yl)butoxy)-2-aminophenol (**11a**)*

Compound **9a** (0.86 g, 1.8 mmol) was dissolved in a mixture of 10% aq HCl (10 mL) and methanol (90 mL) in a Parr hydrogenation bottle. Catalyst (20% $Pd(OH)_2$/C, 0.05 g) was added and the mixture was hydrogenated at 40 psi H_2 for ~40 h. The reaction mixture was rapidly filtered over Celite®, and the filtrate was concentrated and diluted with ethyl acetate. The solution was washed with 5% aq sodium carbonate, dried, and concentrated to give **11a** (0.61 g, 95%) as a brown solid: ^{1}H NMR ($CDCl_3$) δ 7.56 (s, 1 H), 7.05 (s, 1 H), 6.96 (s, 1 H), 6.52 (t, *J* = 7.2 Hz, 1 H), 6.44 (s, 1 H), 6.37 (d, *J* = 8.0 Hz, 1 H), 3.98 (m, 4 H), 2.66 (t, *J* = 6.2 Hz, 2 H), 2.49 (bs, 8 H), 2.41 (t, *J* = 6.5 Hz, 2 H), 1.78 1.68 (m, 2 H); ^{13}C NMR ($CDCl_3$) δ 147.6, 145.5, 128.6, 124.9, 119.4, 117.3, 108.7,

103.7, 68.1, 58.4, 58.2, 53.0, 50.4, 44.7, 27.5, 23.3; MS (ES^+) *m/z* 360.1 $(M+H)^+$.

*1-(4-(4-(2-Amino-3-hydroxyphenoxy)butyl)piperazin-1-yl)-2-(1H-imidazol-1-yl)ethanone (**11b**)*

Compound **10** (0.37 g, 0.75 mmol) was dissolved in a mixture of 10% aq HCl (5 mL) and methanol (45 mL) in a Parr hydrogenation bottle. Catalyst (20% $Pd(OH)_2/C$, 0.02 g) was added and the mixture was hydrogenated at 40 psi H_2 for ~40 h. Workup as described above for the synthesis of **11a** gave **11b** (0.27 g, 98%) as a brown solid: ^1H NMR (CD_3OD) δ 7.78 (s, 1 H), 7.13 (s, 1 H), 7.06 (s, 1 H), 6.58 (m, 1 H), 6.43 (m, 2 H), 5.08 (s, 2 H), 4.03 (t, J = 5.9 Hz, 2 H), 3.66 (s, 2 H), 3.62 (s, 2 H), 2.75 (s, 2 H), 2.65 (m, 4 H), 1.82 (m, 4 H); ^{13}C NMR (CD_3OD) δ 174.8, 165.8, 148.0, 145.8, 138.1, 126.0, 123.0, 121.3, 118.2, 107.8, 103.5, 67.7, 57.3, 52.1, 51.8, 43.5, 40.9, 26.8, 22.2, 20.1; MS (ES^+) *m/z* 374.1 $(M+H)^+$.

*Benzoxazinorifamycin (**2b**)*

A mixture of aminophenol **7** (0.336 g, 1.5 mmol), rifamycin S (**12**; 2.085 g, 3 mmol) and 1,4-dioxane (20 mL) was stirred at room temperature overnight. The mixture was then concentrated to a black solid that was dissolved in 20 mL of methanol and treated with MnO_2 (0.3 g, 3.45 mmol). The mixture was stirred at room temperature for 30 min, filtered over Celite®, and the filtrate concentrated to a dark residue that was purified by flash silica gel chromatography eluting with dichloromethane : methanol (95 : 5 to 90 : 10). Product fractions were pooled and concentrated to give partially purified **2b** as a deep purple solid. Further purification by preparative TLC was conducted on a 20 mg scale, eluting the plate with dichloromethane : methanol (90 : 10). The yield was ~55%: R_f 0.58 (dichloromethane : methanol, 85 : 15); HPLC t_R 6.1 min (95.4% purity);

^{1}H NMR ($CDCl_3$) δ 7.48 (t, J = 8.4 Hz, 1 H), 6.92 (d, J = 8.2 Hz, 2 H), 5.98 (d, J = 15.4 Hz, 2 H), 5.14 (bs, 2 H), 4.97 (m, 1 H), 4.41 (t, J = 11.6, 2 H), 3.29 (s, 2 H), 3.13 (s, 1 H), 3.08 (s, 3 H), 3.01 (d, J = 9.3, 2 H), 2.65 (m, 4 H), 2.29 (s, 3 H), 2.09 (s, 3 H), 2.05 (s, 3 H), 1.79 (s, 3 H), 1.70 (m, 2 H), 1.60 (m, 2 H), 1.25 (s, 3 H), 1.15 (t, J = 7.1 Hz, 6 H), 0.94 (d, J = 7.1 Hz, 3 H), 0.76 (d, J = 6.9 Hz, 3 H), 0.63 (d, J = 7.1 Hz, 3 H); MS (ES^+) *m/z* 900.1 $(M+H)^+$; HRMS (MALDI) calcd for $C_{49}H_{61}N_3O_{13}$ [$(M + H)^+$], 900.4277; found 900.4269.

*Benzoxazinorifamycin (**2c**)*

A mixture of aminophenol **11a** (80 mg, 0.22 mmol), rifamycin S (**12**; 220 mg, 0.32 mmol) and 1,2-dichloroethane (10 mL) was stirred at room temperature for 16 h. The reaction mixture was then concentrated to a black solid that was dissolved in 10 mL of methanol and treated with MnO_2 (80 mg, 0.92 mmol). The mixture was stirred at room temperature for 30 min, filtered over Celite®, and concentrated to a dark residue that was purified by flash silica gel chromatography eluting with dichloromethane : methanol : NH_4OH (94 : 6 : 0.5). Product fractions were pooled and concentrated to give a solid that was further purification by preparative TLC, eluting the plate with dichloromethane : methanol (92 : 8). The product band was processed to give **2c** (170 mg, 74%) as a dark purple solid: HPLC t_R 5.15 min (91.7% purity); ^{1}H NMR ($CDCl_3$) δ 7.56 (s, 1 H), 7.48 (t, J = 8.4 Hz, 1 H), 7.04 (s, 1 H), 6.98 (s, 1 H), 6.92 (d, J = 8.3 Hz, 1 H), 6.80 (d, J = 8.2 Hz, 1 H), 5.97 (m, 2 H), 5.12 (bs, 2 H), 4.94 (m, 1 H), 4.24 (t, J = 5.6 Hz, 2 H), 4.03 (t, J = 6.5 Hz, 2 H), 3.09 (s, 3 H), 3.01 (d, J = 9.3 Hz, 1 H), 2.68 (m, 2 H), 2.52 (bs, 11 H), 2.29, (s, 3 H), 2.09 (s, 3 H), 2.05 (s, 6 H), 1.80 (s, 5 H), 1.69 (m, 2 H), 1.60 (m, 2 H), 1.25 (s, 3 H), 0.93 (s, 3 H), 0.75 (s, 3 H), 0.64 (s, 3 H); MS (ES^+) *m/z* 1035.1 $(M+H)^+$; HRMS

(MALDI) calcd for $C_{49}H_{61}N_3O_{13}$ [$(M + H)^+$], 1035.5074; found 1035.5095.

*Benzoxazinorifamycin (**2d**)*

Reaction of a mixture of aminophenol **11b** (30 mg, 0.08 mmol), rifamycin S (**12**; 102 mg, 0.15 mmol) and 1,2-dichloroethane (4 mL) and subsequent purification was carried out exactly as described above for the synthesis of **2c** to provide **2d** (29 mg, 34.5%) as a dark purple solid: HPLC t_R = 5.11 min (91.8% purity); ^{1}H NMR ($CDCl_3$) δ 7.50 (m, 2 H), 7.10 (s, 1 H), 6.95 (m, 2 H), 6.87 (d, *J* = 8.3 Hz, 1 H), 5.98 (s, 1 H), 5.96 (s, 1 H), 5.30 (s, 2 H), 4.95 (m, 1 H), 4.76 (m, 2 H), 4.25 (m, 2 H), 3.68 (s, 1 H), 3.63 (s, 1 H), 3.49 (s, 1 H), 3.44 (s, 1 H), 3.11 (s, 3 H), 3.03 (s, 1 H), 2.58 (m, 2 H), 2.51 (m, 4 H), 2.29 (s, 3 H), 2.09 (s, 3 H), 2.06 (s, 3 H), 1.86 (d, *J* = 8.5 Hz, 1 H), 1.80 (s, 3 H), 1.68 (s, 2 H), 1.61 (bs, 9 H), 1.25 (s, 3 H), 0.94 (s, 3 H), 0.75 (s, 3 H), 0.65 (s, 3 H). MS (ES^+) *m/z* 1049.2 $(M+H)^+$; HRMS (MALDI) calcd for $C_{49}H_{61}N_3O_{13}$ [$(M + H)^+$], 1049.4866; found 1049.4857.

*RLZ analogue (**2e**)*

A mixture of benzoxazinorifamycin **2d** (5.5 mg, 0.005 mmol), 1-(2-methylpropyl)piperazine (2.3 mg, 0.016 mmol; Oakwood Products Inc.), MnO_2 (5 mg, 0.055 mmol) and DMSO (0.5 mL) was stirred at room temperature for 24 h and then filtered over Celite®. The filtrate was concentrated and purified by preparative TLC, eluting with dichloromethane : methanol (90 : 10). The product band was processed to give **2e** (4.6 mg, 74%) as a dark blue solid: HPLC t_R 5.33 min (95.3% purity); MS (ES^+) *m/z* 1189.5 $(M+H)^+$; HRMS (MALDI) calcd for $C_{49}H_{61}N_3O_{13}$ [$(M + H)^+$], 1189.6180; found 1189.6193.

Appendix IV-3

Confirmation of MTB RNAP subunits and MTB RNAPs Inhibition

Before moving further with the studies, it was important to confirm the bands observed on the SDS-PAGE were the MTB RNAP subunits rather than *E. coli* subunits or a mixture of the two. Previously, the identity of MTB α subunit was confirmed by Michigan Proteome Consortium via mass spectrometry. Furthermore, the identity of the contaminating proteins were also determined as we especially wanted to confirm the band at ~70 kDa was not the *E. coli* sigma factor, σ^{70}.

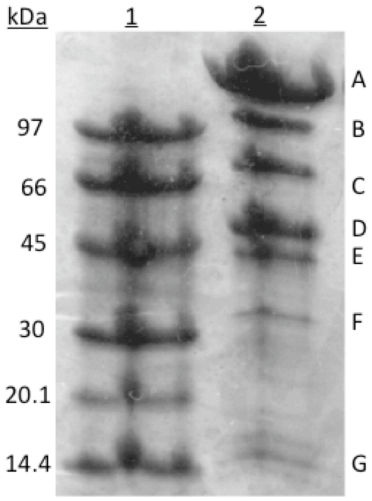

Figure IV-A3: SDS-PAGE of WT MTB RNAP after size exclusion chromatography. Lane 1, LMW standard; Land 2, WT MTB RNAP.

The seven bands (labeled A-G in Figure IV-A3) were sent to Applied Biomics where the identity of each band was determined. As can be seen in Appendix Table IV-A1, band A contains both MTB β and β' subunits and MTB α subunit is band E. However, the MTB ω subunit was not confirmed because band G (assumed to be MTB ω subunit) resulted in being 50S ribosomal protein L28 (MW 9 kDa). To be certain that the MTB ω subunit does not share homology with 50S ribosomal protein L28, the amino acid

sequences of the two proteins were aligned and very low sequence identity/homology was observed. Therefore, the faint band right above band G could possibly be the MTB ω subunit (since the MW of MTB ω subunit is 11.8 kDa). Although MTB ω subunit has not been confirmed, the ω subunit has been reported to assist in assembling the RNAP and does not affect the activity of the enzyme. Therefore, the confirmation of the main catalytic MTB RNAP subunits (α, β, β') is sufficient to eliminate the uncertainty of *E. coli* RNAP being present. To conclude, the activity observed in the assays was due to the MTB RNAP and not *E. coli* RNAP. It was important to confirm that the *E. coli* sigma factor was not bound to the MTB RNAP since the assay for rifalazil analogues and the *in vitro* plasmid based transcription assay require using the MTB sigma factor, SigA. The MTB SigA can be added knowing that the *E. coli* sigma factor is not already bound. Band C at ~70 kDa was confirmed to not be the *E. coli* σ^{70}. The amino acid sequence of *E. coli* σ^{70} and the fused UDP-L-Ara4N formyltransferase/UDP-GlcA C-4'-decarboxylase were aligned to confirm there is low identity/homology between the two proteins.

Table IV-A1: MTB RNAP Subunit Confirmation

Band/Method	**MW**	**Identity (%)**
A (NanoLC)	146.6 kDa (beta') 129.8 kDa (beta)	DNA-directed RNA polymerase beta' and beta subunits (*M. bovis*) (100%)
B (MALDI-TOF/TOF)	104.9 kDa	Oxoglutarate dehydrogenase (succinyl-transferring), E1 component (*E. coli*) (100%)
C (MALDI-TOF/TOF)	74.2 kDa	Fused UDP-L-Ara4N formyltransferase/UDP-GlcA C-4'-decarboxylase (*E. coli*) (100%)
D (MALDI-TOF/TOF)	44 kDa	Dihydrolipoamide succinyltransferase (*Shigella boydii*) (100%)
E (MALDI-TOF/TOF)	37.7 kDa	DNA-directed RNA polymerase alpha subunit (MTB) (100%)
F (MALDI-TOF/TOF)	42.7 kDa	Penicillin-binding protein pbpA (MTB) (90%) *low confidence
G (MALDI-TOF/TOF)	9 kDa	50S ribosomal protein L28 (*Reinekea sp.*) (100%)

The NanoLC method was preferred for Band A since it is more sensitive and able to identify more than one protein.

Table IV-A2: Log IC_{50}s and Standard Errors of the Fits for RLZ (**2a**) and Analogues (**2b** – **2e**) against RNAP

Log IC_{50}[a] (standard error of fit[b], Hill Slope[c])					
	2a (RLZ)	**2b**	**2c**	**2d**	**2e**
WT RNAP (-σ^A)	-1.9407 (0.048, 1.09)	-2.5282 (0.026, 2.29)	-2.5103 (0.038, 2.38)	-2.4916 0.066, 1.22)	-1.7666 (0.040, 0.88)
WT RNAP (+σ^A)	-2.4614 (0.068, 1.16)	-2.5442 (0.038, 1.65)	-2.5653 (0.055, 1.51)	-2.348 (0.096, 0.85)	-1.6819 (0.064, 0.72)
D435V (+σ^A)	2.7331 (0.038, 2.02)	1.2946 (0.035, 0.95)	0.94796 (0.064, 0.87)	1.1085 (0.046, 0.88)	2.0472 (0.156, 0.62)
H445Y (+σ^A)	2.2355 (0.069, 0.71)	2.2337 (0.138, 0.41)	2.6407 (0.140, 0.64)	2.7592 (0.180, 0.53)	3.0311 (0.214, 0.61)
S450L (+σ^A)	2.0692 (0.157, 0.63)	1.2054 (0.056, 0.81)	-2.5103 (0.038, 2.38)	2.0881 (0.069, 0.67)	1.8917 (0.068, 0.74)

[a] The log IC_{50} values are such that the IC_{50} values will be in μM. Negative log IC_{50} values reflect IC_{50} values less than μM (e.g., in the nM range). Values were fit to a four parameter logistic regression model with the top and bottom limits set at 100 and 0 respectively. [b] The average error is ~10 %, which roughly translates to 20-25% in the IC_{50}. [c] The average Hill slope is 1.02.

Table IV-A3: Mean Relative Fluorescence Units (RFU)[a] for RMP (**1**) and Benzoxazinorifamycins (**2a** – **2e**) in the hPXR Activation Assay

	RMP (1)		**2a (RLZ)**	**2b**	**2c**	**2d**	**2e**
20 µM	48427	**100 µM**	35250	11137	10881	11625	29476
10 µM	59067	**25 µM**	63418	11591	12218	43077	24305
5 µM	61839	**6.25 µM**	70784	43495	49297	66941	47757
1 µM	64852	**1.56 µM**	73704	68860	60314	68172	50761
0.5 µM	59756	**0.39 µM**	74950	69532	63570	68936	43211
0.1 µM	63078	**0.098 µM**	72399	71149	65632	68628	43120

[a] RFU is a measure of cell viability in the assay. For controls, 1% DMSO = 67021 RFU; Dosing media = 59992 RFU.

Appendix IV-4

Microsome Stability and Pharmacokinetic (PK) Studies

Microsome stability

Test compound stock solutions were prepared at 200 μM in acetonitrile. Two microliters was added to 198 uL PBS containing 1 mg/mL human or mouse microsome. After mixing, 25 uL aliquots were dispensed in triplicate in 96-well plates. Control and reaction wells received 25 uL of PBS and of 2 mM NADPH in PBS, respectively. Plates were incubated for 30 min at 37 °C with shaking at 600 rpm. Internal standard solution (150 μL) was added to each well to quench the reaction. For controls, quenching was done prior to incubation. Plates were centrifuged at 4000g for 30 min. at 4°C and the supernatant was collected for analysis. The percentage of compound remaining and half-life of compound in microsomes were calculated according to the following formula:

$$\text{Percentage remaining} = \frac{\text{Reaction}}{\text{Control}} \times 100$$

$$\text{Half-life (min)} = -\frac{(\text{Incubation time}) * \text{Ln2}}{\text{Ln}(\text{Percentage remaining}/100)}$$

Pharmacokinetics of Analogue 2b

(Previously described methods were followed (*47, 48*))

Single dose study: Analogue **2b** was prepared in 0.5% CMC at 1 mg/mL. Healthy female BALB/c mice were administered 10mg/kg of the suspension via oral gavage. Two mice per time point were used and 0.4 mg/kg fentanyl was given 15 min prior to bleeding by intraperitoneal injection. For each mouse, at least 100 μL of venous blood was collected via retro-orbital bleeding in BD Vacutainer® spray-coated K2EDTA tubes at 0.5, 1, 2, 4, 8 and 24 h post-dose. Tubes were inverted several times and kept on

ice. Blood was transferred to polypropylene tubes and centrifuged at 4,000*g* for 30 min at 4˚C. The harvested plasma was transferred to new polypropylene tubes and stored at -80˚C until analysis. To each sample, 3x volume of chilled acetonitrile was added containing 0.2 μM internal standard (IS). The solution was vortexed and then subsequently centrifuged at 10,000*g* for 15 min. Calibration standard samples were prepared by spiking the stock solution of analogue **2b** in acetonitrile into mouse plasma to yield the following concentrations: 0.097656, 0.195313, 0.390625, 0.78125, 1.5625, 3.125, 6.25, 12.5, 25, 50 μM. Supernatant was injected into an LC-MS/MS for analysis. In addition, a blank (blank plasma extracted with 3x volume of IS) and a double blank (blank plasma extracted with 3x volume of pure acetonitrile) were prepared. The concentration of **2b** in blood sample for each time point was then determined.

Multiple dose study: Mice were dosed once daily for 5 consecutive days by oral gavage. Blood samples at time points 0.5, 1, 2, 4, 8 and 24h were collected and analyzed in the same way as the single dose study. After collecting the blood, the mice were sacrificed by carbon dioxide asphyxiation. Lung tissue was aseptically removed, rinsed in 3 mL PBS, air dried on sterilized gauze pads, weighed and suspended in 4x (solvent/tissue; w/v) PBS buffer. Lung tissue was homogenized, mixed and extracted with 3x acetonitrile containing internal standard at 0.2 μM and centrifuged at 10,000 *g* for 15 min at 4 ˚C. The supernatant was collected for LC-MS/MS analysis. Calibration standard lung samples were prepared by spiking the stock solution of compound (in methanol or acetonitrile) into homogenized mouse lungs and extracting with 3x volume acetonitrile to yield the following concentrations: 0.024, 0.049, 0.098, 0.195, 0.39, 0.78, 1.56, 3.12, 6.25, 12.5, 25, 50 μM. In addition, a blank (blank lung tissue extracted with

3x volume of IS) and a double blank (blank lung tissue extracted with 3x volume of pure acetonitrile) were prepared. The concentration of **2b** in lung tissue for each time point was then determined.

(a) Single dose

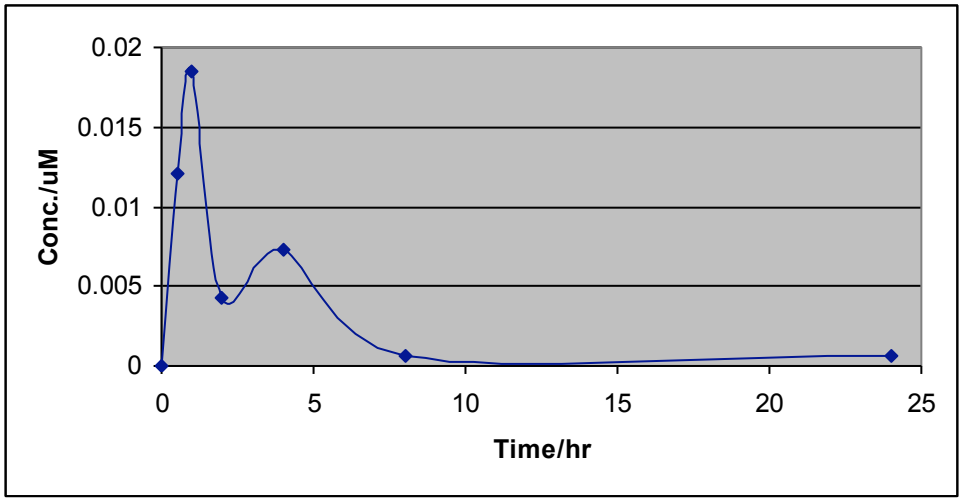

(b) Multiple dose

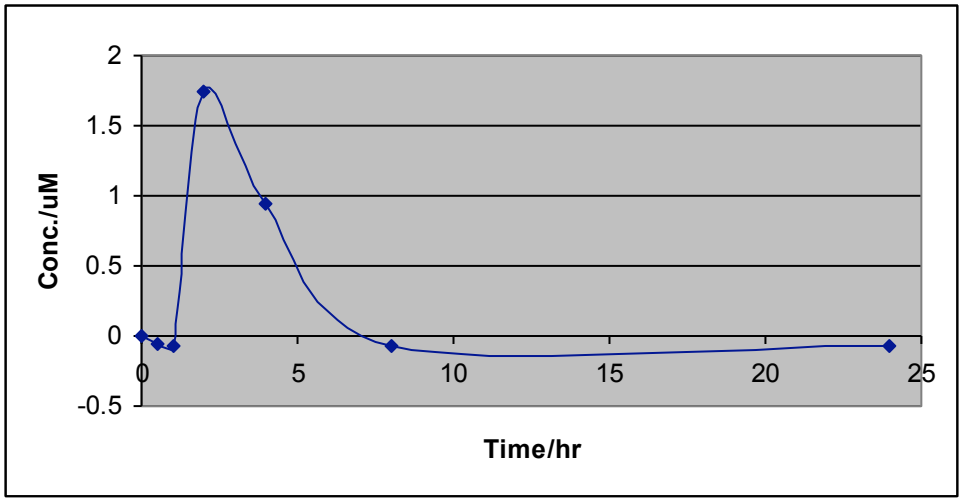

Figure IV-A4: Linear plasma mean concentration vs. time profile for analogue **2b** in (a) single dose and (b) multiple dose studies

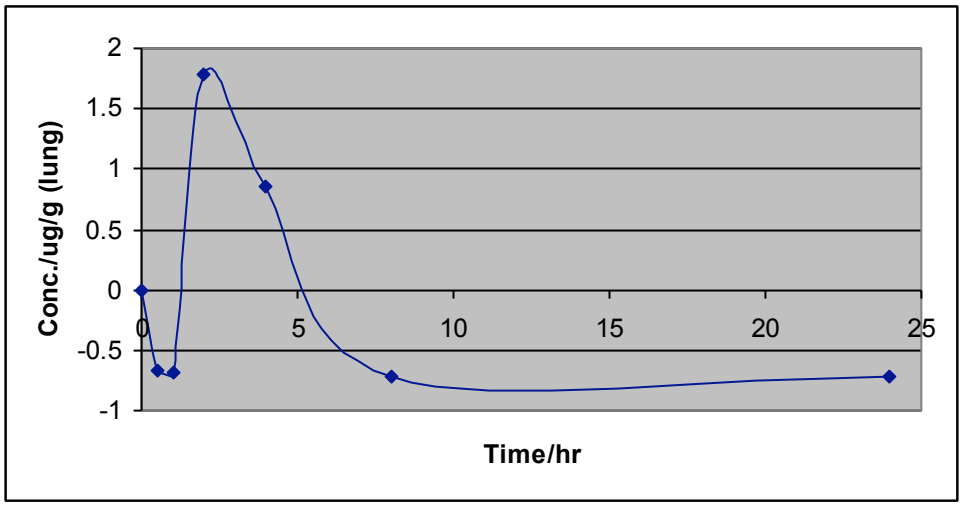

Figure IV-A5: Linear lung tissue mean concentration vs. time profile for analogue **2b** in a multiple dose study.

References

1. World-Health-Organization, "WHO Report 2010: Global Tuberculosis Control" *Report* (2010).

2. D. L. Cohn, M. D. Iseman, Treatment and Prevention of Multidrug-Resistant Tuberculosis. *Res. Microbiol.* **144**, 150 (Feb, 1993).

3. Y. L. Janin, Antituberculosis drugs: Ten years of research. *Bioorg. Med. Chem*. **15**, 2479 (Apr, 2007).

4. A. B. Garcia *et al.*, Strong in vitro activities of two new rifabutin analogs against multidrug-resistant Mycobacterium tuberculosis. *Antimicrobial Agents and Chemotherapy* **54**, 5363 (Dec, 2010).

5. A. Koul, E. Arnoult, N. Lounis, J. Guillemont, K. Andries, The challenge of new drug discovery for tuberculosis. *Nature* **469**, 483 (Jan, 2011).

6. M. I. Siddiqi, A. Kumar, Review of knowledge for rational design and identification of anti-tubercular compounds. *Expert Opinion on Drug Discovery* **4**, 1005 (2009).

7. C. Lienhardt, A. Vernon, M. C. Raviglione, New drugs and new regimens for the treatment of tuberculosis: review of the drug development pipeline and implications for national programmes. *Current opinion in pulmonary medicine* **16**, 186 (May, 2010).

8. H. Saito *et al.*, In vitro antimycobacterial activities of newly synthesized benzoxazinorifamycins. *Antimicrob. Agents Chemother.* **35**, 542 (1991).

9. T. Yamane *et al.*, Synthesis and biological activity of 3'-hydroxy-5'aminobenzoxazinorifamycin derivatives. *Chem. Pharm. Bull.* **41**, 148 (1993).

10. R. Mariani, S. I. Maffoli, Bacterial RNA polymerase inhibitors: an organized overview of their structure, derivatives, biological activity and current clinical development. *Current Med. Chem*. **16**, 430 (2009).

11. S. D. Zorov, J. V. Yuzenkova, K. V. Severinov, Low-molecular-weight inhibitors of bacterial DNA-dependent RNA polymerase. *Molecular Biology* **40**, 875 (Nov-Dec, 2006).

12. N. Lounis, G. Roscigno, In vitro and in vivo activities of new rifamycin derivatives against mycobacterial infection. *Current Pharmaceutical Design* **10**, 3229 (2004).

13. J. Luna-Herrera, M. Venkata Reddy, P. R. J. Gangadharam, In vitro activity of the benzoxazinorifamycin KRM-1648 against drug-susceptible and multidrug-resistant tubercle bacilli. *Antimicrob. Agents Chemother.* **39**, 440 (1996).

14. H. Tomioka, Current status of some antituberculosis drugs and the development of new antituberculous agents with special reference to their in vitro and in vivo antimicrobial activities. *Current Pharmaceutical Design* **12**, 4047 (2006).

15. T. Yamamoto *et al.*, In vitro bactericidal and in vivo therapeutic activities of a new rifamycin derivative, KRM-1648, against Mycobacterium tuberculosis. *Antimicrob. Agents Chemother.* **40**, 426 (1996).

16. T. Hirata *et al.*, In-Vitro and In-Vivo Activities of the Benzoxazinorifamycin KRM-1648 Against Mycobacterium-Tuberculosis. *Antimicrob. Agents Chemother.* **39**, 2295 (Oct, 1995).

17. Y. K. Park *et al.*, Cross-resistance between rifampicin and KRM-1648 is associated with specific rpoB alleles in Mycobacterium tuberculosis. *Int. J. Tuberc. Lung Dis.* **6**, 166 (Feb, 2002).

18. A. Telenti *et al.*, Detection of rifampicin-resistance mutation in *Mycobacterium tuberculosis*. *Lancet* **341**, 647 (1993).

19. S. Mullin, D. M. Rothstein, C. K. Murphy, Activity of novel benzoxazinorifamycins against rifamycin-resistant Streptococcus pyogenes. *Antimicrob. Agents Chemother.* **50**, 1908 (2006).

20. P. M. Roblin, T. Reznik, A. Kutlin, M. R. Hammerschlag, In vitro activities of rifamycin derivatives ABI-1648 (rifalazil, KRM-1648), ABI-1657, and ABI-1131 against Chlamydia trachomatis and recent clinical isolates of Chlamydia pneumoniae. *Antimicrob. Agents Chemother.* **47**, 1135 (2003).

21. M. S. Xia *et al.*, Activities of rifamycin derivatives against wild-type and rpoB mutants of Chlamydia trachomatis. *Antimicrob. Agents Chemother.* **49**, 3974 (Sep, 2005).

22. J. E. Chrencik *et al.*, Structural disorder in the complex of human pregnane X receptor and the macrolide antibiotic rifampicin. *Molecular Endocrinology* **19**, 1125 (May, 2005).

23. L. M. Rose, D. J. Porubek, A. B. Montgomery, in *US Appl.* . (Kaneka Corp., USA, 2003), pp. 28.

24. R. Dietze *et al.*, Safety and bactericidal activity of rifalazil in patients with pulmonary tuberculosis. *Antimicrob. Agents Chemother.* **45**, 1972 (2001).

25. P. J. Barry, T. M. O'Connor, Novel agents in the management of Mycobacterium tuberculosis disease. *Curr Med Chem* **14**, 2000 (2007).

26. J.-L. Portero, M. Rubio, New anti-tuberculosis therapies. *Expert Opin. Ther. Patents* **17**, 617 (2007).

27. E. A. Campbell *et al.*, Structural mechanism for rifampicin inhibition of bacterial RNA polymerase. *Cell* **104**, 901 (2001).

28. I. Artsimovitch *et al.*, Allosteric modulation of the RNA polymerase catalytic reaction is an essential component of transcription control by rifamycins. *Cell* **122**, 351 (Aug 12, 2005).

29. P. Labute, LowModeMD - Implicit Low Mode Velocity Filtering Applied to Conformational Search of Macrocycles and Protein Loops. *J. Chem. Inf. Model.* **50**, 792 (2010).

30. I. Chemical Computing Group. (Montreal, 2010).

31. J.-F. Jacques, S. Rodrigue, R. Brzezinski, L. Gaudreau, A recombinant Mycobacterium tuberculosis in vitro transcription system. *FEMS Microbiology Letters* **255**, 140 (Feb, 2006).

32. L. Collins, S. Franzblau, Microplate alamar blue assay versus BACTEC 460 system for high- throughput screening of compounds against Mycobacterium tuberculosis and Mycobacterium avium. *Antimicrob. Agents Chemother.* **41**, 1004 (May 1, 1997, 1997).

33. S. H. Cho *et al.*, Low-Oxygen-Recovery Assay for High-Throughput Screening of Compounds against Nonreplicating Mycobacterium tuberculosis. *Antimicrob. Agents Chemother.* **51**, 1380 (April 1, 2007, 2007).

34. R. E. Watkins *et al.*, The human nuclear xenobiotic receptor PXR: structural determinants of directed promiscuity. *Science* **292**, 2329 (Jun 22, 2001).

35. R. E. Watkins *et al.*, 2.1 A crystal structure of human PXR in complex with the St. John's wort compound hyperforin. *Biochemistry* **42**, 1430 (Feb 18, 2003).

36. D. G. Teotico, J. J. Bischof, L. Peng, S. A. Kliewer, M. R. Redinbo, Structural basis of human pregnane X receptor activation by the hops constituent colupulone. *Mol Pharmacol* **74**, 1512 (Dec, 2008).

37. D. L. Williams *et al.*, Contribution of rpoB mutations to development of rifamycin cross-resistance in Mycobacterium tuberculosis. *Antimicrob. Agents Chemother.* **42**, 1853 (1998).

38. J. Wang, J. Huang, H. Li, S. Zhang, Synthesis of benzoxazinorifamycin derivatives and preliminary study of antibacterial activity. *Huaxi Yaoxue Zazhi* **18**, 241 (2003).

39. H. G. Floss, T.-W. Yu, Rifamycin-mode of action, resistance, and biosynthesis. *Chem. Rev.* **105**, 621 (2005).

40. K. Fujii, H. Saito, H. Tomioka, T. Mae, K. Hosoe, Mechanism of action of antimycobacterial activity of the new benzoxazinorifamycin KRM-1648. *Antimicrob. Agents Chemother.* **39**, 1489 (1995).

41. M. W. Sinz, Pregnane X receptor: prediction and attenuation of human CYP3A4 enzyme induction and drug-drug interactions. *In Annual Reports in Medicinal Chemistry* **43**, 405 (2008).

42. T. Mae *et al.*, Effect of a new rifamycin derivative, rifalazil, on liver microsomal enzyme induction in rat and dog. *Xenobiotica* **28**, 759 (1998).

43. T. Yamane *et al.*, Synthesis and biological activity of 3'-hydroxy-5'-aminobenzoxazinorifamycin derivatives. *Chem Pharm Bull (Tokyo)* **41**, 148 (Jan, 1993).

44. K. Dhingra, M. E. Maier, M. Beyerlein, G. Angelovski, N. K. Logothetis, Synthesis and characterization of a smart contrast agent sensitive to calcium. *Chemical Communications*, 3444 (2008).

45. A. Binggeli *et al.*, P. P. Application, Ed. (2007).

46. H. J. Havera, R. D. Johnson, H. Vidrio. (United States, 1976), vol. US 3995041

47. R. Jayaram *et al.*, Pharmacokinetics-pharmacodynamics of rifampin in an aerosol infection model of tuberculosis. *Antimicrobial Agents and Chemotherapy* **47**, 2118 (Jul, 2003).

48. R. Jayaram *et al.*, Isoniazid pharmacokinetics-pharmacodynamics in an aerosol infection model of tuberculosis. *Antimicrobial Agents and Chemotherapy* **48**, 2951 (Aug, 2004).

CHAPTER V

Developing a Direct Binding Assay Using a Dansyl-Conjugated Rifamycin

Rifampin (RMP) is a tight binding inhibitor of wild-type (WT) RNA polymerase (RNAP), forming a stable noncovalent 1:1 complex. RMP binds to and inhibits both the core RNAP and the holoenzyme (*1-3*). The binding constant (K_D; equilibrium dissociation constant) for prokaryotic RNAP is in the range of 10^{-8} M (*4-7*). Previously, the K_D has been determined for WT *E. coli* RNAP to be 10^{-9} M via radiochemical and fluorescence assays (*5, 6, 8*); however, the K_D value for WT and rifamycin-resistant (RifR) MTB RNAPs has not been reported.

Recently, Feklistov and colleagues have chemically attached fluorescein to the *E. coli* sigma factor (σ^{70}) to study rifamycin-RNAP interaction (*8, 9*), but there are no reports of developing a direct binding assay using a fluorophore-labeled rifamycin. To characterize the interactions between MTB RNAP and our synthetic rifamycin analogues, we decided to develop a direct binding assay using a fluorescently labeled rifamycin. This would enable the use of competition binding assays to determine binding constants for an array of rifamycin analogues. The dansyl group was selected as the fluorophore for our first attempt because it has been previously used to prepare fluorescent drug analogues (*10, 11*) and has a long history of use in probing binding interactions.

The K_D values of rifamycins and MTB RNAPs will allow for changes in binding free energy to be calculated. We will then correlate the changes in binding free energy to

the predicted changes in molecular interactions between the rifamycins and the RNAP (based on the published crystal structure models (*12, 13*)). Our goal is to use this information to enhance our understanding of the molecular mechanisms responsible for resistance and guide the development of new analogues with improved binding to the MTB RNAP and RifR mutants.

Materials and Methods

Unless otherwise specified, all reagents were purchased from Sigma-Aldrich (St. Louis, MO). Kool^{TM} NC-45^{TM} Universal RNA Polymerase template was from Epicentre (Madison, WI). Carbenicillin (disodium salt), corning microplates, bactotryptone, and yeast extract were from Fisher Scientific (Hampton, NH). The *E. coli* BL21 (DE3) CodonPlus-RIPL and *Epicurian coli* XL2-Blue Ultracompetent cells were from Agilent Technologies (Santa Clara, CA). Quanti-iT^{TM} RiboGreen RNA Reagent and RNaseOUT^{TM} Recombinant Ribonuclease Inhibitor were from Invitrogen (Carlsbad, CA). The Ni-NTA His•Bind® resin was from Novagen (San Diego, CA). The nucleotide triphosphates (NTPs) were from Roche Applied Science (Indianapolis, IN). PhastGel Precast Gels and SDS Buffer Strips were from VWR (Arlington Heights, IL). The Bio-Rad Protein Assay kit was from Bio-Rad (Hercules, CA). The EC2880 strain (permeable strain with *tolC*$^{-}$ and *imp*$^{-}$ mutations) was a generous gift from Dr. Michael Hubband (Pfizer Scientific). Rifamycin S was from AAPharmaSyn LLC. Rifampin was from Boche Scientific. Dansyl chloride and dansyl amide were from Sigma-Aldrich.

Synthesis of Dansyl-Conjugated Rifamycin (HX52)

The dansyl-conjugated rifamycin (HX52) was synthesized by Hao Xu (3rd year Medicinal Chemistry student) using the scheme outlined in Figure V-1.

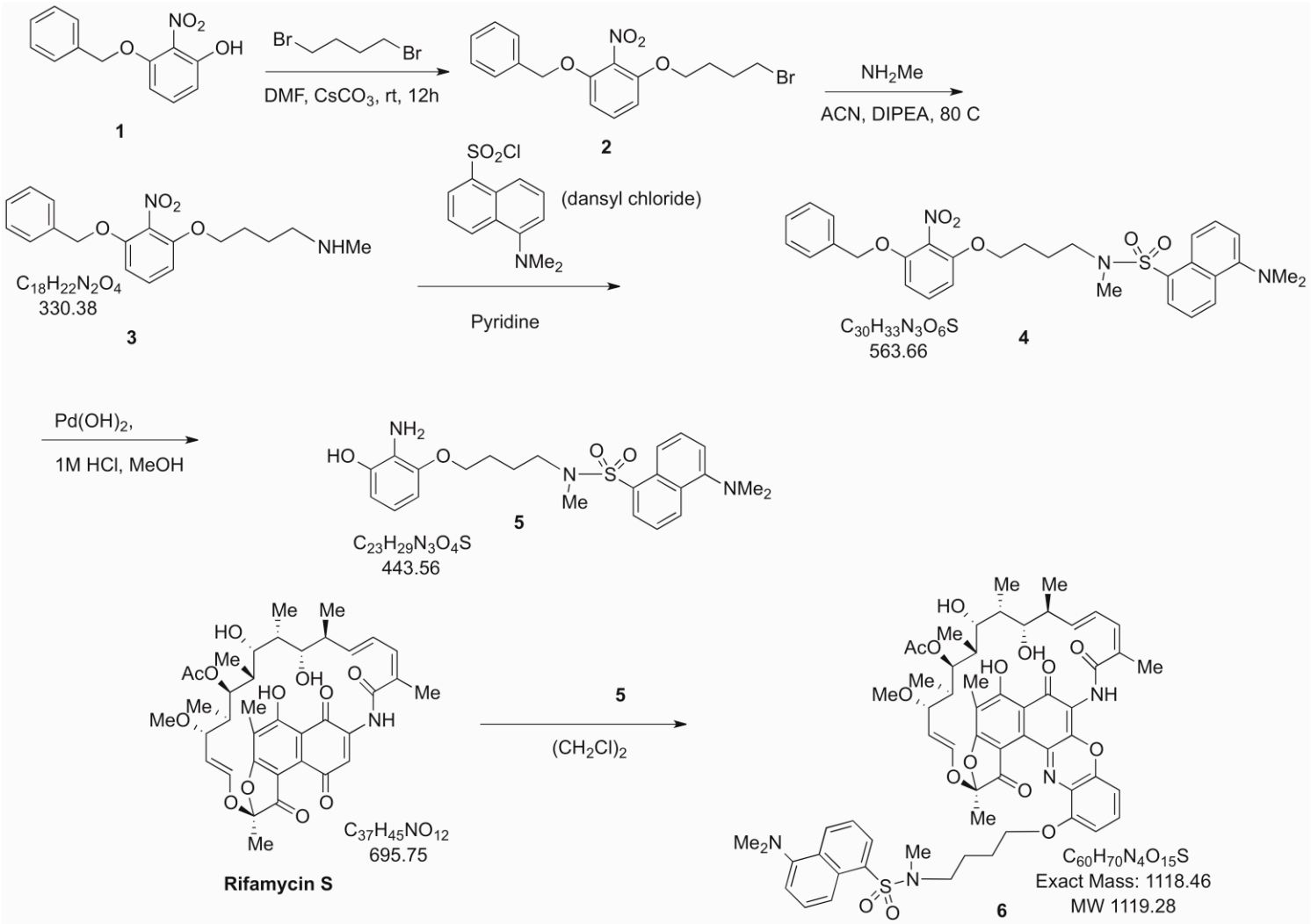

Figure V-1: Dansyl-conjugated Rifamycin (Compound 6; HX52)

Expression and Purification of MTB RNAP (WT and RifR mutants) and MTB SigA (σ^A)

The WT and RifR MTB RNAPs and MTB SigA were prepared as described earlier in Chapter II and IV.

In vitro Transcriptional Activity of MTB RNAPs and Dose Response Curves

The RNAP activity and inhibition was estimated by the production of RNA synthesis as described (*14*). The IC_{50} values were determined via dose response studies (Table V-1). HX52 (**6**) was tested in duplicate (n=2). The final concentration of the WT MTB RNAP was 10 nM, whereas the final concentrations of the RifR RNAPs were 100 nM in the reactions.

Determination of Minimal Inhibitory Concentration (MIC) Against MTB $H_{37}R_v$ Strains

The compound was also evaluated for MIC_{90} vs. MTB $H_{37}R_V$ using the Microplate Alamar Blue Assay (MABA) and the Low Oxygen Recovery Assay (LORA) (*14-16*). Additionally, the MIC_{90} values were determined for *E. coli* by the microdilution method described previously (*17, 18*).

HX52 Absorbance/Fluorescence Studies

Absorbance and fluorescence spectra were measured using the Synergy H1 Hybrid Multi-Mode Microplate Reader (BioTek) in half area 96-well black plates.

Results

In this work, the dansyl-conjugated rifamycin (HX52, **6**) was synthesized by Hao Xu using the scheme illustrated in Figure V-1. The dansyl group reacted with the secondary amine of (**3**) to yield the dansyl amide derivative (**4**) that was then modified and attached to rifamycin S.

Inhibition Studies

The IC_{50} values of HX52 against WT and RifR MTB RNAPs were determined (Table V-1). This dansyl-conjugated rifamycin does potently inhibit the WT MTB RNAP (with and without sigma factor, σ^A) with the IC_{50} values in the 10^{-9} M (nM) range; whereas, the RifR MTB RNAPs ($+\sigma^A$) were inhibited at higher concentrations with the IC_{50} values in the 10^{-6} M (μM) range.

Table V-1. *In vitro* RNAP IC_{50} Values (μM) for HX52

	IC_{50} values
WT RNAP ($-\sigma^A$) (C_f = 10 nM)	0.0146
WT RNAP ($+\sigma^A$) (C_f = 10 nM)	0.0152
D435V ($+\sigma^A$) (C_f = 100 nM)	343
H445Y ($+\sigma^A$) (C_f = 100 nM)	267
S450L ($+\sigma^A$) (C_f = 100 nM)	97

The MIC_{90} values are also reported against the MTB virulent strain ($H_{37}R_V$) and three selected *E. coli* strains (Table V-2). HX52 inhibited MTB with MIC_{90} values 9 nM and 0.93 μM for MABA and LORA, respectively. The MIC_{90} values were higher for *E. coli* strains including the *tolC* knockout strain (EC2880).

Table V-2. HX52 MIC_{90} values against MTB and *E. coli*

	MIC_{90} values (μM)
MTB ($H_{37}R_V$)	
MABA	0.009
LORA	0.93
***E. coli* strains**	
TG2	> 100
DH5α	> 100
EC2880 (*ΔtolC*)	> 12.5 (75% inhibited)

Absorbance/Fluorescence Studies

Compound HX52 was initially dissolved in DMSO to make a high concentration stock. The compound was then diluted in RNAP storage buffer (10 mM Tris-HCl (pH 7.9), 0.1 mM EDTA, 0.1 mM DTT, 0.1 M NaCl) to the final concentration of 100 nM in a total volume of 100 μL. The dansyl conjugated compound excitation and emission maxima vary between 350-370 nm and 490-540 nm, respectively. Unfortunately, when the sample, in the above buffer, was excited at 350 nm, there was no fluorescence emission observed (400-600 nm). The absorbance of different rifamycins was measured from 250-600 nm (Figure V-2). The dansyl-conjugated rifamycin (HX52) has a broad peak around the 350-370 nm region. Possible explanations for this lack of fluorescence include: the tetracyclic chromophore (benoxazinonaphthyl) of the rifamycin moiety might quench the fluorescence of the dansyl group or fluorescence could be quenched due to the polarity/pH of the buffer.

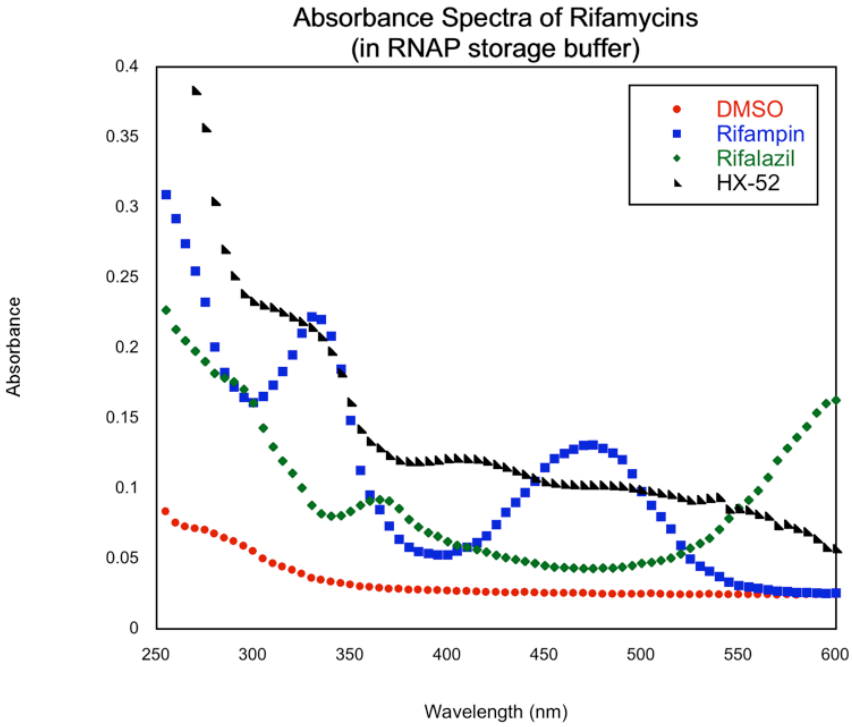

Figure V-2: Absorbance Spectra of Rifamycins.

To investigate which of these explanations might apply, the following steps were taken. The NMR of D–Cl and HX52 confirmed that the starting material and the end product were pure and stable (data not shown). To see if the tetracyclic moiety of rifamycin quenches the fluorescence of the dansyl group, a direct comparison of fluorescence emission spectra of compound **5** and HX52 would have been ideal. Unfortunately, all of compound **5** was used to synthesize HX52 thus the fluorescence could not be determined. Instead the fluorescence of dansyl amide (CAS# 1431-39-6; λ_{ex}=340 nm; λ_{em}=555–565 nm) was measured because dansyl amide is a fluorescent side product observed when D–Cl is attached to amino acids (Figure V-3). We would have expected to see a similar fluorescence emission spectrum of our dansyl-conjugated rifamycin as the one observed for dansyl amide since the dansyl group reacted with an amine to form a dansyl amide derivative. The dansyl amide was incubated with RMP to

determine if fluorescence is quenched in the presence of rifamycins but the data was inconclusive.

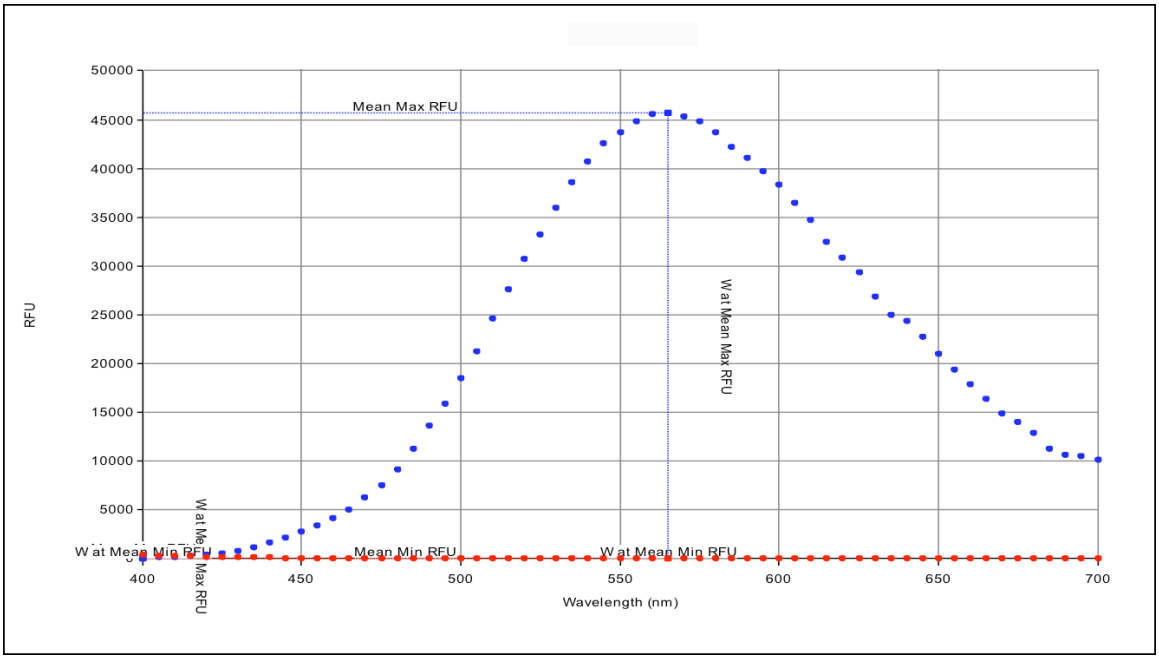

Figure V-3: Fluorescence emission spectrum of Dansyl-amide (in blue) in RNAP storage buffer. The sample was excited at 340 nm and the emission spectrum was measured from 400-700 nm. DMSO (control) can be seen in red.

It is possible that the fluorescent dansyl tail is stacking on top of the tetracyclic moiety of HX52, thereby quenching the fluorescence. To probe this, compound HX52 was preincubated with RNAP for 10 min at 37^{o}C, with the idea that the key interactions between the rifamycin core and RNAP would free the dansyl tail, but unfortunately fluorescence was not observed under these conditions (data not shown). The dansyl group is a sensitive probe where the fluorescence is polarity/pH dependent; therefore, the HX52 itself was dissolved in different solvents (methanol, acetone, acetonitrile) and tested in different buffers (Tris buffers, bicarbonate buffers, phosphate buffers) at different pH values but still no fluorescence was observed (data not shown). To make sure that a component of the buffer was not quenching the fluorescence, the compound

was tested in water and the same results were seen. However, the compound was fluorescent when it was dissolved in 100% DMSO. Optimal fluorescence was observed when λ_{ex}=360 nm with emission spectra from 400-700 nm. The DMSO concentration was titrated in RNAP buffer (Figure V-4) to determine the effect of DMSO concentration on fluorescence. Fluorescence was not seen at less than 60% DMSO. Optimal fluorescence was observed at high DMSO concentrations (80-100% DMSO). To determine if fluorescence could be seen when bound to RNAP, the compound was preincubated with the RNAP but fluorescence was not observed (data not shown).

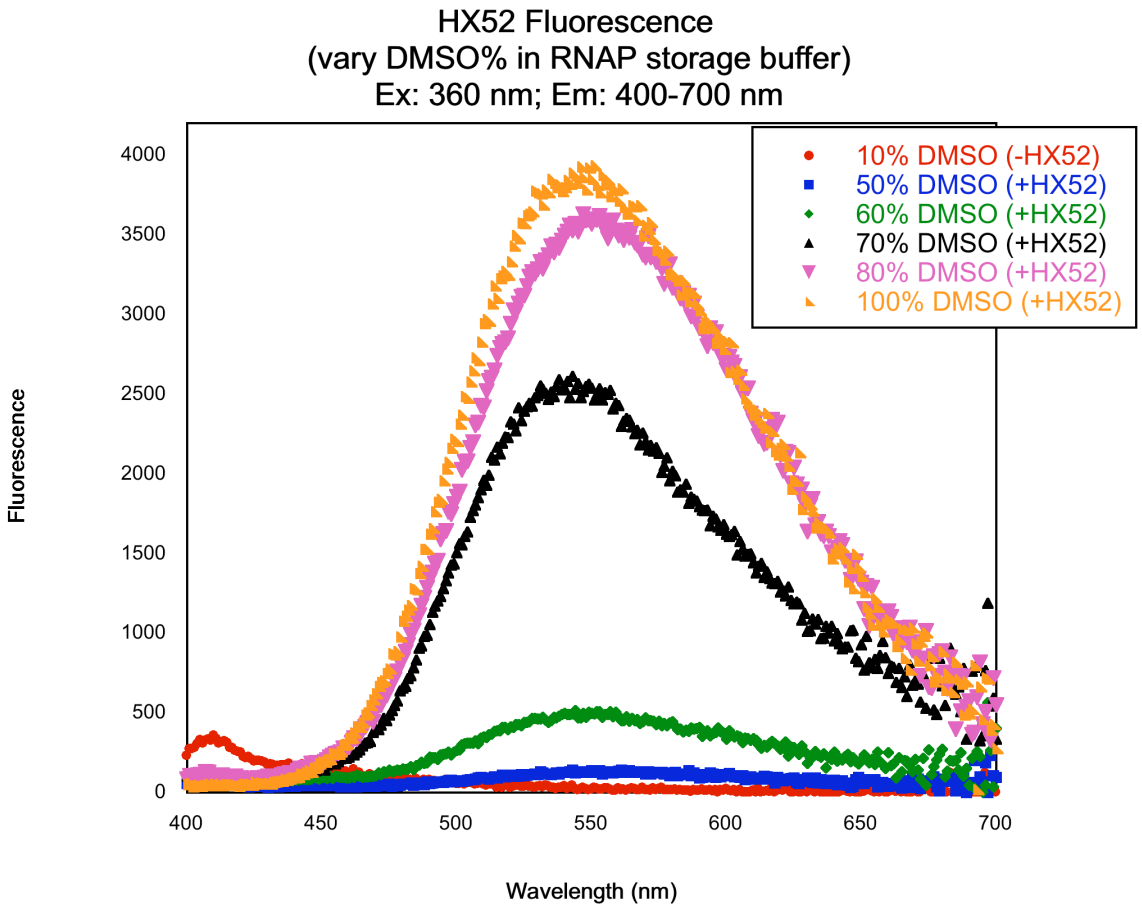

Figure V-4: Fluorescence emission spectra of dansyl-conjugated rifamycin (HX52) in RNAP storage buffer with increasing amount of DMSO.

Discussion

Previously, the reported equilibrium dissociation constant for wild-type *E. coli* RNAP and RMP is 10^{-9} M at 37°C determined via radioactive and fluorescence assays (*5, 6, 8, 19*). The radioactive assay consisted of using dextran-coated charcoal and radiolabeled [^{14}C] RMP to determine the K_D value (*5, 19*). The [^{14}C] RMP was mixed with the enzyme where the unbound RMP was adsorbed on the charcoal and the larger antibiotic-enzyme complex remained in solution. The K_D has also been determined via direct fluorescence titration where the binding of RMP leads to the partial quenching of the RNAP tryptophan residue (*20*). Recently, Feklistov *et al*. have calculated the association, dissociation, and equilibrium constants by measuring rifampin-RNAP via monitoring the quenching of the fluorescence emission of fluorescein-labeled sigma factor (*8*). Fluorescein, a fluorescent probe, was inserted at residue 517 of σ^{70}. The probe was the FRET donor and the naphthyl group of rifampin was the FRET acceptor (*9*).

Fluorescent probes are relatively small modifying agents used to label protein, nucleic acids, and drugs. Advantages of a fluorescent assay include: nonradioactive, does not require separation of bound and free ligand, higher sensitivity, and adaptable to low volumes (*10, 21*). There are a wide range of fluorescent probes available: fluorescamine, dialdehydes, ATTO-TAG reagents, FITC and other isothiocyanates, succinimidyl esters, and sulfonyl chlorides (www.invitrogen.com). We elected to add the dansyl probe to make the rifamycin fluorescent. Dansyl chloride (a sulfonyl chloride) is a well known reagent that has been utilized in areas such as pharmacology, toxicology, organic synthesis, and biochemistry (*11*). Furthermore, it is useful in preparing fluorescent drugs

that are expected to bind to hydrophobic sites in proteins, membranes, or other biological receptors.

The dansyl-conjugated rifamycin (HX52) was synthesized and assayed in inhibition studies. The compound behaves similar to other rifamycins and binds to the WT MTB RNAP with a strong affinity and exhibits loss of affinity with the RifR MTB RNAPs. From the MTB MIC_{90} values, it can be seen that the compound is able to permeate through the mycobacterial cell wall. However, higher MIC_{90} values were observed with *E. coli* (including the Δ*tolC* strain) indicating that the compound is less able to permeate through Gram-negative bacteria and the higher MIC_{90} values do not appear to be due to efflux pump activity.

Previously, dansyl-conjugated analogues have been reported to be highly fluorescent (λ_{ex}=350 nm; λ_{em}=490–540 nm). Therefore, the addition of the dansyl probe to a rifamycin was expected to make the dansyl-conjugated rifamycin compound fluorescent. Unfortunately, this dansyl-conjugated rifamycin (HX52) was not fluorescent in aqueous buffers. Most likely the dansyl probe overlaps with the tetracyclic moiety of our synthesized rifamycin probe (due to the length and flexibility of the linker), which quenches the fluorescence. As mentioned earlier, the intrinsic chromophore within rifamycins can be used as acceptors in fluorescence resonance energy transfer (FRET) measurements (*6, 9, 20*). When the compound is in DMSO (a highly polar, aprotic solvent), the dansyl probe is presumably free in solution and fluorescent. This is problematic because RNAP is not stable in ≥30% DMSO solutions and fluorescence of HX52 itself is not observed at that concentration of DMSO (*19*). When HX52 was in less polar, aprotic solvents (acetone, acetonitrile), fluorescence quenching was observed.

Conclusions

Unfortunately, the dansyl-conjugated rifamycin resulted in a nonfluorescent derivative. In the future, a different fluorophore can be introduced that is not so sensitive to the assay conditions or else reduce the length of the linker such that the dansyl group cannot overlap with the rifamycin chromophore and quench the fluorescence. Another option to attach the fluorophore to the RNAP/sigma factor (as described earlier by Feklistov and colleagues) or use radiolabeled RMP. Due to the fact that rifamycins are retained by nitrocellulose filters, a nitrocellulose filter binding assay cannot be used to study rifamycin-RNAP interactions (*22*). Once a direct binding assay has been established, the effects of WT and mutant MTB RNAPs will be analyzed to determine the equilibrium binding constant. The K_D values will allow the loss of binding free energy to be calculated. This value will help answer the following questions: Does this value correlate to the loss of just one hydrogen bond? Are other interactions being affected by the mutation?

Notes to Chapter V

We gratefully acknowledge Hao Xu and Dr. Hollis Showalter for the synthesis of the dansyl-conjugated rifamycin (HX52). We thank Dr. Scott Franzblau (Institute for Tuberculosis Research at University of Illinois at Chicago) for providing the antitubercular activity data. We acknowledge generous support by the University of Michigan College of Pharmacy Ella and Hans Vahlteich and UpJohn Research Funds. We would also like to acknowledge additional funding by the University of Michigan Office of the Vice President for Research, and the Rackham Graduate School.

Abbreviations used: TB, tuberculosis; RNAP, DNA-dependent RNA polymerase; SigA, MTB housekeeping sigma factor A; WT, wild-type; RifR, Rifamycin-resistant; MTB, *Mycobacterium tuberculosis*; K_D, equilibrium dissociation constant; D-Cl, dansyl-chloride; HX52, dansyl-conjugated rifamycin; RMP, rifampin; NTP, ribonucleotide triphosphate; EDTA, ethylenediaminetetraacetic acid; DTT, dithiothreitol; RNA, ribonucleic acid; MABA, Microplate Alamar Blue Assay; LORA, Low Oxygen-Recovery Assay; IC_{50}, concentration of rifamycin resulting in 50% inhibition of transcription; MIC_{90}, concentration of rifamycin that results in 90% inhibition of bacterial growth

References

1. W. K. Wehrli, F; Schmid, K.; Staehelin, M., Interaction of rifamycin with bacterial RNA polymerase. *Proc. Nat. Acad. Sci. USA* **61**, 667 (1968).

2. E. Dimauro *et al.*, Rifampicin Sensitivity of Components of DNA-Dependent RNA Polymerase. *Nature* **222**, 533 (1969).

3. W. Wehrli, M. Staehelin, Actions of the rifamycins. *Bacteriological Reviews* **35**, 290 (1971).

4. H. G. Floss, T.-W. Yu, Rifamycin-mode of action, resistance, and biosynthesis. *Chem. Rev.* **105**, 621 (2005).

5. E. Wyss, W. Wehrli, Use of Dextran-Coated Charcoal for Kinetic Measurements - Interaction Between Rifampicin and DNA-Dependent RNA-Polymerase of *Escherichia coli*. *Analytical Biochemistry* **70**, 547 (1976).

6. W. Bahr, W. Stender, K. Scheit, T. Jovin, in *RNA Polymerase,* R. Losick, M. Chamberlin, Eds. (Cold Spring Harbor Laboratory Press, Cold Spring Harbor, 1976), pp. 369-396.

7. G. Hartmann, W. Behr, K.-A. Beissner, K. Honikel, A. Sippel, Antibiotics as inhibitors of nucleic acid and protein synthesis. *Angew. Chem. internat. Edit.* **7**, 693 (1968).

8. A. Feklistov *et al.*, Rifamycins do not function by allosteric modulation of binding of Mg2+ to the RNA polymerase active center. *Proceedings of the National Academy of Sciences of the United States of America* **105**, 14820 (Sep 30, 2008).

9. J. L. Knight, V. Mekler, J. Mukhopadhyay, R. H. Ebright, R. M. Levy, Distance-Restrained Docking of Rifampicin and Rifamycin SV to RNA Polymerase Using Systematic FRET Measurements: Developing Benchmarks of Model Quality and Reliability. *Biophys. J.* **88**, 925 (February 1, 2005, 2005).

10. M. A. Martin, B. Lin, B. Delcastillo, The Use of Fluorescent-Probes in Pharmaceutical Analysis. *J. Pharm. Biomed. Anal* **6**, 573 (1988).

11. R. Bartzatt, Fluorescent labeling of drugs and simple organic compounds containing amine functional groups, utilizing dansyl chloride in Na_2CO_3 buffer. *J. Pharmacol. Toxicol. Methods* **45**, 247 (May-Jun, 2001).

12. E. A. Campbell *et al.*, Structural mechanism for rifampicin inhibition of bacterial RNA polymerase. *Cell* **104**, 901 (2001).

13. I. Artsimovitch *et al.*, Allosteric modulation of the RNA polymerase catalytic reaction is an essential component of transcription control by rifamycins. *Cell* **122**, 351 (Aug 12, 2005).

14. S. K. Gill, Xu, H., Kirchhoff, P.D., Wan, B., Zhang, N., Peng, K., Franzblau, S., Garcia, G.A., Showalter, H.D., Structure-based Design of Novel Benzoxazinorifamycins with Potent Binding Affinity to Wild-type and Rifampin-resistant Mutant Mycobacterium tuberculosis RNA polymerase. *Journal of Medicinal Chemistry* (2012) **DOI: 10.1021/jm201716n**.

15. S. H. Cho *et al.*, Low-Oxygen-Recovery Assay for High-Throughput Screening of Compounds against Nonreplicating Mycobacterium tuberculosis. *Antimicrob. Agents Chemother.* **51**, 1380 (April 1, 2007, 2007).

16. L. Collins, S. G. Franzblau, Microplate alamar blue assay versus BACTEC 460 system for high- throughput screening of compounds against Mycobacterium tuberculosis and Mycobacterium avium. *Antimicrob Agents Chemother* **41**, 1004 (1997 May, 1997).

17. I. Wiegand, K. Hilpert, R. E. W. Hancock, Agar and broth dilution methods to determine the minimal inhibitory concentration (MIC) of antimicrobial substances. *Nat. Protoc.* **3**, 163 (2008).

18. S. K. Gill, G. A. Garcia, Rifamycin inhibition of WT and Rif-resistant Mycobacterium tuberculosis and Escherichia coli RNA polymerases in vitro. *Tuberculosis* **91**, 361 (Sep, 2011).

19. W. Wehrli, Handschin, J., and Wunderli, W., in *RNA Polymerase,* R. Losick, M. Chamberlin, Eds. (Cold Spring Harbor Laboratory Press, Cold Spring Harbor, 1976), pp. 397-412.

20. C. W. Wu, Goldthwa.Da, Studies of Nucleotide Binding to Ribonucleic Acid Polymerase by a Fluorescence Technique. *Biochemistry* **8**, 4450 (1969).

21. D. M. Jameson, J. A. Ross, Fluorescence Polarization/Anisotropy in Diagnostics and Imaging. *Chemical Reviews* **110**, 2685 (May, 2010).

22. R. K. Neogy, Chowdhur.K, I. Kerr, Nitrocellulose Filter Retention Method for Studying Drug-Nucleic Acid Interactions. *Biochimica Et Biophysica Acta* **374**, 96 (1974).

CHAPTER VI

Summary

Tuberculosis (TB), an infectious disease caused by *Mycobacterium tuberculosis* (MTB), remains an important global public health problem (*1, 2*), mainly because of the number of multi-drug resistant and extensively-drug resistant strains that have become more prevalent over the years (*3*). The existing anti-TB drugs are unable to treat these resistant strains and the number of new anti-TB drugs in clinical trials is limited to only nine candidates (*4, 5*). Novel drug targets are proving to be increasingly difficult to identify and effectively attack. One approach is to revisit proven targets and attempt to address deficiencies such as drug resistance. In order to modify antibiotics to control the resistant strains, a better understanding of resistance needs to be achieved at the molecular level. The mechanism of known drugs (*e.g.,* rifampin and other rifamycins) needs to be thoroughly understood that will then lead to improved drug design and a better understanding of the resistant (*e.g.,* RifR) mutants to guide further research.

Rifampin (RMP) is a semi-synthetic rifamycin derivative that demonstrates strong bactericidal activity via inhibition of RNA polymerase (RNAP). The mechanism of inhibition reported and confirmed (via crystal structure) for rifamycins is the "steric occlusion model" where rifamycins bind to the β-subunit and clash with the 5'-phosphate of the growing RNA chain during the initiation stage of transcription (*6, 7*). Resistance to RMP is mainly due to point mutations within the 81 base pair region (amino acids 424-

456, MTB numbering) of the β-subunit, which alter the rifamycin-binding site leading to decreases in affinity for the rifamycins. The three most prevalent RifR mutations found in MTB clinical isolates are Asp435Val, His445Tyr, and Ser450Leu, which result in disrupting key interactions between the enzyme and RMP (*7*-*9*). Even though these mutations have been clinically isolated and studied in resistant MTB strains, no *in vitro* studies of purified resistant MTB RNAPs with rifamycins have been reported. It is conceivable that a more potent rifamycin, which could potentially be active against these resistant strains, can be developed from the information obtained from these *in vitro* studies. The purpose of this dissertation is to address the issue of rifamycin resistance in MTB and screen novel rifamycin analogues against RifR MTB RNAPs.

We report the construction of co-overexpression vectors containing *rpo* genes that co-express the core subunits of wild-type and RifR mutants of MTB RNAP preceded by a single T7 promoter. The three aforementioned amino acids were each mutated to the most prevalent substitution found in the MTB clinical isolates in the *rpoB* gene via site directed mutagenesis. Initially, only the expression of MTB α subunit was observed; therefore, conditions (*e.g.,* expression cell lines, expression temperature, and concentration of IPTG) were varied to express all 4 subunits. The expression of MTB RNAP was successful in *E. coli* BL21 (DE3) CodonPlus RIPL cell line when expressed at 19^{o}C for 20-24 hours. The enzyme was then purified via nickel affinity chromatography and gel filtration. The *in vitro* activity of the wild-type and RifR mutant MTB RNAPs was assessed via rolling circle transcription assay. The final concentration of enzyme that was determined to be optimal (lowest concentration that gives a consistent and reliable signal) was 10 nM. The apparent IC_{50} values for three key rifamycins

(rifampin, rifabutin, and rifaximin) were determined via dose response studies and these results indicate that the mutant RNAPs demonstrate greater than 10^3-fold losses in affinity for rifamycins relative to wild-type MTB RNAP.

Along with screening known rifamycins, a novel series of rifamycin S and rifampin analogues incorporating 8-amino, 8-thio, and 1,8-pyrazole substituents was also assayed. The most prevalent mutation seen in clinical isolates is the mutation of amino acid Ser450 to Leu where the Ser450 residue directly interacts with the C-8 hydroxyl group of RMP via a hydrogen bond thus the Ser450Leu mutation affects the binding of the rifamycin (*7-9*). The results from this screen confirm that the C-8 hydroxyl of RMP does form a hydrogen bond with Ser450 and that rifamycin resistance in the Ser450Leu mutant is due to loss of this hydrogen bond and loss of affinity for rifamycins. Unfortunately, none of the C-8 analogues displayed superior potency to their parent scaffolds.

In addition, we report the screening of benzoxazinorifamycin derivatives. The design of these analogues was based upon recent crystal structures in order to develop a more potent rifamycin by making additional contacts with the other RNAP subunits. (*7, 10*). The sigma factor and core RNAP were preincubated to form a holoenzyme prior to the addition of the analogue in case the analogue does make additional contacts with the sigma factor. Overall, these novel benzoxazinorifamycin analogues displayed superior affinity toward wild-type and RifR mutants of the MTB RNAP compared to RMP but the IC_{50} values were still in the 10^{-6} M (μM) range with the RifR MTB RNAPs.

RMP is a potent inducer of cytochrome P450 3A4 (CYP3A4, a drug metabolizing enzyme); whereas, rifalazil is not thus suggesting the design of rifamycins can be

improved where CYP3A4 induction is absent. The expression of CYP3A4 is up-regulated when the human pregnane X receptor (hPXR) is activated. In order to determine if these novel series of rifamycins (C-8 analogues and benzoxazinorifamycin analogues) activate the receptor, the analogues were assessed using the hPXR activation assay. Some of the analogues of the latter series exhibited lowered activation of hPXR suggesting a potential for reduced Cyp3A4 induction activity. These studies demonstrate proof of principle for this subclass of rifamycins and support further expansion of structure-activity relationships (SAR) toward uncovering analogues with development potential.

Previously, it has been reported that Gram-positive bacteria (particularly mycobacteria) are more sensitive to rifamycins than Gram-negative bacteria (*11*). The IC_{50} values of known rifamycins for wild-type and RifR mutants of MTB and *E. coli* RNAPs (wild-type and corresponding mutants) were determined and found to be very similar; therefore, the difference in sensitivity toward rifamycins is not due to the RNAP. The correlation between the sensitivity of rifamycins and permeability into cells was evaluated using the wild-type *E. coli* strains and a mutant strain with efflux pump defects (EC2880, $tolC^{-}/imp^{-}$). The MIC values were drastically lower in the EC2880 strain, consistent with previous reports that the differential sensitivity of MTB and *E. coli* to rifamycins is not related to the RNAP, but rather has to do with efflux pump activity in *E. coli*.

In addition to screening rifamycin derivatives, work on the development of two additional assays (direct binding assay and MTB promoter based plasmid assay) was carried out. Due to the limitations of the rolling circle transcription assay, a more

sensitive direct binding assay needs to be developed to determine the affinity of MTB RNAPs and rifamycins. The equilibrium dissociation constant (K_D) of wild-type and RifR RNAPs will then be compared. The loss of free energy for each mutation will then be correlated to what interaction(s) is/are being disrupted. The focus has been on developing the direct binding assay by attaching a fluorophore (*e.g.,* dansyl group) directly to the rifamycin to determine the K_D value. Unfortunately the fluorescence of a rifamycin-dansyl probe was quenched in aqueous buffer. To conclude if the fluorescence is essentially quenched due to the naphthyl ring of the rifamycin, a variety of different fluorophores and linkers need to be tested. Another disadvantage of the rolling circle transcription assay is the non-native promoterless DNA nanocircle template. Therefore, to enhance the affinity of the MTB RNAP for the template, a MTB promoter-based plasmid has been constructed using the P1 and P3 promoters of the MTB rrn operon that would be recognized by the MTB holoenzyme. The promoter region is followed by malachite green aptamer repeat sequences, which allows the amount of the malachite green aptamer mRNA transcribed to be directly measured via fluorescence upon the addition of malachite green. Once the optimal conditions are determined, this assay will be followed up by high-throughput screening of small molecule libraries that might lead to the discovery of potential lead compounds that bind at the same position of rifamycins or at other positions that act against the antibiotic resistant strains.

Prior to our studies, the *E. coli* RNAP and rifampin had been extensively studied but little is known about the molecular mechanisms involved in resistance due to the lack of *in vitro* studies of RifR MTB RNAPs. The successful expression and purification of wild-type and RifR MTB RNAPs from co-overexpression vectors allowed us to directly

investigate the level of inhibition by known and novel rifamycins. The similar IC_{50} values determined for known rifamycins with MTB and *E. coli* RNAPs (WT and RifR) allowed us to conclude that the difference in sensitivity between MTB and *E. coli* is not due to the RNAP. The issue of sensitivity was further investigated by using a mutant *E. coli* strain (deficient in the TolC efflux pump) where the strain was much more sensitive to rifamycins suggesting that the difference in sensitivity is due to the *E. coli* efflux pumps. The C-8 modifications (8-amino, 8-thio, and 1,8-pyrazole) did not result in a more effective rifamycin against the most prevalent mutation (Ser450Leu) found in MTB clinical isolates. This study also confirmed that the C-8 position is limited in the number of modifications at this position since it is involved in critical interactions with key residues of the RNAP. The next set of analogues was based on rifalazil and crystal structure information since rifalazil is more potent than RMP and does not induce CYP3A4. The benzoxazinorifamycin analogues were designed to make additional contacts with the RNAP. While the desired level of inhibition was not obtained, the limited number of compounds synthesized provided proof of concept for expansion of SAR in this series. The linker was also thought to lower the affinity of the benzoxazinorifamycins to the hPXR binding site because of the additional bulk, but since the hPXR binding site is large and able to adapt to different ligands, activation was still observed which could be due to the flexibility of the linker. The results from these studies will lead us to improve the design of rifamycins to develop a more potent rifamycin against RifR RNAPs.

In the future, the completion of the direct binding assay and the *in vitro* MTB promoter based plasmid transcription assay experiments allow for a greater understanding

of the interactions between rifamycins with the wild-type and mutant MTB RNAP. The small molecules identified from the HTS can then be transformed into new broad-spectrum antibiotics since prokaryotic RNAPs are conserved. Furthermore, it would be beneficial to obtain structural information by X-ray crystallography of the MTB RNAP bound to various rifamycins, especially the benzoxazinorifamycin analogues. These experiments will hopefully provide useful information to understand the molecular mechanisms responsible for resistance and guide the development of new analogues with the potential of enhanced activity against resistant strains.

References

1. World-Health-Organization, "WHO Report 2010: Global Tuberculosis Control" *Report* (2010).

2. D. M. Morens, G. K. Folkers, A. S. Fauci, The challenge of emerging and re-emerging infectious diseases. *Nature* **430**, 242 (Jul, 2004).

3. WHO, Multidrug and Extensively Drug-Resistant TB (M/XDR-TB): 2010 Global Report on Surveillance and Response. http://whqlibdoc.who.int/publications/2010/9789241599191_eng.pdf, (2010).

4. A. Koul, E. Arnoult, N. Lounis, J. Guillemont, K. Andries, The challenge of new drug discovery for tuberculosis. *Nature* **469**, 483 (Jan, 2011).

5. N. R. Gandhi *et al.*, Multidrug-resistant and extensively drug-resistant tuberculosis: a threat to global control of tuberculosis. *Lancet* **375**, 1830 (May, 2010).

6. W. R. McClure, C. L. Cech, On the mechanism of rifampicin inhibition of RNA synthesis. *J. Biol. Chem*. **253**, 8949 (1978).

7. E. A. Campbell *et al.*, Structural mechanism for rifampicin inhibition of bacterial RNA polymerase. *Cell* **104**, 901 (2001).

8. A. Telenti *et al.*, Detection of Rifampicin-Resistance Mutations in *Mycobacterium tuberculosis*. *Lancet* **341**, 647 (Mar, 1993).

9. D. L. Williams *et al.*, Contribution of rpoB mutations to development of rifamycin cross-resistance in Mycobacterium tuberculosis. *Antimicrob. Agents Chemother.* **42**, 1853 (1998).

10. I. Artsimovitch *et al.*, Allosteric modulation of the RNA polymerase catalytic reaction is an essential component of transcription control by rifamycins. *Cell* **122**, 351 (Aug 12, 2005).

11. H. G. Floss, T.-W. Yu, Rifamycin-mode of action, resistance, and biosynthesis. *Chem*. *Rev*. **105**, 621 (2005).

12. N. Zenkin, A. Kulbachinskiy, I. Bass, V. Nikiforov, Different Rifampin Sensitivities of Escherichia coli and Mycobacterium tuberculosis RNA Polymerases Are Not Explained by the Difference in the {beta}-Subunit Rifampin Regions I and II. *Antimicrob. Agents Chemother.* **49**, 1587 (April 1, 2005, 2005).

APPENDIX

Construction of MTB Promoter Based Plasmid

In prokaryotes, gene expression is mediated by the holoenzyme (core RNAP + sigma factor) (*1*). An *in vitro* transcription assay mimics these conditions by using a DNA template with a specific promoter that is recognized by the sigma factor. For the assay, a strong promoter is required to be confident it will recognized by the holoenzyme hence leading to the expression of the gene following the promoter. Previously, *E. coli* has been the best-studied prokaryote where the *E. coli* RNAP and promoters are well known. However, mycobacterial promoters are not well characterized since majority of the promoters are weak (*2*). Mycobacterial promoters have also been difficult to study because the promoters do not function well in *E. coli* (*1, 2*). Due to the fact that prokaryotic RNAPs recognize different promoters, the activity of MTB RNAP will be assessed directly using a native mycobacterial template that will be recognized by the housekeeping MTB sigma factor, (SigA, σ^A), which is one of the thirteen MTB sigma factors, all of the σ^{70} type (*1, 3, 4*).

In general, prokaryotic promoters contain two hexamers at -35 and -10 from the transcription start point (TSP). Different parts of the sigma factor recognize different regions of the promoter (σ region 2.4 binds to the -10 region and σ region 4.2 binds to the -35 region of the promoter) (*1, 3, 5*). The -10 region of mycobacterial promoters is similar to *E. coli* but the -35 region is not as strongly conserved (*2, 6*). The consensus

sequence recognized by SigA is TTGAC(A/T) (-35 hexamer) $N_{18/17}$ TATA(A/C)T (-10 hexamer) (*1, 5*). Only a few strong MTB promoters have been identified that transcribe the following genes: 16S rRNA, *cpn*-60 gene, and 85A antigen gene (*6-9*). Even though the slow-growing MTB has a low content of RNA, the majority (80%) of the RNA pool is the ribosomal RNA (rRNA), which is an essential component that is involved in decoding the mRNA and interacting with the tRNA. MTB has a single ribosomal RNA (*rrn*) operon containing the genes for 16S, 23S, and 5S rRNA that is driven by two promoters, P1 and P3 (*10, 11*). The complete promoter region of *rrn* operon is approximately 650 bp, but previous studies have shown that a 310 bp fragment containing the +1 of mature 16S rRNA and both P1 and P3 *rrn* promoters is highly active (*8*). The P3 promoter has been identified as the stronger *rrn* promoter in MTB, approximately twice as active as P1. The sequence of the P3 promoter is TTGACT (-35 hexamer) N_{18} TAGACT (-10 hexamer), similar to the consensus sequence recognized by SigA (*8*). Therefore, our lab will use the MTB rrn operon (containing the P1 and P3 promoters) as the promoter region.

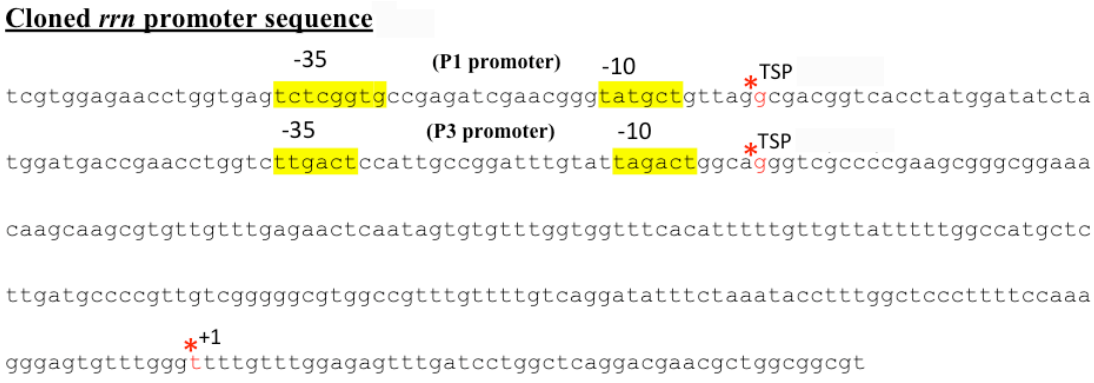

Appendix Figure–1: The 369 bp sequence of MTB rrn operon containing the P1 and P3 promoter. The -35 and -10 regions of both promoters are highlighted in yellow. The transcription sites are indicated after the -10 hexamer as 'TSP' and the translation start point is indicated as +1 (*7-9*).

Another important component of the assay is the detection of the transcribed product. Previously, radioisotopically tagged ribonucleotides have been used in *in vitro* transcription assays. Some disadvantages involved with this method include: high reagent costs, high disposal costs, and variable reagent shelf life (*12*). A non-radioisotopic approach is to measure the RNA via Ribogreen, a fluorescent dye. A disadvantage to this method is the dye binds to both RNA and DNA; therefore, an additional step is required that removes DNA by DNase digestion and ultrafiltration (*12*). Molecular beacons can also be used to detect the mRNA. These exist in RNA hairpin structures in the absence of target with the fluorophore in close proximity to the quencher. When the molecular beacon binds to the specific target, a strong fluorescence signal is observed due to the dissociation of the hairpin (concurrent with annealing to the target RNA) and the consequent physical separation of the fluorophore and quencher moieties. This method allows for high signal to noise ratio, but is prohibitively expensive to be used for an HTS assay (*13*). Another method is use an aptamer, which is short single stranded RNA that binds to a molecule with high binding affinity and specificity (*14, 15*). To visualize the amount of mRNA produced in this assay, we have elected to insert the malachite green aptamer (MGA) gene sequence after the MTB P1/P3 promoter. MGA has been reported to bind to triphenylmethane dyes (*i.e.,* malachite green (MG)) and upon binding a $\geq$ 2,000 fold increase in fluorescence signal is observed (*16*). The fluorescence emission spectra is measured at an excitation wavelength of 610 nm with the maximum emission wavelength being at 640-650 nm.

(38 nt) ggaucccgacuggcgagagccagguaacgaauggaucc

(4xMGA RNA 173 nt)

5′ggaucccgacuggcgagagccagguaacgaauggauccuaaaaacgg
aucccgacuggcgagagccagguaacgaauggauccuaaaaacggauc
ccgacuggcgagagccagguaacgaauggauccuaaaaacggaucccg
acuggcgagagccagguaacgaauggaucc 3′

(8xMGA RNA 365 nt)

5′ggaucccgacuggcgagagccagguaacgaauggauccuaaaaacgg
aucccgacuggcgagagccagguaacgaauggauccuaaaaacggauc
ccgacuggcgagagccagguaacgaauggauccuaaaaacggaucccg
acuggcgagagccagguaacgaauggauccucuagagcgguaagucga
cggaucccgacuggcgagagccagguaacgaauggauccuaaaaacgg
aucccgacuggcgagagccagguaacgaauggauccuaaaaacggauc
ccgacuggcgagagccagguaacgaauggauccuaaaaacggaucccg
acuggcgagagccagguaacgaauggaucc 3′

Appendix Figure–2: The malachite green aptamer (MGA) mRNA sequence. The 4xMGA and 8xMGA repeat sequences are shown underneath with the MGA sequence underlined.

Professor Jaya Sivaswami Tyagi (All India Institute of Medical Sciences) was kind enough to send us the prrn plasmid containing the 369 bp rrn operon (with P1 and P3 promoter) followed by the *gfp* gene (Appendix Figure–1) (*9*). The plasmid is in an *E. coli*-mycobacterial shuttle plasmid (pFPV-27) and is hygromycin B antibiotic resistant. The plasmids containing MGA (pLee345.3.3 and pTJ141) were a generous gift from Professor Nilsen-Hamilton (Iowa State University). Plasmid pLee345.3.3 has the sequence of four repeats of MGA (4xMGA) and plasmid pTJ141 has eight repeats (8xMGA) where each MGA repeat sequence is separated by 7 bases. Since the aptamer domain is only 38 nucleotides long (Appendix Figure–2), the multiple repeats of MGA might enhance fluorescence signal further.

Once the plasmids were received, unique restriction sites were incorporated to allow for subcloning the MGA repeats into the MTB promoter containing plasmid (Appendix Figure–3). It was challenging to identify unique sites because we did not have

the sequence file of prrn. The unique sites used were *Bsu361* and *PacI*. These sites were introduced into prrn plasmid via site-directed mutagenesis. After the *Bsu361* site was inserted after the P3 TSP, the sequence of several plasmids showed there was a deletion of a single nucleotide at various positions of the P3 promoter: ΔT from P3 spacer region, ΔT from P3 -10 region, and ΔG before P3 TSP. QC primers were designed to insert +T to the -10 region, but after multiple trials, the reaction was still unsuccessful. For MGA sequence, the sites were introduced via PCR.

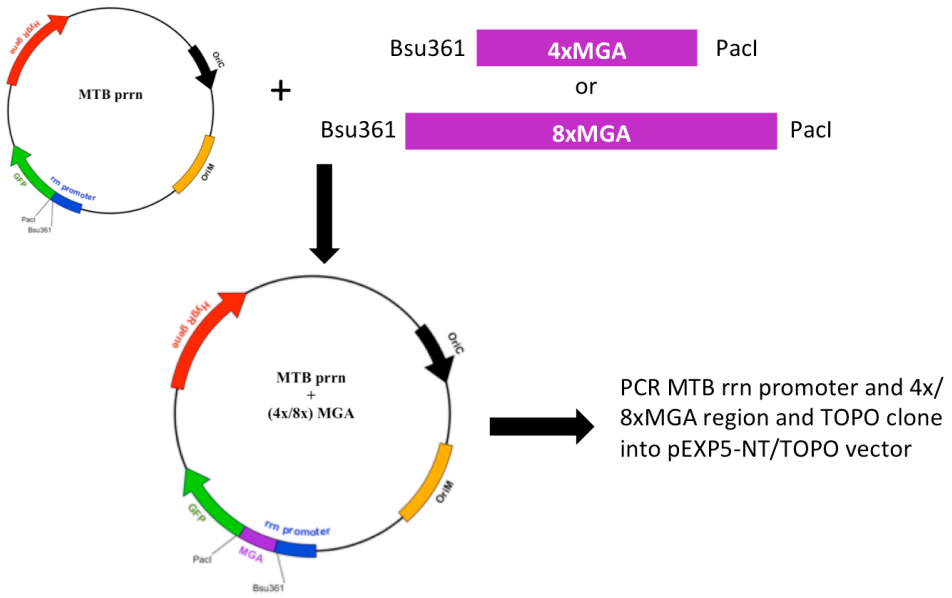

Appendix Figure–3: MTB Promoter based plasmid + MGA. All the oligonucleotides used to sequence and construct the plasmid are listed in Appendix Table 1.

After the restriction sites were introduced, the PCR product of 4xMGA and 8xMGA and prrn (containing the *Bsu361* and *PacI* sites) were treated with *Bsu361* and *PacI* via sequential digestion. The PCR product of the MGA repeats was subcloned into treated prrn. Along the way plasmids containing only two repeats of the MGA were also obtained. The resulting plasmids that we have constructed are listed below (unfortunately we were unable to get a plasmid that did not contain a deletion):

- prrn (ΔT from P3 spacer region) + 2xMGA
- prrn (ΔG before P3 TSP) + 2xMGA
- prrn (ΔT from P3 spacer region) + 4xMGA
- prrn (ΔT from P3 -10 region) + 4xMGA
- prrn (ΔG before P3 TSP) + 4xMGA
- prrn (ΔT from P3 spacer region) + 8xMGA
- prrn (ΔG before P3 TSP) + 8xMGA

Now that these plasmids have been constructed, initial studies need to be conducted including one that determines if the holoenzyme binds to the DNA template via DNA binding assays. Control experiments (with no inhibitor present) will then be setup to find the optimal conditions for the *in vitro* transcription assay. Furthermore, the MGA sequence from the original plasmids (pLee345.3.3 and pTJ141) is preceded by the T7 promoter thus the amount of MGA synthesized by T7 RNAP can be isolated and quantified to determine a standard curve using MG. The amount of fluorescence observed with the MTB promoter assay can be used to quantify the amount of RNA transcribed. Rifampin and rifamycin analogues will then be assayed with the wild-type and mutant MTB RNAPs. In the absence of rifamycins, the MTB RNAP will be expected to transcribe the MGA domain and when MG is added a distinct fluorescence signal will be observed; whereas, in the presence of rifamycins, the aptamer domain will not be transcribed because the RNAP will be inhibited thus no fluorescent signal.

Once preliminary runs are successful, the assay can then be developed into an HTS assay. Small molecule libraries will be screened using the different MTB RNAPs. Any hits will be confirmed and characterized via secondary assays (e.g., *in vitro*

MGA•MG binding assay to screen for inhibitors of MG binding to MGA and the direct binding assay (see Chapter V) to probe for competition with rifamycins). Ideally the HTS will identify novel scaffolds that inhibit the MTB RNAP with a different mechanism of action than the rifamycins thus not subject to cross-resistance.

In this appendix, we have described an approach to analyze *in vitro* transcription in the presence of MTB RNAP using the malachite green aptamer that specifically binds to malachite green. The SigA driven MTB RNAP binds to the MTB *rrn* operon promoters hence leads to the transcription of the malachite green aptamer mRNA. This method is convenient with reduced steps, which makes it favorable to be developed into a HTS assay. The advantages of this method include: reduced cost, fewer steps, high signal to noise ratio, high binding affinity of target, and non-radiolabeled nucleotides. Since RNAP is conserved among prokaryotes, small molecules that target and inhibit RNAP in HTS assay could potentially lead to finding a novel MTB antibiotic.

Appendix Table 1. Oligonucleotides Used to Construct the Plasmids.

Oligonucleotides	**Primer Sequence (5'-3')**
(QC/PCR Primers)	
prrn Plasmid	
(Add Bsu361 site after P3 TSP start site and PacI site after translation start site)	
prrn QC FWD Primer (+Bsu361)	gtattagactggcagggtcgccccTaagGgggcggaaacaagcaagcgtgttg
prrn QC REV Primer (+Bsu361)	caacacgcttgcttgtttccgcccCcttAggggcgaccctgccagtctaatac
prrn QC FWD Primer (+PacI)	ctggctcaggacgaacgctggcggcTtaatTaAtagtgaattcgatatcaagcttatc
prrn QC REV Primer (+PacI)	gataagcttgatatcgaattcactaTtAattaAgccgccagcgttcgtcctgagccag
(Insert "T" in the -10 box of the second promoter (P3))	
prrn QC FWD Primer (+T)	gccggatttgtattagacTggcagggtcgcccctaag
prrn QC REV Primer (+A)	cttaggggcgaccctgccAgtctaatacaaatccggc
(To amplify WT MTB rrn promoter + GFP)	
PCR FWD Primer	gaagctGGATCCcccgggctgcagg
PCR REV Primer	agcttcGCATGCctgcaggtctggac
(QC/PCR Primers)	
(p4xMGA Plasmid; pLee345.3.3)	
p4xMGA PCR FWD (+Bsu361)	cagcgaCCTAAGGagcacgtcgacggatcccgac
p4xMGA PCR REV (+PacI)	gaagctTTAATTAAtccgctctagaggatccattcg
(p8xMGA Plasmid; pTJ141)	
p8xMGA PCR FWD (+Bsu361)	cagcgaCCTAAGGctcttcaggtaagtcgacggatcccgac
p8xMGA PCR REV (+PacI)	gaagctTTAATTAAtccaccgctctagaggatccattcgttacc
(to amplify 4xMGA and 8xMGA from original plasmids pLee345.3.3 and pTJ141)	
PCR FWD Primer (4x/8xMGA)	cagaGATTACGAATTTAATACGACTC
PCR REV Primer (4x/8xMGA)	gagtCTAGTAAAAAGCGGACCGAAGTC

Appendix Table 1. (continued)

Oligonucleotides	**Primer Sequence (5'-3')**
PCR primers (to amplify MTB rrn promoter region (including ~150 bp upstream) + 4x/8xMGA without GFP sequence)	
PCR FWD Primer	cagaCTTGGTCGATACCAAGCCATTTC
PCR REV Primer	gagtGATATCGAATTCACTATTAATTAATC

References

1. P. Sachdeva *et al.*, The sigma factors of Mycobacterium tuberculosis: regulation of the regulators. *Febs Journal* **277**, 605 (Feb, 2010).

2. N. Agarwal, A. K. Tyagi, Mycobacterial transcriptional signals: requirements for recognition by RNA polymerase and optimal transcriptional activity. *Nucleic Acids Res.* **34**, 4245 (Sep, 2006).

3. S. Rodrigue, R. Provvedi, P.-E. Jacques, L. Gaudreau, R. Manganelli, The Sigma factors of *Mycobacterium tuberculosis*. *FEMS Microbiology Reviews* **30**, 926 (2006).

4. J. H. Lee, P. C. Karakousis, W. R. Bishai, Roles of SigB and SigF in the *Mycobacterium tuberculosis* sigma factor network. *J. Bacteriol.* **190**, 699 (Jan, 2008).

5. R. Manganelli, R. Provvedi, S. Rodrigue, J. Beaucher, L. Gaudreau, I. Smith, Sigma factors and global gene regulation in *Mycobacterium tuberculosis*. *J. Bacteriol.* **186**, 895 (Feb, 2004).

6. M. D. Bashyam, D. Kaushal, S. K. Dasgupta, A. K. Tyagi, A study of the mycobacterial transcriptional apparatus: Identification of novel features in promoter elements. *J. Bacteriol.* **178**, 4847 (Aug, 1996).

7. J. A. GonzalezyMerchand, M. J. Colston, R. A. Cox, The rRNA operons of Mycobacterium smegmatis and Mycobacterium tuberculosis: Comparison of promoter elements and of neighbouring upstream genes. *Microbiology-(UK)* **142**, 667 (Mar, 1996).

8. A. Verma, A. K. Sampla, J. S. Tyagi, Mycobacterium tuberculosis rrn promoters: Differential usage and growth rate-dependent control. *J. Bacteriol.* **181**, 4326 (Jul, 1999).

9. S. Chauhan, J. S. Tyagi, Cooperative binding of phosphorylated DevR to upstream sites is necessary and sufficient for activation of the Rv3134c-devRS operon in Mycobacterium tuberculosis: Implication in the induction of DevR target genes. *J. Bacteriol.* **190**, 4301 (Jun, 2008).

10. Y. E. Ji, M. J. Colston, R. A. Cox, Nucleotide-Sequence and Secondary Structures of Precursor 16s Ribosomal-RNA of Slow-Growing Mycobacteria. *Microbiology-(UK)* **140**, 123 (Jan, 1994).

11. A. Verma, A. K. Kinger, J. S. Tyagi, Functional-Analysis of Transcription of the *Mycobacterium tuberculosis* 16s RNA-Encoding Gene. *Gene* **148**, 113 (Oct, 1994).

12. P. Kuhlman, H. L. Duff, A. Galant, A fluorescence-based assay for multisubunit DNA-dependent RNA polymerases. *Analytical Biochemistry* **324**, 183 (Jan, 2004).

13. W. Tan, K. Wang, T. J. Drake, Molecular beacons. *Current Opinion in Chemical Biology* **8**, 547 (Oct, 2004).

14. J. E. Weigand, B. Suess, Aptamers and riboswitches: perspectives in biotechnology. *Appl. Microbiol. Biotechnol.* **85**, 229 (Nov, 2009).

15. M. Mandal, R. R. Breaker, Gene regulation by riboswitches. *Nature Reviews Molecular Cell Biology* **5**, 451 (Jun, 2004).

16. J. R. Babendure, S. R. Adams, R. Y. Tsien, Aptamers switch on fluorescence of triphenylmethane dyes. *J. Am. Chem. Soc.* **125**, 14716 (Dec, 2003).